UNIVERSITÀ
DEGLI STUDI
DI PADOVA

Università degli Studi di Padova
Sede amministrativa: Padova
Dipartimento di Fisica e Astronomia "Galileo Galilei"
SCUOLA DI DOTTORATO DI RICERCA IN FISICA
CICLO XXVI

Tesi di dottorato:

Search for heavy lepton partners of neutrinos in the context of type III seesaw mechanism in 2012 LHC CMS data

Direttore della Scuola: **Prof. Andrea Vitturi**

Supervisore: **Dott. Ezio Torassa**

Co-Supervisore: **Prof. Ugo Gasparini**

Co-Supervisore: **Dott. Gaetano Maron**

Dottorando: **Andrea Gozzelino**

Signatures

Direttore della Scuola: **Prof. Andrea Vitturi**

Supervisore: **Dott. Ezio Torassa**

Co-Supervisore: **Prof. Ugo Gasparini**

Co-Supervisore: **Dott. Gaetano Maron**

Dottorando: **Andrea Gozzelino**

Thesis delivery: January, 31st 2014

Month of the defense: March 2014

Riassunto

Questa tesi di fisica sperimentale delle alte energie tratta una ricerca dedicata al meccanismo dell'altalena con mediatori tripletti deboli di fermioni pesanti (tipo III). La ricerca é basata sui processi dove i mediatori del modello ad altalena sono prodotti attraverso un bosone vettoriale carico e virtuale, e decadono in bosoni vettoriali reali e leptoni carichi standard. Gli stati finali considerati contengono esattamente tre leptoni carichi e standard, energia trasversa mancante, che rivela indirettamente la presenza di neutrini standard, e jets. La somma della carica elettrica dei tre leptoni considerata ha valore unitario, di ambo i segni. Il campione di dati analizzati é stato raccolto dall'esperimento Compact Muon Solenoid (CMS) all'acceleratore Large Hadron Collider (LHC) del CERN, in Ginevra (Svizzera), nel corso del periodo di presa dati in collisioni protone-protone, relativo al 2012. Tale campione di dati consta di una luminositá integrata pari a 19.7 fb^{-1} con energia disponibile nel centro di massa di 8 TeV. Gli algoritmi di trigger selezionati richiedono due leptoni carichi (dileptoni) con impulso trasverso sopra le soglie di 17 GeV e 8 GeV, rispettivamente. I contributi di fondo agli eventi di segnale provengono da processi del modello standard, principalmente dibosoni, conversioni asimmetriche di fotoni (Dalitz) e leptoni provenienti da vertici secondari (Fake). Dalitz e Fake sono stimati attraverso due metodi, che usano le informazioni provenienti dai dati. L'incertezza sistematica relativa al fondo é dominante rispetto agli errori statistici. Il modello dell'altalena di tipo III é studiato dettagliatamente nelle fasi di generazione. Il segnale é modellato attraverso una tecnica di simulazione Monte Carlo per diversi valori di massa dei mediatori nell'intervallo tra 140 GeV e 340 GeV. Un possibile contributo di segnale nel campione di dati analizzati é investigato con il metodo dell'esperimento taglia e conta. Non c'é evidenza statistica di segnale rispetto al fondo previsto dal modello standard nei dati del 2012, cosí si conclude che nessun indizio di nuova fisica da modello di seesaw tipo III é presente. La sensitivitá dell'analisi é stata calcolata nell'ipotesi di solo fondo. Sono presentati i limiti superiori sulle sezioni d'urto di produzione dei mediatori nel modello dell'altalena moltiplicati per il rappporto di decadimento nelle catene che portano stati finali con leptoni carichi. Poi, i limiti superiori sono tradotti in limite inferiore sul valore di massa dei mediatori: il limite osservato é 240 GeV.

Abstract

In the thesis the analysis performed for the search for seesaw mechanism with heavy fermion weak triplets mediators (type III) is presented. The search is based on the process of seesaw mediators via virtual charged boson with the subsequent decay in real vector boson and standard charged leptons. The considered final states host exactly three charged standard leptons and missing transverse energy, which displays indirectly standard neutrinos, and jets. The investigated electric charge sum of three leptons has unit value, both signs. The analysed data sample has been recorded by the Compact Muon Solenoid (CMS) experiment at the CERN Large Hadron Collider (LHC) in Geneva, Switzerland, during the 2012 proton-proton collisions data-taking period. The data sample consists of a total integrated luminosity of 19.7 fb^{-1} at center of mass energy 8 TeV. The selected trigger algorithms require two charged leptons (dilepton) with transverse momentum above thresholds of 17 GeV and 8 GeV, respectively. The background contributions to the signal events come from standard model processes, mainly involving di-bosons, photon asymmetric conversion (Dalitz), and non prompt leptons (Fake). Dalitz and Fake are estimated through two methods using data information. The systematic uncertainty related to the background is dominant with respect the statistic errors. The seesaw type III model is in details studied in generation phases. The signal is modelled through Monte Carlo simulation technique for different mediators mass values in the range from 140 GeV to 340 GeV. A possible signal contribution in the analysed data sample is investigated through a cut and count experiment. There is no statistical evidence of signal respect the expected standard model background in the 2012 pp collisions data, so no hints of new physics from seesaw type III model is present. The sensitivity of the analysis has been calculated in the background only hypothesis. An upper limits on the production cross sections of the seesaw mediators times the branching ratio of the decays with three charged leptons in final states are presented. Then, the upper limits are translated into lower limits on mediators mass value: the observed limit is 240 GeV.

Contents

Introduction

The Standard Model (SM) of fundamental interactions [1–4] is the best description of the phenomena involving elementary particles at different energy scales and it reproduces almost all experimental physics results obtained so far at many accelerator and non-accelerator experiments. SM is not a definitive theory, but it is the best effective theory in place. However, it does not explain neutrinos masses, the gravity as unified mediated force, and it does not provide a complete model for the violation of conjugate charge and the parity symmetry. Moreover, SM leaves open questions concerning the dark matter in the Universe, and the so called hierarchy and naturalness problems. Searches for physics beyond the SM (BSM) are attractive: many theories have been developed by theoreticians and all of them need to be tested. The most common theory BSM is the Super Symmetry (SUSY), but the field is open. The experiments at Large Hadron Collider (LHC) explore also signatures and final states for different theories with dedicated studies called ”exotica searches”.

In the context of ”exotica searches”, a specific search is devoted to test the possible existence of heavy partners of neutrino, and the results are interpreted in the framework of the so called ”seesaw type III” mechanism. One of the explanations for standard neutrinos light masses - not included in the SM - is the seesaw mechanism. The final states characterized by the presence of three leptons and missing transverse energy and jets are investigated. As it will be discussed in the thesis, no evidence of events above SM backgrounds is seen. Limits on production cross sections and mediators masses are set using 2012 data at center of mass energy 8 TeV, collected by Compact Muon Solenoid (CMS) experiment.

Chapter 1

The Standard Model of fundamental interactions and its possible extensions

1.1 Standard Model

SM gives the best description of the phenomena involving elementary particles and fundamental interactions. It is a quantum field theory (QFT), which includes the Quantum Cromo Dynamics (QCD), describing the strong interaction, and the electroweak theory (EWK), describing the electromagnetic and weak interactions. It is based on the gauge group:

$$SU(3)_{color,C} \otimes SU(2)_{weakisospin,T} \otimes U(1)_{hypercharge,Y}. \tag{1.1}$$

Related to this local symmetry group, twelve gauge bosons with spin 1 arise:

- eight gluons (g) related to $SU(3)_C$ generators;
- three gauge bosons W_i related to $SU(2)_T$ generators;
- one gauge bosons B related to $U(1)_Y$ generator.

The neutral Z boson, mediator of the weak neutral current, and photon γ, mediator of the electromagnetic interaction, are linear combinations of gauge bosons W_3 e B. Fermions, particles with semi integer spin, are quarks or leptons: the former have both strong and electroweak interactions, the latter only the electroweak. Both quarks and leptons are divided into three families, with different masses but identical interactions. Right-handed or left-handed Weyl spinors, with two components, describe all fermions. Although, mass terms are not present in the Lagrangian: they would destroy the gauge symmetry. Fermions have masses only if symmetry is broken. The Higgs mechanism, proposed in 1964 by Higgs, Englert and Brout and others, breaks the symmetry group and gives masses to particles, preserving the possible renormalization of the theory. The mechanism introduces scalar fields as a weak isospin doublet $SU(2)_T$ with hypercharge Y $= -\frac{1}{2}$ to leave $SU(3)_C \otimes U(1)_Y$:

$$\Phi = \begin{pmatrix} \Phi^0 \\ \Phi^- \end{pmatrix}$$

In the SM Lagrangian, the potential term V(Φ) is introduced in addition to the fermions and gauge fields, kinetic and interaction terms:
$L = L(f, G) + L(f, \Phi) + L(G, \Phi) + L(G) - V(\Phi)$
where f stays for fermion, G for gauge bosons, Φ for Higgs doublet. The scalar potential is:

$V = \mu^2 \Phi^\dagger \Phi + \lambda (\Phi^\dagger \Phi)^2$.

If μ^2 is negative, by definition the neutral component has vacuum expectation value not zero:

$$<\Phi> = \begin{pmatrix} 0 \\ v \end{pmatrix} * \frac{1}{\sqrt{2}}$$

where v $= \sqrt{\frac{-\mu^2}{\lambda}}$.

Symmetry $SU(2)_T \otimes U(1)_Y$ is broken, but symmetry $U(1)_{em}$ is in place. The vectorial charged boson

$$W^{\pm} = \frac{W^1 \pm W^2}{\sqrt{2}}$$

have mass

$$M_W = \frac{g_2 * v}{2}$$

and the linear combination of neutral bosons

$$Z = \frac{1}{\sqrt{g_1^2 + g_2^2}} * (-g_2 W^3 + g_1 B)$$

has mass

$$M_Z = \frac{v * \sqrt{g_1^2 + g_2^2}}{2}$$

but the orthogonal combination

$$A = \frac{1}{\sqrt{g_1^2 + g_2^2}} * (g_1 W^3 + g_2 B)$$

is still mass less. g_1 and g_2 are the coupling constants in $U(1)_Y$ and $SU(2)_T$. The SM Higgs scalar boson has mass $M^2_{Higgs} = -2\mu^2$. Parameters v,g_1 e g_2 are related to the Fermi constant G_F and the electromagnetic constant e:

$$G_F = \frac{\sqrt{2} * g_2^2}{8 * M_W^2}$$
$$e = g_2 \sin\theta_W = g_1 \cos\theta_W$$

where the electromagnetic mixing angle, called Weinberg's angle, is $\tan\theta_W = \frac{g_1}{g_2}$. The Weinberg's angle is not fixed, but its experimental value gives an handle to test the SM. After spontaneous symmetry breaking the Lagrangian for the fermion fields contains: the Weinberg's angle, the positron electric charge, the mass less photon field, the two massive and neutral weak boson fields, the quark masses. In the presence of right-handed neutrinos, the Lagrangian gives

rise also to Dirac neutrinos masses. If neutrinos and anti neutrinos are the same particle, they are Majorana neutrinos. In addition, there is a physical neutral Higgs scalar field H which is the only remaining part of the doublet Φ after spontaneous symmetry breaking. In non-minimal models there are additional charged and neutral scalar Higgs particles. The Higgs particles discovered by ATLAS and CMS collaborations on July 4th 2012 is like H, till now. The SM has three free parameters excluding masses. A set of those is: the fine structure constant α, determined from the electron positron anomalous magnetic moment and the quantum Hall effect, the Fermi constant G_F, determined from the muon lifetime, the Z boson mass, measured from the Z-line shape scan at Large Electron Positron collider (LEP). The SM is a re normalizable theory which, after proper computation of radiative corrections at leading or next-to-leading order of the perturbation expansion, gives precise predictions on many physical observables. Experiments tested and stressed it with many precise measurements, but no deviations are claimed till now from its predictions. However, SM leaves open questions concerning the dark matter in the Universe, and the so called hierarchy and naturalness.

1.2 Higgs boson

The SM of elementary particles provides a remarkably accurate description of results from many accelerator and non-accelerator based experiments. The SM comprises quarks and leptons as the building blocks of matter, and describes their interactions through the exchange of force carriers: the photon for electromagnetic interactions, the W and Z bosons for weak interactions, and the gluons for strong interactions. The electromagnetic and weak interactions are unified in the electroweak theory. Although the prediction of the SM have been extensively confirmed, the question of how the W and Z gauge bosons acquire mass whilst the photon remains mass less was open till July 2012. Nearly fifty years ago it was proposed that the spontaneous symmetry breaking in gauge theories could be achieved through the introduction of a scalar field. Applying this mechanism to the electroweak theory through a complex scalar doublet fields leads to the generation of the W and Z masses, and the prediction of the existence of the SM Higgs boson H. The scalar field also give mass to the fundamental fermions through the Yukawa interaction. The mass m_H of the SM Higgs boson is not predicted by theory. However, general considerations suggest that m_H should be smaller than 1 TeV, while precision electroweak measurements imply that $m_H < 152$ GeV at 95% confidence level (CL). Over the past twenty years, direct searches for the Higgs boson have been carried out at the LEP collider, leading to a lower bound of $m_H > 114.4$ GeV at 95% CL, and at the Tevatron proton-antiproton collider, excluding the mass range [162;166] GeV at 95% CL and detecting an excess of events in the range [120;135] GeV. First direct searches at the LHC are based on data from proton-proton collisions corresponding to an integrated luminosity of 5 fb^{-1} collected at the center-of-mass energy $\sqrt{s} = 7$ TeV. The CMS experiment excluded at 95% CL a range of masses [127;600] GeV. The ATLAS experiment excluded at 95 % CL the ranges [111.4;116.6], [119.4;122.1] and [129.1;541] GeV. Within the remaining allowed mass region, an excess of events near 125 GeV was reported by both the experiments. In 2012 the proton-proton center-of-mass energy was increased to 8 TeV and by the end of June and additional integrated luminosity of more than 5 fb^{-1} had been recorded by ATLAS and CMS experiments. The Higgs boson search was performed in five decay modes: $H \to \gamma\gamma$, $H \to ZZ$, $H \to W^+W^-$, $H \to \tau^+\tau^-$, $H \to b\bar{b}$, in the low-mass range from 110 to 160 GeV. In this mass range the Higgs boson production cross section is predicted to have value between 23 (29) and 10 (14) pb at $\sqrt{s} = 7$ (8) TeV. The natural width of SM Higgs boson over the same range is less than 100 MeV, so that the width of any observed peak would be entirely dominated by instrumental mass resolution. CMS observed an excess of events above the expected background, with a local significance of 5.0 standard

deviations, at a mass near 125 GeV, signaling the production of a new particle. The expected significance for a standard model Higgs boson of that mass is 5.8 standard deviations [5]. The data samples corresponding to integrated luminosities of up to 5.1 fb^{-1} at 7 TeV and 5.3 fb^{-1} at 8 TeV. The evidence is strongest in the two final states with the best mass resolution, namely H $\rightarrow \gamma\gamma$ and H $\rightarrow ZZ$ (with Z bosons decaying to electrons or muons): a fit to these signals gives a mass of 125.3 $\pm$ 0.4 (stat.) $\pm$ 0.5 (syst.) GeV. The decay to two photons indicates that the new particle is a boson with spin different from one. ATLAS observed a clear evidence for the production of a neutral boson with a measured mass of 126.0 $\pm$ 0.4 (stat.) $\pm$ 0.4 (syst.) GeV. This observation, which has a significance of 5.9 standard deviations, corresponding to a background fluctuation probability of $1.7*10^{-9}$, is compatible with the production and decay of the Standard Model Higgs boson [6]. Finally, the ATLAS measurement of the mass of the newly discovered boson using the full data set of events collected in 2011 and 2012 (corresponding to a total integrated luminosity of $\sim 25\ fb^{-1}$) is 125.5 $\pm$ 0.2 (stat.) $\pm$ 0.5 (syst.) GeV [7]. The new boson is observed as a narrow resonance with a local significance of 6.8 standard deviations, a measured mass of 125.6 $\pm$ 0.4 (stat.) $\pm$ 0.2 (syst.) GeV and a total width <3.4 GeV at a 95% CL in four leptons final state at CMS [8]. The determination of the properties of the new observed boson, such as its couplings to other particles, mass, and quantum numbers, including spin and parity, is crucial for establishing the nature of this boson. Many channels help to reach the goal. The pseudo scalar and spin-one boson hypotheses are excluded at a 99% CL or higher. All tested spin-two boson hypotheses are also excluded at a 95% CL or higher [8]. In details, the spin-parity $J^P = 0^+$ hypothesis is favored against a narrow resonance with $J^P = 2^+$ or $J^P = 0^-$ that decays to a W-boson pair. This result provides strong evidence for a Higgs-like boson decaying to a W-boson pair [9]. The observed signal cross section times the branching fraction to WW for H mass $m_H = 125.6$ GeV is $0.72^{+0.20}_{-0.18}$ times the standard model expectation. More data are required to determine whether all properties are compatible with predictions from the SM, as they are till now.

1.3 Standard Model problems

To date there is no known discrepancy between the SM and the experiments. The discovered new boson is a particle compatible with the SM Higgs, confirming the symmetry-breaking mechanism. At moment there are no hints of non SM particles in LHC data. The great achievement of the Glashow-Weinberg-Salam model was the unification of the weak and electromagnetic interactions, but the couplings arise from different sources. SU(2) $\otimes$ U(1) gauge group is a product of two disconnected groups of gauge transformations and the coupling forces g and g' are not related by the theory. Their ratio has to be measured experimentally and it is the Weinberg angle. A more general unifying group G contains SU(2) $\otimes$ U(1), and the Clebsh-Gordan coefficients of G would predict the relationship between g and g'.

The SM is completed by the inclusion of the SU(3) color group of gauge transformations which describes the strong interactions. This group is disconnected from the electroweak groups so it is natural to attempt to unify the strong, the weak and the electromagentic interactions. The grand-unifying group must have at least four commuting generators corresponding to the third component and the hypercharge of weak isospin and the same quantities of the color group: it must have rank four at least. The simplest group satisfying the requirement is SU(5). In the SU(5) the predicted value of $\sin^2\theta_{Weinberg}$ is 0.205, somewhat lower than the measured value of (0.2325 $\pm$ 0.0008). Many attempts have been made to formulate Grand Unified Theories (GUTs), starting from the simplest model SU(5). In SU(5) it is necessary to accommodate each generation of fermions in two multiplets. In these multiplets quarks and leptons, and quarks and anti quarks appear on the same footing and therefore transitions between them can be in-

duced by the appropriate gauge bosons. As in SM, the color octet of gluons induces transitions between colored quarks, the W bosons couple to weak isospin doublets and the Z and photon to fermion−anti fermion pairs. The new ingredients in SU(5) are the massive gauge bosons X and Y whose existence leads to new and far reaching consequences. These gauge bosons will induce transitions in which baryon number B and/or lepton number L are no longer conserved. As a result, proton decay would no longer be forbidden. Neutrino-less double β decay of nuclei should occur and, provided neutrinos have non zero mass, ΔL different from zero transitions will give rise to neutrino oscillations in which transformations between different neutrino species occur. GUTs predict the existence of magnetic monopoles with masses comparable with the grand unification scale. In the SM neutrinos are assumed to be mass-less and exist in only one helicity state. However, there is no fundamental reason why this should be so. Moreover, the question of neutrino mass has important implications for cosmology. Various astronomical observations indicate that about 90% of the total gravitational mass of the universe consists of invisible or dark matter: a component of this dark matter could be massive neutrinos. Massive neutrinos also provide a solution to the solar neutrino problem, the discrepancy between solar neutrino flux expected from calculations based on the standard solar model and the experimentally observed flux of solar neutrinos. The experiments confirm that neutrinos oscillate, so neutrinos have mass.

The cosmological problem of the existing asymmetry in the universe between matter and antimatter can be understood in terms of a hot big bang model of the origin of the universe and its evolutions related to the grand-unification of interactions of particle physics. Some features of GUTs are unsatisfactory. The most unsatisfactory one is that gravity is not included in the unification schemes. SM of elementary particle physics depends on quantum mechanics in an essential way: the general relativity, although a gauge theory, does not include quantum effects, so it is difficult to insert gravity in a defined unified theory. Another problem is the large discrepancy between aspects of the weak force and gravity. There are no explanations, for example, why the weak force is 10^{32} times stronger than gravity or why the Higgs boson is so much lighter (125 GeV) than the Planck mass (or the grand unification energy, or a heavy neutrino mass scale) 10^{15} GeV. The expected large quantum contributions to the square of the Higgs boson mass would inevitably make the mass huge, comparable to the scale at which new physics appears, unless there is an incredible fine-tuning cancellation between the quadratic radiative corrections and the bare mass. This is the so-called hierarchy problem.

One proposed solution is related to the super symmetry. Super symmetry explains how a tiny Higgs mass can be protected from quantum corrections. It removes the power-law divergences of the radiative corrections to the Higgs mass and solves the hierarchy problem as long as the super symmetric particles are light enough (< 1 TeV). In super symmetry each point like particle is postulated to have a SUSY partner, called sparticle, with spin which differs from that of the particle by half a unit. Except the spin, sparticle and particle have the same quantum numbers. A new multiplicative quantum number, known as R parity, is assigned to the particles. R parity is not necessarily conserved, but it is imposed as a discrete symmetry with the consequence that sparticles are always produced in pairs.

Other models offer solutions to the hierarchy problem, such as extra dimensions. The described SM problems justify the existence of other theories, so experiments search direct or indirect evidence for physics BSM. Fields to be explored are related to neutrinos, gravity, dark matter in connection with astrophysics and cosmological measurements, Higgs mass respect the Plank scale of unification in the hierarchical problem.

1.4 Searches in high energy experimental physics Beyond Standard Model - SUSY

The search for SUSY is a central activity of the LHC physics program. In the framework of the Minimal Super symmetric extension of the Standard Model (MSSM) with R-parity conservation, SUSY particles are created in pairs. At the LHC, the most copiously produced SUSY particles are expected to be the strongly interacting partners of quarks, the squarks, and the partners of gluons, the gluinos. A comprehensive search program for the SUSY particles discovery has been underway at the LHC, since the beginning of the data-taking process. These searches aim for a broad range of possible final states, and the analysis are in general model independent, for example [10],[11]. Hadronic collisions yielding three or more electrons, muons, or taus (which define the multilepton signature) serve as an ideal final state to search for physics BSM, as such final states are relatively rare in the SM but can be produced at high rates in new physics scenarios involving electroweak processes with SUSY partner particles of gauge bosons and leptons. Several exclusive final states are defined by lepton flavor content, hadronic energy, missing transverse energy and the presence or absence of b-tagged jets. Events with several same-sign, isolated leptons from SM processes in proton-proton collisions are extremely rare. Searches for anomalous production of same-sign dileptons can therefore be very sensitive to new physics contributions. The same argument can be applied to other theories like universal extra dimensions, pair production of fermion partners of the top, heavy Majorana neutrinos and same-sign top-pair production. Other signatures without missing transverse energy are sensitive to SUSY models with R-parity violation (RPV) that imply an unstable lightest super symmetric particle (LSP). SUSY processes have cross sections of the order of fb, as reported in Figure 1.1. A summary of mass limits obtained in SUSY searches by the CMS experiments is presented in Figure 1.2.

1.5 Searches in high energy experimental physics Beyond Standard Model - EXOTICA

Searches BSM are extended to more general exotic signatures. They are typically conceived in the framework of extra dimensions or super symmetric scenarios. Searches for signatures from different models are grouped by final states. The exotic searches program is wide, as the map in Figure 1.3 shows.

A non complete list of searches is:

- search for Z', extra dimensions, Z_{KK} with dilepton, dijet, diphoton final states;
- search for graviton exchange, and contact interactions with dilepton, and dijet continuum modification;
- search for heavy neutrino from right-handed W and leptoquark with dileptons and dijets;
- search for direct graviton emission and gravitino with single photon and missing transverse energy;
- search for W' with single lepton and missing transverse energy;
- search for technicolor or leptoquark with multileptons and multijets;
- search for top partners or seesaw mechanism particles with same-sign dileptons;
- search for microscopic black holes in large extra dimensions scenarios with high multiplicity and high sphericity events.

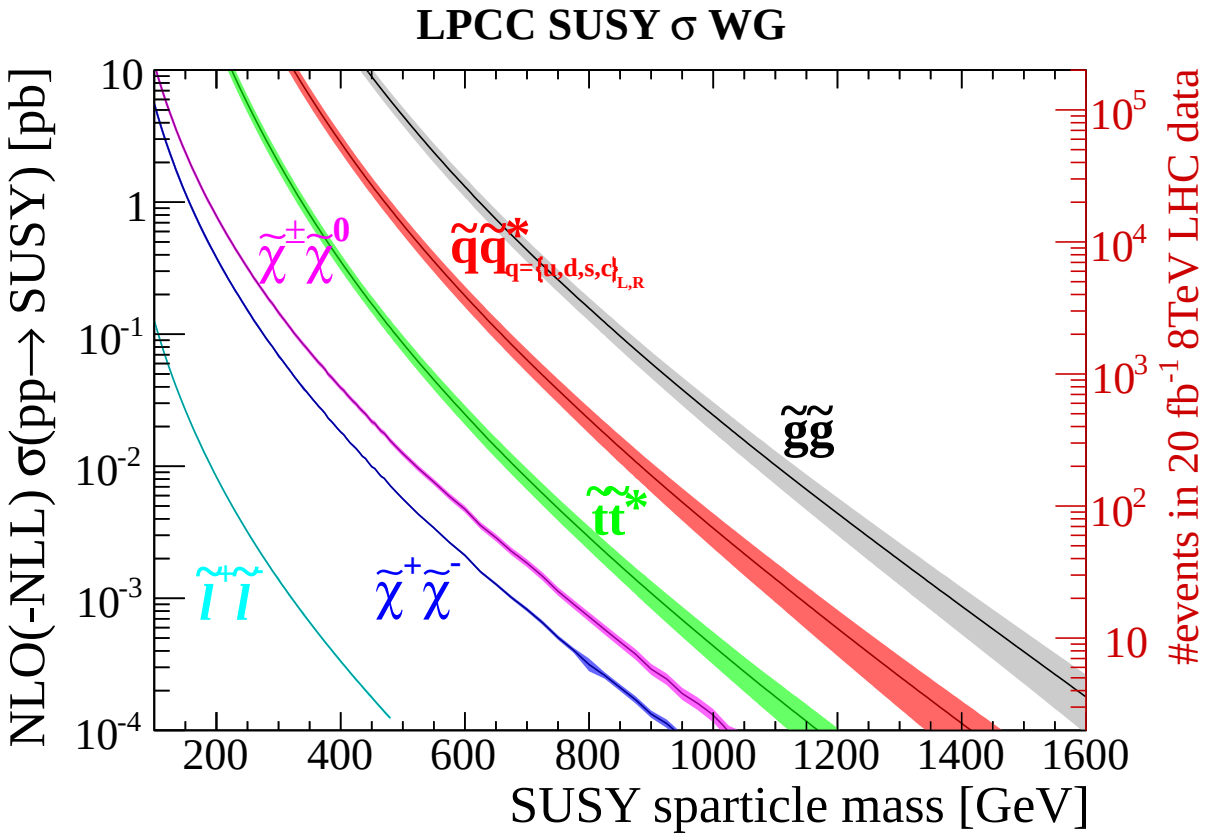

Figure 1.1: Theoretical cross section for selected SUSY pair production processes.

In addition, there are several data analysis which look for the existence of a fourth generation of quarks (B2G). Finally, a number of searches are developed for signatures that involve heavy long lived charged particles and other particles in non minimal SUSY models.

Seesaw models, postulating the existence of heavy neutrino partners, as discussed in the next chapter, are considered in the EXOTICA context.

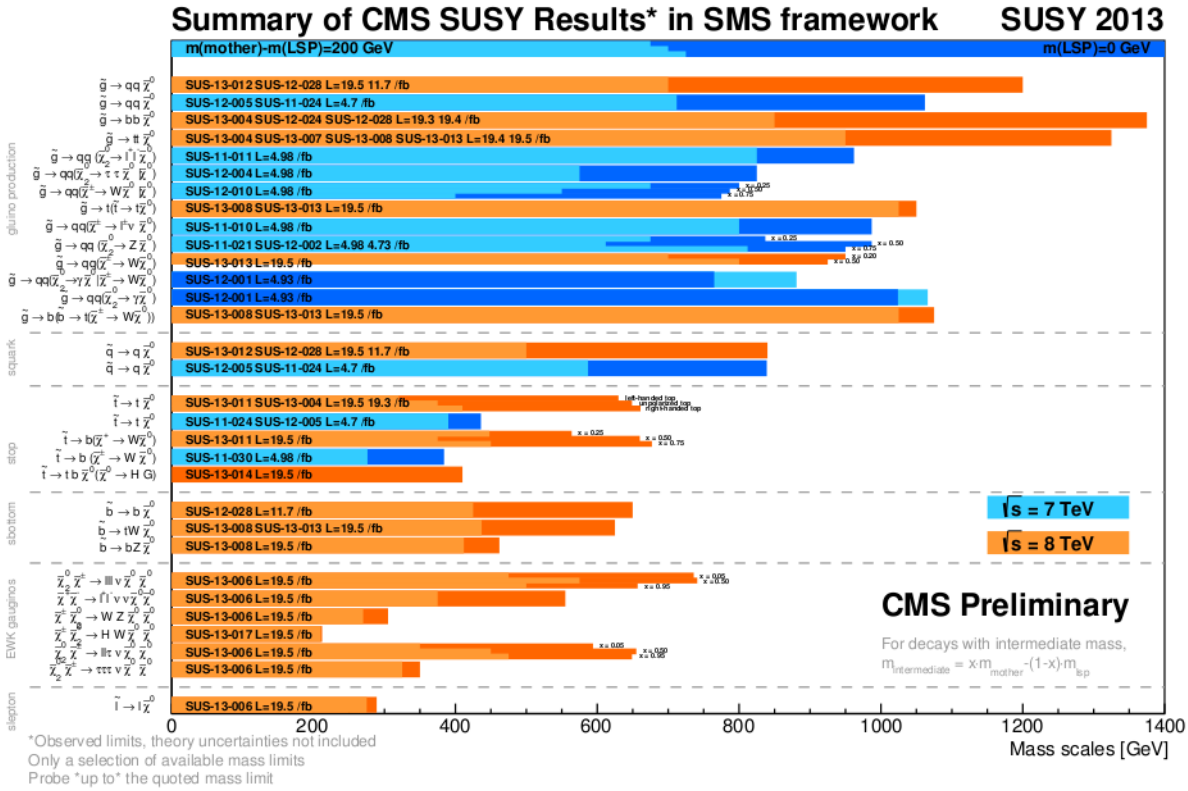

Figure 1.2: Recap map of limits found in SUSY searches at CMS. The x axis is the energy scale in GeV. Best exclusion limits for the masses of the "mother" particles, for m(LSP) = 0 GeV (dark shades) and m(mother) - m(LSP) = 200 GeV (light shades); for each topology, for all results. In this plot, the lowest mass range is m(mother)=0, but results are available starting from a certain mass depending on the analysis and topologies. Branching ratios of one are assumed, values shown in plot are to be interpreted as upper bounds on the mass limits. The theory uncertainties are not included.

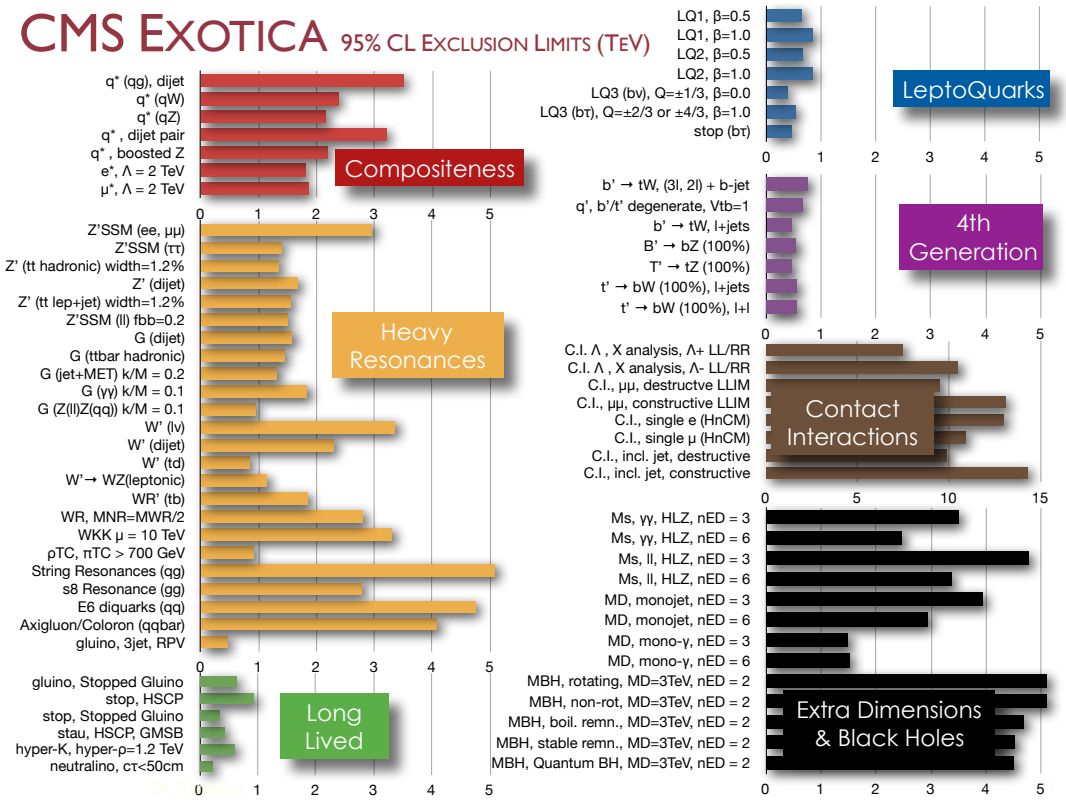

Figure 1.3: Recap map of limits found in exotica searches at CMS. The x axis is the energy scale in TeV.

Chapter 2

Neutrino physics and Seesaw mechanism

2.1 Theoretical introduction

The existence of neutrino particle was first postulated in 1930 by Wolfgang Pauli to preserve the conservation of energy, momentum and angular momentum in β decay described by neutron (n) decay reaction in proton (p) and electron: $n \rightarrow p + e^- + \nu_e$. Neutrino is a fermion, an elementary particle with spin $1/2$, with no electric and color charge. Neutrinos are leptons and interact through weak force and gravity. They are of three types or generations, corresponding to electron, muon and tau. Starting in the late 1960s, several experiments found that the number of electron neutrinos arriving from the sun was between one third and one half the number predicted by the Standard Solar Model (SSM), a discrepancy which became known as the solar neutrino problem and remained unsolved for some thirty years. The idea of neutrino flavor oscillations was first suggested by Bruno Pontecorvo in 1957 to solve the issue, and it was further developed in 1967. According to this theory neutrinos are able to oscillate between the three available flavors while they propagate through space. Pontecorvo's equation gives the probability that a neutrino with energy E of flavor μ oscillate in flavor τ traveling for distance L

$$P_{\mu\tau} = sin^2(2\theta)sin^2(1.27\Delta m^2 LE^{-1}) \tag{2.1}$$

The observation of neutrino flavor oscillations indicates that neutrinos have mass, the factor Δm in the Equation 2.1 being the mass difference between neutrino generations, which is not present in the SM. Neutrino masses could be introduced in the SM with a most conservative hypothesis, i.e.: simply adding Dirac right-handed neutrino, with Yukawa couplings. However, a possibility is described by the seesaw mechanism, as next sections will explain in details.

2.2 Experimental evidence of neutrinos masses

The observation of the supernova SN1987A from February 23rd 1987, the only source of neutrinos from supernova explosion observed till today, establishes that neutrinos have masses sum not above 6 eV [12]. The idea that neutrinos has mass was born when they were predicted. Fermi in 1933 studied a specific region of nuclear process in which neutrinos are emitted: there neutrinos bring minimal kinetic energy, so neutrinos mass effect is amplified. Following the Fermi search line, nuclear processes set limit on neutrinos masses at 2 eV. Fermi called particle neutrino as similar to other particle name neutron. The presence of neutrino explains the continuous spectrum in β decay reactions. In 1956 Cowan and Reines discovered neutrinos in an experiment at the nuclear fission reactor in Savannah River [13, 14]: free neutrinos induce reactions. More stringent limits comes from cosmological studies: the sum of the three known neutrinos masses is below 0.6 eV [15–17]. Observations of neutrinos and anti neutrinos produced in the sun, the atmosphere, reactors, and from particle beams provide overwhelming

evidence that the flavors of neutrinos change (oscillate). The vast majority of experimental results on neutrino flavor oscillations converge towards a simple three-neutrino (3ν) framework, where the flavor states $\nu_{alpha} = (\nu_e, \nu_\mu, \nu_\tau)$ mix with the massive states $\nu_i = (\nu_1, \nu_2, \nu_3)$ via three mixing angles $(\theta_{12}, \theta_{13}, \theta_{23})$ and a possible CP-violating phase δ. The observed oscillation frequencies are governed by two independent differences between the squared masses m_i^2 , which can be defined as $(\delta m)^2 = m_2^2 - m_1^2 > 0$ and $(\Delta m)^2 = m_3^2 - (m_1^2 + m_2^2)/2$, where $(\Delta m)^2 > 0$ and < 0 correspond to normal hierarchy (NH) and inverted hierarchy (IH), respectively. At present five oscillation parameters are known, each one with an accuracy largely dominated by a specific class of experiments, namely: θ_{12} by solar data, θ_{13} by short-baseline (SBL) reactor data, θ_{23} by atmospheric data, mainly from Super-Kamiokande (SK), $(\delta m)^2$ by long-baseline reactor data from KamLAND (KL), and $(\Delta m)^2$ by long-baseline (LBL) accelerator data, mainly from MINOS and T2K. However, the available data are not yet able to determine the mass hierarchy, to discriminate the θ_{23} octant, or to discover CP-violating effects. A worldwide research program is underway to address such open questions and the related experimental and theoretical issues. Global neutrino data analysis, as in Reference [18], are useful to get the most restrictive bounds on the known parameters, via the synergy combination of results from different classes of oscillation searches. At the same time, such analysis provide some guidance about the unknown oscillation parameters, a successful example being represented by the hints of $sin^2(\theta_{13}) \sim 0.02$, which were discussed before the discovery of $\theta_{13} > 0$ at reactors. Including new relevant data which have become available mainly in 2013 and which turn out to have an interesting impact on the global fit results, the actual status has the recent SBL reactor data from Daya Bay [19] and RENO [20], which reduce significantly the range of θ_{13}, the latest published appearance and disappearance event spectra in the LBL accelerator experiments T2K [21][22] and MINOS [23][24], which not only constrain the known parameters $((\Delta m)^2, \theta_{23}, \theta_{13})$ but, in combination with other data, provide some guidance on the θ_{23} octant and on leptonic CP violation. In the light of recent (circa 2013) new results coming from reactor and accelerator experiments, and of their interplay with solar and atmospheric data, the knowledge about 3 ν parameters improves: a significant reduction of the θ_{13} uncertainties, and some changes in the preferred ranges of $((\Delta m)^2, \theta_{23})$ are obtained. Despite of the improvements, neutrinos physics has many open questions to be investigate with different experimental apparatus.

2.3 Seesaw mechanism and models

Explaining the origin of neutrino mass is one of the open issues in particle physics. An appealing possibility to include the neutrino masses and accounting for their smallness is the Seesaw mechanism. The neutrinos masses are small, six or more orders of magnitude smaller than the mass of the electron. In order to account for neutrino masses, the SM should be extended: the discovery of neutrino oscillation can be considered as the first unambiguous evidence for physics BSM. However, which is the correct extension of the SM is not clear at all. In principle one could simply add a right-handed component for the neutrinos and give them a Dirac mass, as for the other fermions. But this would require extraordinary small Yukawa couplings and also the assumption of lepton number conservation, to prevent the right-handed neutrinos to acquire a (heavy) Majorana mass. The most natural explanation appears then to be the one offered by the so-called seesaw models: new heavy particles coupling both to the lepton and the Higgs doublets generate a small Majorana mass for the neutrinos, with the Yukawa couplings suppressed with respect to the massive neutrinos couplings by a factor v/M, where v is the Higgs vacuum expectation and M the mass of the heavy particle. For M large enough (order of 10^{14} GeV), small neutrino masses are generated even for order $\mathcal{O}(\infty)$ Yukawa couplings. On the other hand, if M is smaller, either smaller Yukawa couplings or an alternative suppres-

sion mechanism are required. At tree level, there are three ways of producing the Weinberg operator, which corresponds to neutrinos mass, by exchange of heavy:

- fermion singlet (1C , 1W , Y = 0), called Type I [25],[26],[27];
- scalar weak triplet (1C , 3W , Y = 2), called Type II [28],[29],[30];
- fermion weak triplet (1C , 3W , Y = 0), called Type III [31],[32],[33].

Neutrino masses, in type I and type III, are given by:

$$m_\nu = Y^T \, M^{-1} \, Y \, \frac{v^2}{2} \tag{2.2}$$

where Y is the Yukawa couplings matrix, M is the mass of the heavy partner of the neutrinos and v the Higgs vacuum expectation. Considering mediator masses between 100 and 200 GeV, it is clear that the neutrino masses cannot be small for the v =M suppression. The two possibilities are:

- small Yukawa couplings, leading to small mixing angles between the mediators and the SM fermions; values 10^{-6} is "natural" in case of Majorana neutrinos, in contrast to the 10^{-12} required for a Dirac mass;
- large Yukawa couplings and another suppression scale is in the neutrino formula. This is the case of inverse seesaw [34], where neutrino masses are directly proportional to a small lepton number violating scale.

In the analysis search, the first case is the one considered in seesaw type III context.

2.3.1 Seesaw with heavy fermion singlet mediator (type I)

Seesaw type I is implemented by adding three right-handed current eigenstates $N'_{i,R}$ with i =1,2,3, transforming as singlets under the SM gauge group. The Yukawa interaction for neutrinos is similar to the one for charged leptons. The interaction generates a mass term upon spontaneous symmetry breaking. Since $N'_{i,R}$ are SM singlets, gauge symmetry allows a Majorana mass term. Then, the relevant interaction terms for heavy neutrino mass eigenstates are obtained by diagonalizing the mass matrix and rewriting the interaction in the mass eigenstate basis. Before LHC, direct searches for heavy Majorana neutrinos have been reported by the L3 [35] and DELPHI [36] collaborations at the Large Electron-Positron Collider. Searches are for Z to μ_lN decays and set limits on $|V_{lN}|^2$ as a function of m_N for heavy Majorana-neutrino masses up to approximately 90 GeV. The ATLAS Collaboration at the LHC has also reported limits on heavy Majorana neutrino production in the context of an effective Lagrangian approach and the Left-Right Symmetric Model [37, 38]. Indirect limits on $|V_{lN}|^2$ have been obtained from the non-observation of neutrino less double beta decay, resulting in 90 % confidence level (CL) limits of $|V_{eN}|^2 < 7 * 10^{-5} TeV^{-1}$. Precision electroweak measurements have been used to constrain the mixing parameters resulting in indirect 90 % CL limits of $|V_{eN}|^2 < 0.0066$, $|V_{\mu N}|^2 < 0.0060$, and $|V_{\tau N}|^2 < 0.016$. CMS search [39] follows a model-independent phenomenological approach, with m_N and V_{lN} as free parameters, where V_{lN} is a mixing parameter describing the mixing between the heavy Majorana neutrino and the SM neutrino ν_l of flavor l. CMS reports results using a set of data of integrated luminosity 5.0 fb^{-1} at 7 TeV. The heavy Majorana neutrino can decay to a lepton with positive or negative charge, leading to events containing two leptons with the same or opposite sign. Same-sign events have much lower backgrounds from SM processes and therefore provide an accessible signature of heavy Majorana neutrino production. Signature is event with two isolated leptons of same sign and flavor ($\mu^\pm\mu^\pm$ or $e^\pm e^\pm$) and at least two accompanying jets. Contributions from SM processes to such dilepton final states are very small and the background is dominated by processes such as multijet

production, in which leptons from b-quark decays or from jets are misidentified as isolated prompt leptons. After applying all the final selections the observation is 65 events in data in the muon channel and expect a total SM background of 70 $\pm$ 4 (stat.) $\pm$ 22 (syst.) events, with the dominant contribution of 63 $\pm$ 4 (stat.) $\pm$ 22 (syst.) events arising from the misidentified muon background. Thus, data are in agreement with the estimated background. In the electron channel the observation is 201 events in data, and estimate the total SM background as 219 $\pm$ 6 (stat.) $\pm$ 62 (syst.) events, with the dominant contribution of 177 $\pm$ 5 (stat.) $\pm$ 62 (syst.) events arising from the misidentified electron background. Again, data are in agreement with the estimated background. A 95 % CL exclusion limits on the square of the heavy Majorana-neutrino mixing parameter as a function of m_N, using the CLs method based on the event yields is set. The DELPHI and L3 limits were derived from Z decay to $\nu_l N$ and are thus restricted to masses below approximately 90 GeV. The CMS limits extend well beyond this mass. For $m_N = 90$ GeV values are $|V_{\mu N}|^2 < 0.07$ and $|V_{eN}|^2 < 0.22$. At $m_N = 210$ GeV value is $|V_{\mu N}|^2 < 0.43$, while for $|V_{eN}|^2$ the limit reaches 1.0 at a mass of 203 GeV.

2.3.2 Seesaw with heavy scalar weak triplet mediators (type II)

The observation of a doubly-charged scalar particle could establish the type II seesaw mechanism as the most promising framework for generating neutrino masses. The minimal type II seesaw model is realized with an additional scalar field that is a triplet under $SU(2)_L$ and carries $U(1)_Y$ hypercharge Y = 2. The triplet contains a doubly-charged component Δ^{++} or Δ^{--}, a singly-charged component Δ^{+} or Δ^{-} and a neutral component Δ^0. The Δ^{++} particle carries double electric charge, and decays to same-sign lepton pairs $l^+_\alpha l^+_\beta$ with flavor indices α and β, where α can be equal to or different from β.The Δ^{++} Yukawa coupling matrix Y_Δ is proportional to the light neutrino mass matrix. The search strategy is to look for an excess of events in one or more flavor combinations of same-sign lepton pairs coming from the decays $\Delta^{++} \rightarrow l^+_\alpha l^+_\beta$. Final states containing three or four charged leptons are considered in the CMS search with 2011 data sample [40]. The first limits on the Δ^{++} mass were derived based on the measurements done at PEP and PETRA experiments [41]. Next, the Δ^{++} was searched for at the MARK II detector at SLAC [42], the H1 detector at HERA [43] and the LEP experiments [44],[45],[46]. The more recent results are from the Tevatron [47] and ATLAS [48] experiments, which set lower limits on the Δ^{++} mass between 112 and 355 GeV, depending on assumptions regarding Δ^{++} branching fractions, considering only the pair-production mechanism, and only a small fraction of the possible final state combinations. CMS latest search added associated production and all possible final states and significantly improved the sensitivity. Lower bounds on the Δ^{++} mass are established between 204 and 459 GeV in the 100% branching fraction scenarios, and between 383 and 408 GeV for four benchmark points of the type II seesaw model.

2.4 Seesaw with heavy fermion weak triplet mediators (type III)

In the type III seesaw model the SM is extended with the addition of fermionic weak triplets Σ_i, with zero hypercharge. Then, the total Lagrangian is given by

$$L = L_{SM} + L_K + L_Y + L_M$$

with the following terms:

- L_K referred to the interactions triplets - vector bosons;
- L_Y referred to the interactions Higgs - triplets - leptons;

- L_M referred to the Majorana mass, including interactions Left-Right forbidden in $SU(2)_L$.

The Lagrangian terms are briefly discussed below.

The interactions triplets - vector bosons come from the Lagrangian kinetic term

$$L_K = i\bar{\vec{\Sigma}}_j \cdot \gamma^\mu D_\mu \vec{\Sigma}_j \tag{2.3}$$

with sum over j = 1,2,3 is implicit. The co-variant derivative is

$$D_\mu = \partial_\mu + ig\vec{T} \cdot \vec{W}_\mu \tag{2.4}$$

Using Cartesian components and four components notation, the triplet Yukawa interaction with lepton doublets is described by

$$L_Y = -Y_{ij}\bar{L}'_{iL}(\vec{\Sigma}_j \cdot \vec{\tau})\Phi + h.c. \tag{2.5}$$

with Y a 3X3 matrix, if 3 triplets are introduced. The triplet Majorana mass term is

$$L_M = -\frac{1}{2}M_{ij}(\bar{\vec{\Sigma}}^c_i \cdot \vec{\Sigma}_j) + h.c. \tag{2.6}$$

with M a 3X3 symmetric matrix, if 3 triplets are introduced. All the triplet members Σ_j^1,Σ_j^2,Σ_j^3 have the same mass term. The charge eigenstates are related to the Cartesian components according to Formula 2.7.

$$\Sigma_j^+ = \frac{1}{\sqrt{2}}(\Sigma_j^1 - i\Sigma_j^2), \Sigma_j^0 = \Sigma_j^3, \Sigma_j^- = \frac{1}{\sqrt{2}}(\Sigma_j^1 + i\Sigma_j^2) \tag{2.7}$$

The physical particles are charged Dirac fermions E'_j and neutral Majorana fermions N'_j, where symbol ' indicates the weak interaction eigenstates.

$$E'_{jL} = \Sigma_j^{+c}, E'_{jR} = \Sigma_j^{-c}, N'_{jL} = \Sigma_j^{0c}, N'_{jR} = \Sigma_j^0, \tag{2.8}$$

After spontaneous symmetry breaking the terms in Equations 2.5 and 2.6 lead to the neutrino mass matrix

$$L_{\nu,mass} = -\frac{1}{2}(\bar{\nu}'_L \bar{N}'_L) \begin{pmatrix} 0 & \frac{v}{\sqrt{2}}Y \\ \frac{v}{\sqrt{2}}Y^T & M \end{pmatrix} \begin{pmatrix} \nu'_R \\ N'_R \end{pmatrix} + h.c.$$

The mass matrix for charged leptons, including Yukawa inverse matrix Y^{-1}, is

$$L_{l,mass} = -(\bar{l}'_L \bar{E}'_L) \begin{pmatrix} \frac{v}{\sqrt{2}}Y^l & vY \\ 0 & M \end{pmatrix} \begin{pmatrix} l'_R \\ E'_R \end{pmatrix} + h.c.$$

The term with B_μ is absent because triplets have zero hypercharge. The gauge interactions in the weak eigenstate basis can be derived. Limits on the mixing of fermionic triplets arise from electroweak precision data [49].

The seesaw type III discovery potential at a center of mass energy of $\sqrt{s} = 14$ TeV is discussed in theoretician community [32]. In 2012, a complete evaluation of the signal expected and model

framework at $\sqrt{s} = 7$ TeV are developed [50]. The complete Lagrangian includes SM and SU(2) heavy fermion triplets (Σ) with Y=0. The model requires at least two triplets in order to obtain two non vanishing neutrino masses. The search involves only the lightest triplet, which is the easiest to be discovered. Following the assumption of one triplet, the Yukawa couplings matrix reduces to a one row, three columns matrix, and the mass matrix is a scalar. The Yukawa couplings phases and the PMNS matrix phases do not play role in the discovery process, so they are neglected. The assumption of real parameters allows to write all the couplings in term of the mixing parameters, $V\alpha$, defined by the Formula 2.9, where α labels the couplings to each of the e, μ and τ leptons generation:

$$V_\alpha = \frac{v}{\sqrt{2}} M_\Sigma^{-1} Y_\Sigma \tag{2.9}$$

In particular, given the electric charge of the lepton triplet components, $\Sigma^+, \Sigma^0, \Sigma^-$ the most promising signal for finding a state at $M_v \sim 100$ GeV is through quark-annihilation $qq' \rightarrow \Sigma^0\Sigma^\pm$, followed by decays $\Sigma^0 \rightarrow W^\pm l^\mp$ and $\Sigma^\pm \rightarrow W^\pm \nu$. The total width of the supposed heavy leptons and their decay branching ratios to SM leptons depend on the mixing matrix element V_α. Constraints on the mixing parameters and their products list, coming from electroweak precision data [49], is

- $|V_e| < 0.055$;
- $|V_\mu| < 0.063$;
- $|V_\tau| < 0.063$;
- $|V_e V_\mu| < 0.00000017$;
- $|V_e V_\tau| < 0.00042$;
- $|V_\mu V_\tau| < 0.00049$.

The predicted pair production cross section for the Σ states does not depend on V_α and the production of a lepton α is proportional to the ratios of matrix elements:

$$b_\alpha = \frac{|V_\alpha|^2}{|V_\mathrm{e}|^2 + |V_\mu|^2 + |V_\tau|^2}. \tag{2.10}$$

CMS type III seesaw search at 7 TeV [51] uses three different sets of values V_α, according to the constraints (V_α=0.00041). Very small angles ($V_\alpha \sim 10^{-12}$) imply seesaw mediators with a longer life time and displaced decay vertices in the event. The mixing values $V_\alpha = 10^{-6}$ do not produce visible displaced vertices (see Table 2.1).

The event topology, chosen in the analysis and described in Feyman's diagrams shown in Figure 2.1, includes charged leptons in final state. At LHC, the supposed heavy fermions come from a virtual W boson decay. Then, Σ^0 decays into $W^\pm l^\mp$ and $\Sigma^\pm$ decays into $W^\pm\nu$ or $Zl^\pm$. If Z boson decays hadronically or invisibly, final state has exactly three charged leptons.

Another possible production process is $q\bar{q} \rightarrow Z^*$ or $\gamma^* \rightarrow \Sigma^+\Sigma^-$. Following the decay chain, the final state in this case has at least four leptons. The Σ^0 via virtual Z boson or photon is not produced because it has third isopin component and hypercharge null.

Figure 2.2 shows cross sections for Σ^+ and Σ^- as a function of the common triplet mass. The values for the positive charge are about two times larger than those for the negative charge, with a strong dependence on the mass. Figure 2.3 shows the branching fractions (BR) for $\Sigma^\pm$ and Σ^0; the decay widths are reported in Table 2.1. Decay chain hosts W, Z and H bosons. The

Table 2.1: Decay width and mean value of the decay length for different triplet masses.

Mass	Total decay width (MeV)	Decay length (μm)
140	$1.2\ 10^{-9}$	380
180	$3.6\ 10^{-9}$	104
200	$5.4\ 10^{-9}$	65
220	$7.6\ 10^{-9}$	43
240	$10.4\ 10^{-9}$	29
260	$15.5\ 10^{-9}$	22
280	$17.5\ 10^{-9}$	16
300	$22.0\ 10^{-9}$	12
320	$27.2\ 10^{-9}$	9
340	$33.1\ 10^{-9}$	7

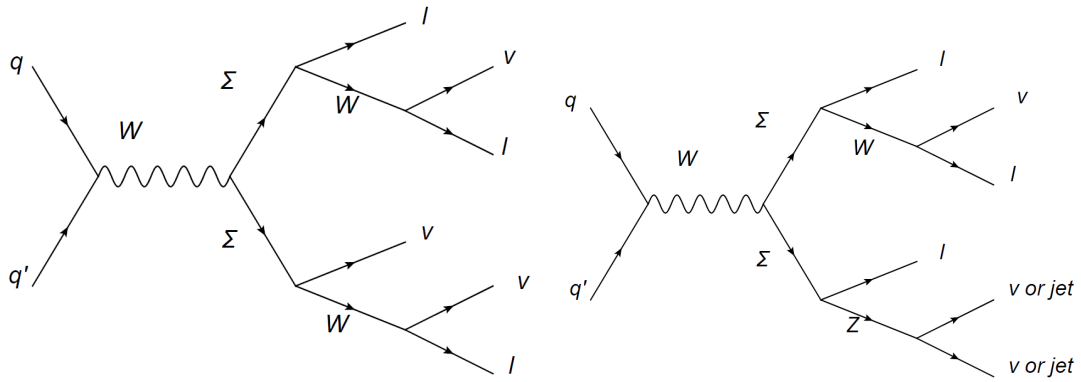

Figure 2.1: Feynman diagrams with the production and the decay of the charged and neutral heavy fermions. The Σ^0 decays into $W^{\pm}l^{\mp}$. The $\Sigma^{\pm}$ decays into $W^{\pm}\nu$ or $Zl^{\pm}$.

BR involving H boson is the smallest one and it is neglected in the search. The production cross sections are listed in Table 2.2.

Table 2.2: Cross section (pb) for $\Sigma^-\Sigma^0$ and $\Sigma^+\Sigma^0$ production.

Sign	140	180	200	220	240	260	280	300	320	340
-	0.0628	0.0190	0.0115	0.0073	0.0048	0.0033	0.0023	0.0016	0.0012	0.0009
+	0.1229	0.0401	0.0252	0.0166	0.0113	0.0079	0.0057	0.0042	0.0031	0.0024

Three mixing parameters V_α are relevant to define the seesaw type III model. CMS search at 8 TeV uses the "natural" values: $V_e = V_\tau = V_\mu = 10^{-6} = V_\alpha$, called flavor democratic scenario (see Section 2.3). Results can be interpreted in other similar seesaw type III models, as in the Reference [51]. A more useful re interpretation is under investigation, according to theoreticians [52]. A general limit in 2D plane [V_{eN};$V_{\mu N}$] gives more information than interpretation in many defined V_α scenarios; it shows exclusion regions in flavor mixing space for values of M_Σ.

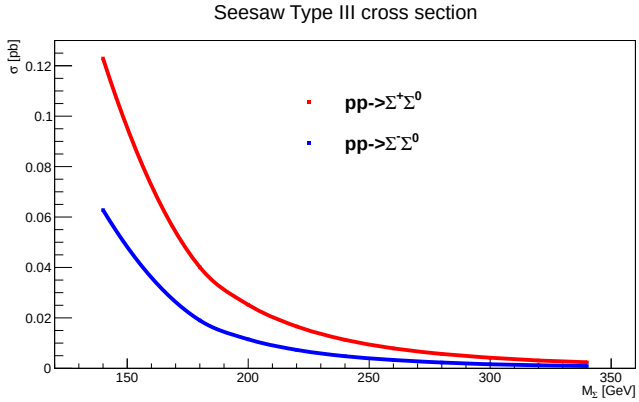

Figure 2.2: Cross sections for the $\Sigma^+\Sigma^0$ and $\Sigma^-\Sigma^0$ production for pp interaction at $\sqrt{s} = 8\ TeV$ as a function of the triplet mass.

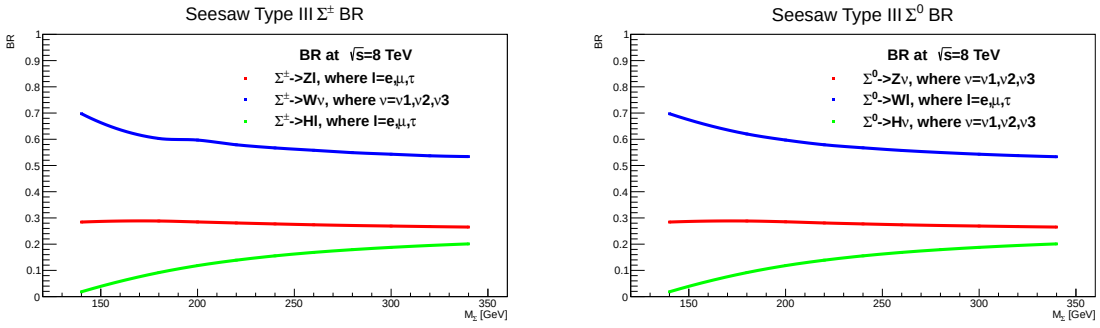

Figure 2.3: Branching fractions for $\Sigma^\pm$ and Σ^0 decays as a function of the triplet mass.

Chapter 3

Signal and background Simulation

3.1 Introduction

High Energy Physics (HEP) analysis results depend on accurate comparisons between theoretical expectations (backgrounds and eventually signal) and the experimental output coming from the detector. Theoretical expectations are computed with computer simulations, based on models. The simulation uses Monte Carlo (MC) techniques to perform simulated experiments using random number generators for evaluating the integrals involved in the calculation. This search uses MC simulations common to other CMS analysis for the SM backgrounds and a dedicated MC simulation for the signal. The minimal seesaw type III model, described in Section 2.4, is implemented and tested.

3.2 Physics of particle collisions

At LHC, two protons beams collide. The structure of the colliding protons is modeled using parton distribution functions (PDFs). PDF define the probability density to find a parton (quark or gluon) with a given longitudinal momentum fraction x at a fixed value of momentum transfer Q^2 of the collisions. PDFs cannot be calculated perturbatively; they are determined by fits to data from processes such as deep inelastic scattering (DIS) and lepton pair production, called Drell-Yan production (DY). PDFs have experimental uncertainties which lead to systematic uncertainty on the cross section measurements of the investigated processes. The collision occurs between partons inside each proton ("hard process"). Lagrangian matrix elements corresponding to the parton interactions describe the various particles production processes and decay. The square of matrix elements gives the probability density for the process. The computer program used in event generation and implemented with the detector simulation includes a tree level or leading order (LO) generators, generally dependent o n the kinematic properties of the event. Higher order effects such as next to leading order (NLO) or next to next leading order (NNLO) are introduced with a multiplicative factor, called k factor, obtained using higher order analytic calculations. The interaction produces also parton showers, hadronizing into collections of hadrons. The primary collision includes QCD radiation from the incoming (Initial State Radiation ISR) and outgoing (Final State Radiation FSR) partons. ISR and FSR depend on Q^2 and, less, on the processes simulation details. The parton kinetic energy is transferred to the color field, where it produces additional partons from the vacuum. Then, partons in the showers hadronize and build neutral color combinations, called jets. The hadronization step is not well described in theory: it is modeled phenomenologically with the Lund string model [53]. The remaining partons from the protons represent the so called underlying events. They are typically soft and semi-phenomenological or perturbation models describe them. In a single bunch crossing is possible to have interactions between several proton pairs. The ef-

fect is called PileUp (PU). The number of proton interactions is estimated with the number of the reconstructed primary vertices (PV). PU is simulated in the generated events by superimposing minimum bias events (QCD events with low transverse energy), on the events in the nominal samples, according to the number of primary vertices distribution observed in 2012 data. Figure 3.1 shows the PU distribution for 2012 data.

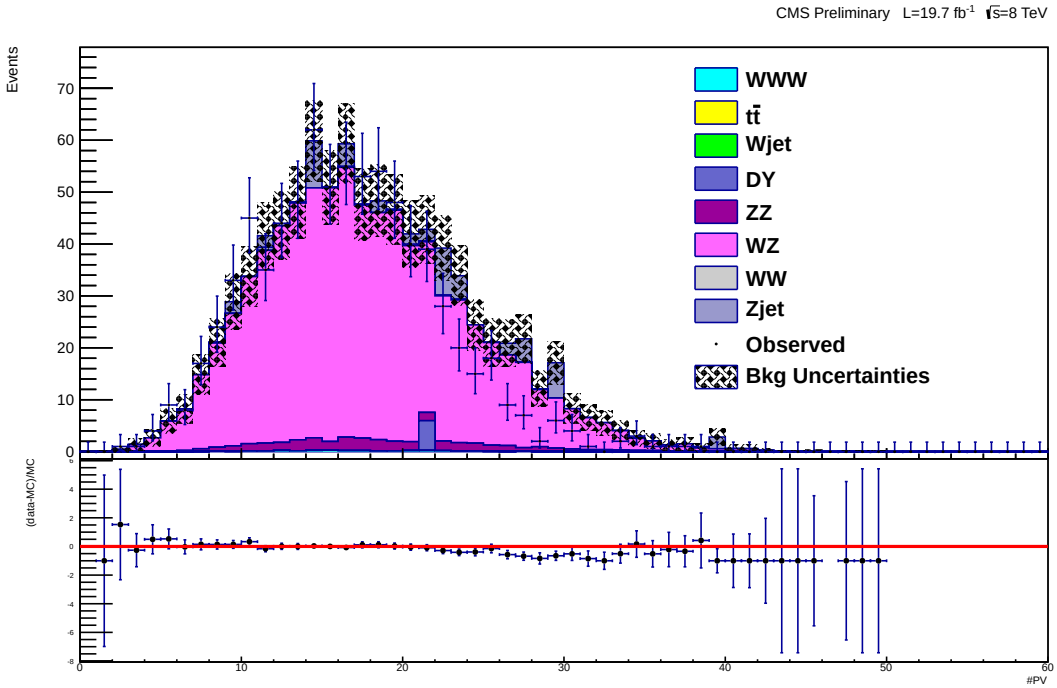

Figure 3.1: Number of Primary Vertex (PV) distribution after analysis selections, described in Chapter 5.

3.3 Event simulation chain

MC event generation proceeds in steps: implementation of the matrix element calculation for the hard scattering, parton shower generation, underlying event and hadronization process simulation. Different programs are typically used to perform each step of the simulation chain. The list of the software used, with the corresponding reference, is:

- Feynman rules and couplings calculations, models building: FeynRules [54];
- Matrix Element (ME) calculations, hard process and decays: MADGRAPH 5 (MG) [55];
- Parton showering, hadronization, underlying events: Pythia6 [56];
- CMS detector simulation, digitization and reconstruction: CMSSW Full Simulation [57].

FeynRules is a Mathematica package that allows the calculation of Feynman Rules in momentum space for any QFT physics model. Input parameters are related to the new model description (model file with extension fr). The information is used to calculate the set of Feynman rules associated with the Lagrangian. The Feynman rules calculated by the code are input for MC LO generators. A set of dedicated interfaces are in place.

MADGRAPH requires three type of cards in text format: parameter cards coming out from Universal FeynRules Output (UFO) models [58], process cards, and run card. The cards used in the seesaw type III search are described in details in the Appendix B. Parameter cards are divided in blocks needed to describe CKM matrix, particles mass, mixing scenarios, SM constants, Yukawa couplings, particles decays including SM bosons, quantum number of the new states. Process cards invoke particles definition, UFO model and processes chains. Finally, a run card includes information about the energy, the number of events, the collisions and the final states objects.

PYTHIA is a program for the generation and hadronization of high-energy physics events, i.e. for the description of collisions at high energies between elementary particles. It contains theory and models for a number of physics aspects, including hard and soft interactions, parton distributions, initial-and final-state parton showers, multiple interactions, fragmentation and decay. PYTHIA is completely integrated with CMSSW software and it is one of the official parton tools used by the CMS collaboration. Details about the hadronization fragment are in Appendix C.

CMSSW software is the official framework used in the CMS collaboration. All detector related codes and packages are implemented in CMSSW, from trigger to simulation. Physics events generation includes simulation (SIM), digitization (DIGI) and reconstruction (RECO). The CMS detector Full Simulation is based on GEANT4 [59], a toolkit used to model the interactions of particles in the detector and the detector electronics response. The algorithm incorporates information on the materials budget between the interaction point and the detectors, the magnetic fields and the geometry features. Generated particles pass through the toolkit. Then, the detector response to the simulated particles is determined in the digitization phase. Physics objects are reconstructed for the analysis (reconstruction step), after the emulation of the triggering process. The best calibration and alignment conditions are considered in this stage.

3.4 Seesaw signal models and generation

UFO models [58] are build from Feyman Rules using the Mathematica program [60]. Ten models are build corresponding to the ten triplet mass values in the range from 140 to 340 GeV. The following approximations are applied to reduce the process time and to simplify the models:

- the Cabibbo angle in the CKM matrix is set to zero;
- the light quarks and all leptons mass are set to zero;
- the Higgs boson is coupled only with the top quark;
- the Higgs mass is set to 125.3 GeV;
- the masses of the three heavy partners of the neutrinos are not split;
- the Yukawa couplings with light quark (including charm) and all leptons (including tau) are set to zero.

The process under investigation is the production of pairs of these supposed massive particles, via virtual boson W^* in the s channel. Production processes via real W' or virtual Z or real Z' have different theoretical frameworks and they are not included. The search considers final states where three charged leptons with transverse momentum p_T above defined thresholds are present and the sum of their electric charge is ± 1. Final states host also neutrinos and jets. The processes implemented in MADGRAPH are the following:

$p\,p \to \Sigma^+\,\Sigma^0$, $(\Sigma^+ \to W^+\,\nu, W^+ \to l^+\,\nu)$, $(\Sigma^0 \to W^+\,l^-, W^+ \to l^+\,\nu)$
$p\,p \to \Sigma^+\,\Sigma^0$, $(\Sigma^+ \to W^+\,\nu, W^+ \to l^+\,\nu)$, $(\Sigma^0 \to W^-\,l^+, W^- \to l^-\,\nu)$
$p\,p \to \Sigma^+\,\Sigma^0$, $(\Sigma^+ \to Z\,l^+, Z \to \nu\,\nu)$, $(\Sigma^0 \to W^+\,l^-, W^+ \to l^+\,\nu)$
$p\,p \to \Sigma^+\,\Sigma^0$, $(\Sigma^+ \to Z\,l^+, Z \to \nu\,\nu)$, $(\Sigma^0 \to W^-\,l^+, W^- \to l^-\,\nu)$
$p\,p \to \Sigma^+\,\Sigma^0$, $(\Sigma^+ \to Z\,l^+, Z \to \text{jet jet})$, $(\Sigma^0 \to W^+\,l^-, W^+ \to l^+\,\nu)$
$p\,p \to \Sigma^+\,\Sigma^0$, $(\Sigma^+ \to Z\,l^+, Z \to \text{jet jet})$, $(\Sigma^0 \to W^-\,l^+, W^- \to l^-\,\nu)$

$p\,p \to \Sigma^-\,\Sigma^0$, $(\Sigma^- \to W^-\,\nu, W^- \to l^-\,\nu)$, $(\Sigma^0 \to W^+\,l^-, W^+ \to l^+\,\nu)$
$p\,p \to \Sigma^-\,\Sigma^0$, $(\Sigma^- \to W^-\,\nu, W^- \to l^-\,\nu)$, $(\Sigma^0 \to W^-\,l^+, W^- \to l^-\,\nu)$
$p\,p \to \Sigma^-\,\Sigma^0$, $(\Sigma^- \to Z\,l^-, Z \to \nu\,\nu)$, $(\Sigma^0 \to W^+\,l^-, W^+ \to l^+\,\nu)$
$p\,p \to \Sigma^-\,\Sigma^0$, $(\Sigma^- \to Z\,l^-, Z \to \nu\,\nu)$, $(\Sigma^0 \to W^-\,l^+, W^- \to l^-\,\nu)$
$p\,p \to \Sigma^-\,\Sigma^0$, $(\Sigma^- \to Z\,l^-, Z \to \text{jet jet})$, $(\Sigma^0 \to W^+\,l^-, W^+ \to l^+\,\nu)$
$p\,p \to \Sigma^-\,\Sigma^0$, $(\Sigma^- \to Z\,l^-, Z \to \text{jet jet})$, $(\Sigma^0 \to W^-\,l^+, W^- \to l^-\,\nu)$

Two charged leptons arise from the neutral Σ^0 decay chain, the third charged lepton comes from the charged $\Sigma^\pm$ decay chain. The processes where Z boson decays leptonically have different final states, with four or five or six charged leptons. They have smaller cross sections than final states with three leptons. A study was performed in case of sign + and mass point 140 GeV to inquire the eventual contribution from different final states. Case with four charged leptons has a cross section of 8.6 fb; for comparison, case with three charged leptons has a cross section of 122.9 fb. All cross sections are at LO, computed with MADGRAPH. The potential excluded additional contribution is $\approx 7\%$. The cases with five or six charged leptons in final states have smaller cross sections than four leptons case. Final state with two leptons have a very large backgrounds. Natural value $V_\alpha = 10^{-6}$ and flavor democratic scenario are chosen (see Section 2.4). Tables 3.1 and 3.2 summarize the branching ratio for $\Sigma^\pm$, Σ^0 values coming from MADGRAPH in the analysis.

Table 3.1: Branching ratios for $\Sigma^\pm$.

BR Decay	140	180	200	220	240	260	280	300	320	340
$\Sigma^\pm \to \nu_1 W^\pm$	0.2325	0.2010	0.1990	0.1930	0.1890	0.1860	0.1830	0.1810	0.1790	0.1780
$\Sigma^\pm \to \nu_2 W^\pm$	0.2325	0.2010	0.1990	0.1930	0.1890	0.1860	0.1830	0.1810	0.1790	0.1780
$\Sigma^\pm \to \nu_3 W^\pm$	0.2325	0.2010	0.1990	0.1930	0.1890	0.1860	0.1830	0.1810	0.1790	0.1780
$\Sigma^\pm \to e^\pm Z$	0.0948	0.0961	0.0949	0.0936	0.0924	0.0913	0.0904	0.0897	0.0890	0.0884
$\Sigma^\pm \to \mu^\pm Z$	0.0948	0.0961	0.0949	0.0936	0.0924	0.0913	0.0904	0.0897	0.0890	0.0884
$\Sigma^\pm \to \tau^\pm Z$	0.0948	0.0961	0.0949	0.0936	0.0924	0.0913	0.0904	0.0897	0.0890	0.0884
$\Sigma^\pm \to e^\pm h$	0.0061	0.0305	0.0394	0.0463	0.0518	0.0562	0.0597	0.0626	0.0650	0.0670
$\Sigma^\pm \to \mu^\pm h$	0.0061	0.0305	0.0394	0.0463	0.0518	0.0562	0.0597	0.0626	0.0650	0.0670
$\Sigma^\pm \to \tau^\pm h$	0.0061	0.0305	0.0394	0.0463	0.0518	0.0562	0.0597	0.0626	0.0650	0.0670

To conclude, search is performed in three charged leptons channel as a reasonable compromise between signal cross sections and backgrounds; signal is generated with the twelve processes listed above, at ten different mass values.

3.5 Signal samples validation

Before proceeding to the full simulation chain, some checks are needed at the signal generation level, to validate the main characteristics of the processed samples. To this end, a special format

Table 3.2: Branching ratios for Σ^0.

BR Decay	140	180	200	220	240	260	280	300	320	340
$\Sigma^0 \to \nu_1 Z$	0.0948	0.0961	0.0949	0.0936	0.0924	0.0913	0.0904	0.0897	0.0890	0.0884
$\Sigma^0 \to \nu_2 Z$	0.0948	0.0961	0.0949	0.0936	0.0924	0.0913	0.0904	0.0897	0.0890	0.0884
$\Sigma^0 \to \nu_3 Z$	0.0948	0.0961	0.0949	0.0936	0.0924	0.0913	0.0904	0.0897	0.0890	0.0884
$\Sigma^0 \to e^+ W^-$	0.1162	0.1034	0.0995	0.0965	0.0946	0.0929	0.0916	0.0905	0.0896	0.0889
$\Sigma^0 \to \mu^+ W^-$	0.1162	0.1034	0.0995	0.0965	0.0946	0.0929	0.0916	0.0905	0.0896	0.0889
$\Sigma^0 \to \tau^+ W^-$	0.1162	0.1034	0.0995	0.0965	0.0946	0.0929	0.0916	0.0905	0.0896	0.0889
$\Sigma^0 \to e^- W^+$	0.1162	0.1034	0.0995	0.0965	0.0946	0.0929	0.0916	0.0905	0.0896	0.0889
$\Sigma^0 \to \mu^- W^+$	0.1162	0.1034	0.0995	0.0965	0.0946	0.0929	0.0916	0.0905	0.0896	0.0889
$\Sigma^0 \to \tau^- W^+$	0.1162	0.1034	0.0995	0.0965	0.0946	0.0929	0.0916	0.0905	0.0896	0.0889
$\Sigma^0 \to e^\pm h$	0.0061	0.0305	0.0394	0.0463	0.0518	0.0562	0.0597	0.0626	0.0650	0.0670
$\Sigma^0 \to \mu^\pm h$	0.0061	0.0305	0.0394	0.0463	0.0518	0.0562	0.0597	0.0626	0.0650	0.0670
$\Sigma^0 \to \tau^\pm h$	0.0061	0.0305	0.0394	0.0463	0.0518	0.0562	0.0597	0.0626	0.0650	0.0670

for event description, called Les Houches Events (LHE) file format, has been developed in agreement with theoreticians to properly define matrix element input (PDF evaluation, phase space boundaries, processes amplitudes, masses and widths of new particles and their spin correlations) in a common language. The checks are performed at this LHE interface level.

As an example, Figure 3.2 shows the Σ particle mass distributions.

Figure 3.3 shows the lepton multiplicity distributions; similar number of events with three electrons and with three muons are shown, as expected. Events with three leptons are the most frequent, so the final state is favorite. Values are similar for all mass values, so only one marker per bin is shown. The p_T mean values in the distributions are used in calculation of the decay distance means, reported in Table 2.1.

Figures 3.4 and 3.5 show lepton transverse momentum p_T distributions coming from Σ and W boson, respectively.

Figures 3.6 and 3.7 show distributions of missing transverse energy E_T^{miss} (see Section 5.2.6), hadron activity H_T (see Section 5.2.9), and first jet in p_T Combined Secondary Vertex (CSV) algorithm b tag value (see Section 5.2.4). Each line is related with a Σ mass value.

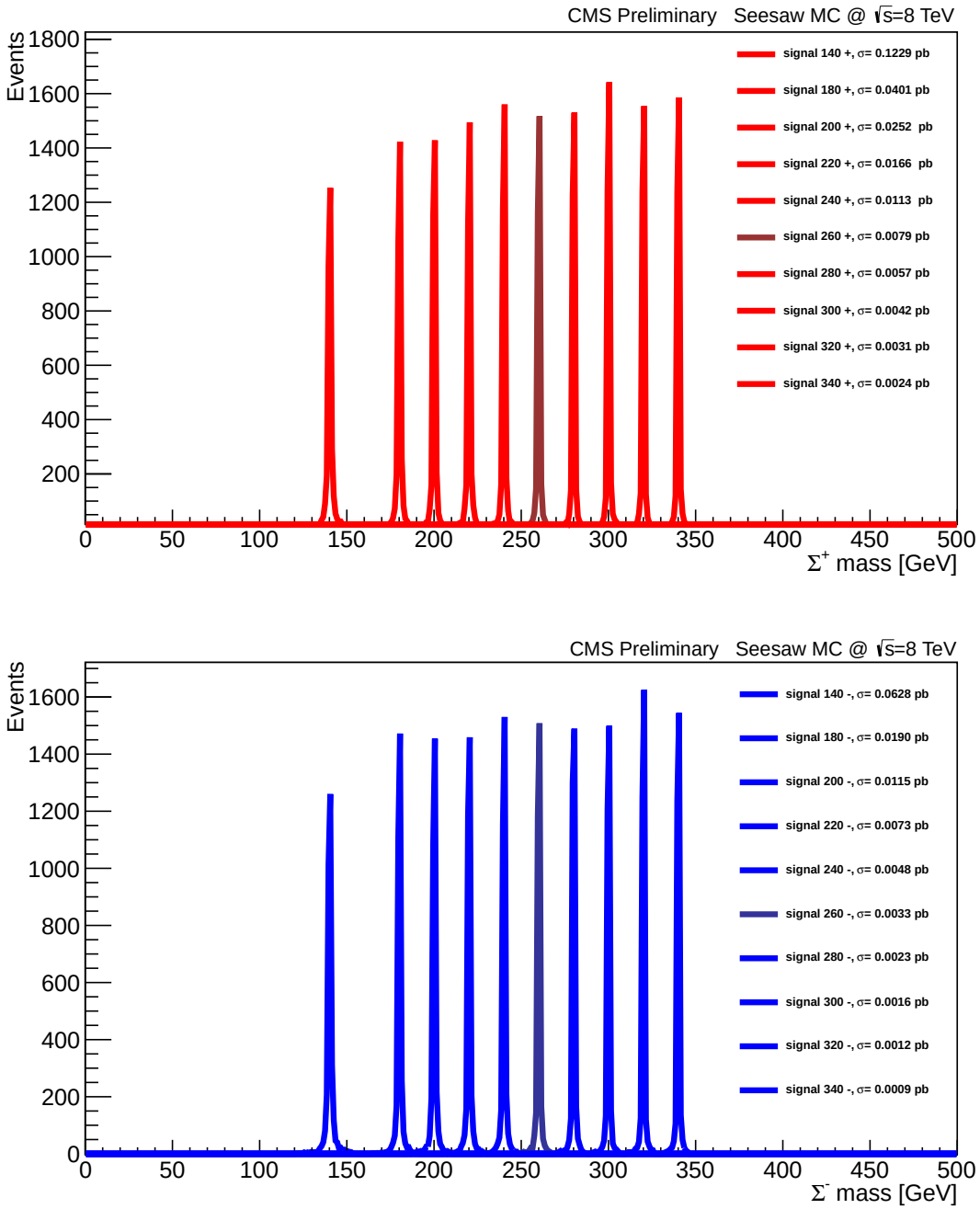

Figure 3.2: Σ^+ and Σ^- particle mass, at generated values.

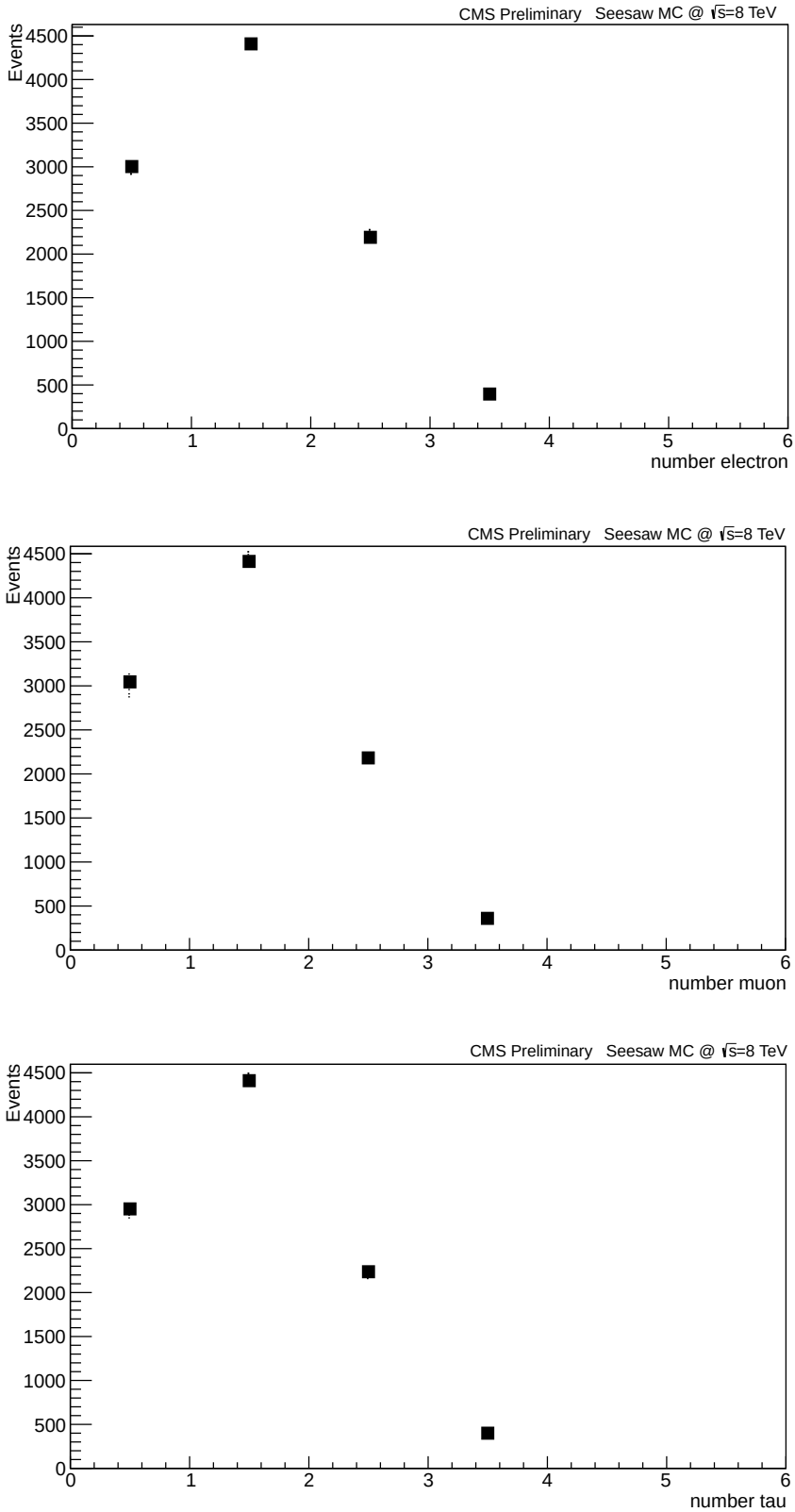

Figure 3.3: Lepton multiplicity distributions (flavors e, μ, τ).Values are similar for all mass values, so only one marker per bin is shown. As example, case + is shown.

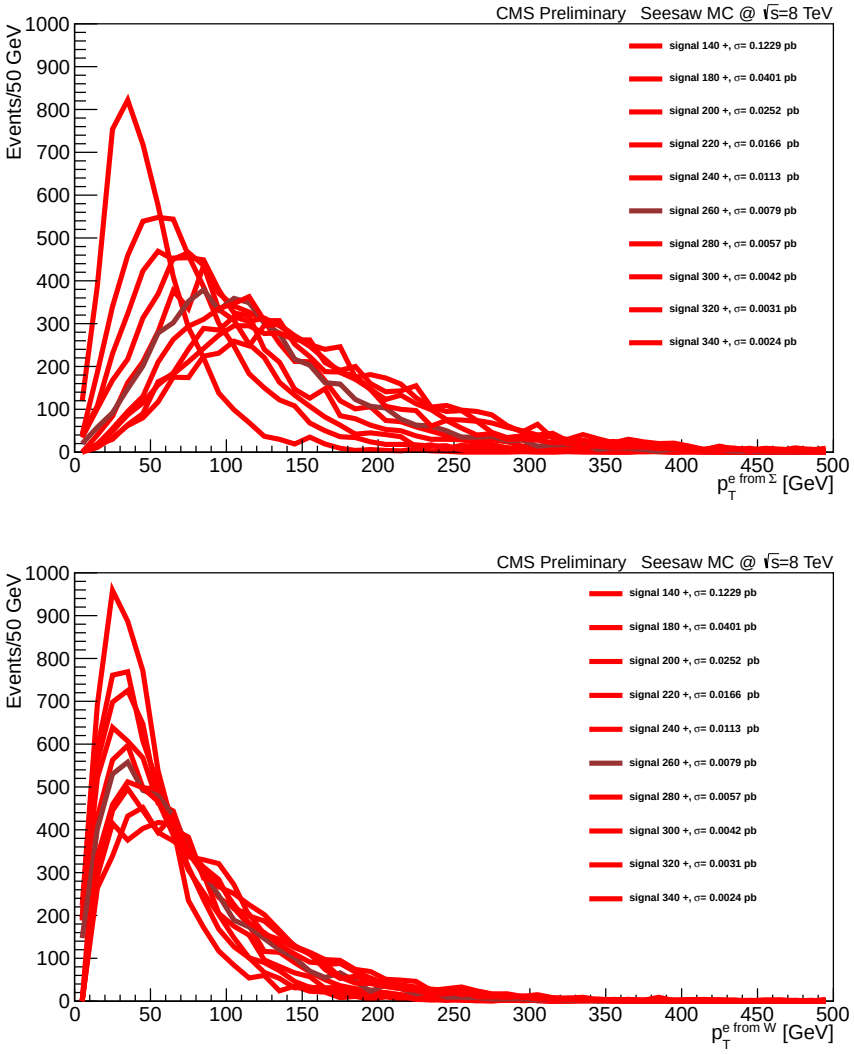

Figure 3.4: Electron from Σ and W p_T distributions. Sign + signal of ten mass points are shown.

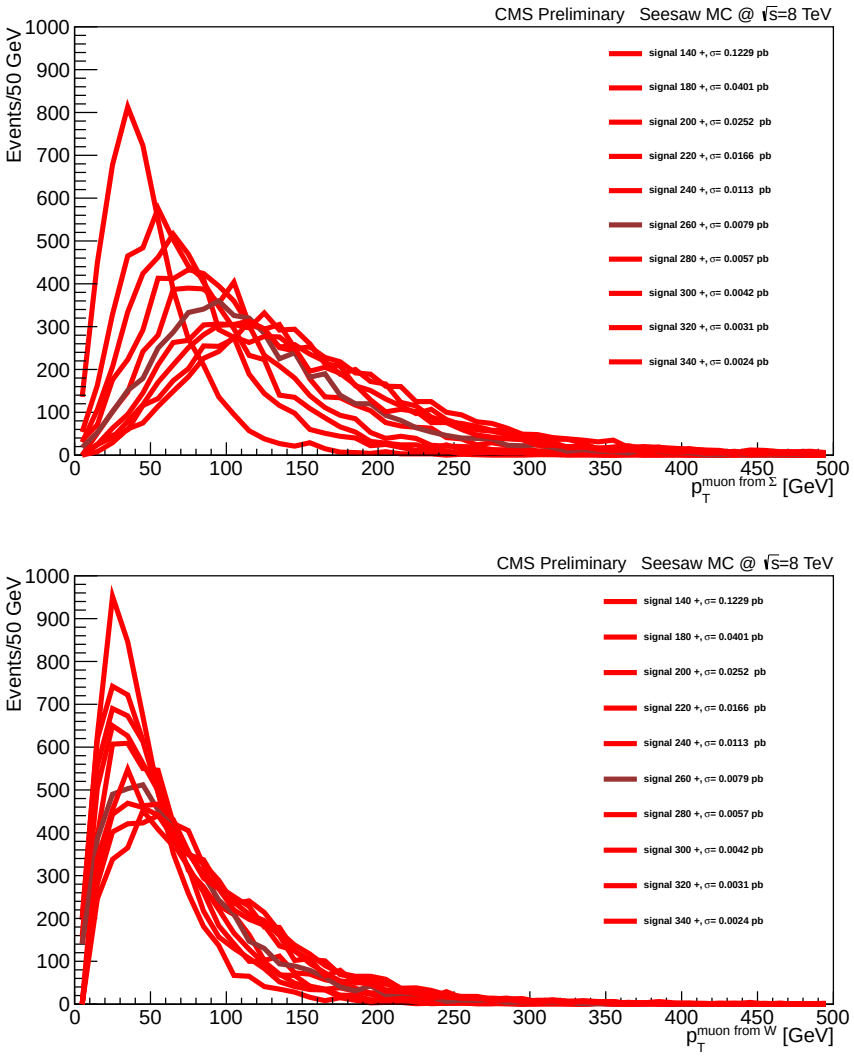

Figure 3.5: Muon from Σ and W p_T distributions. Sign + signal of ten mass points are shown.

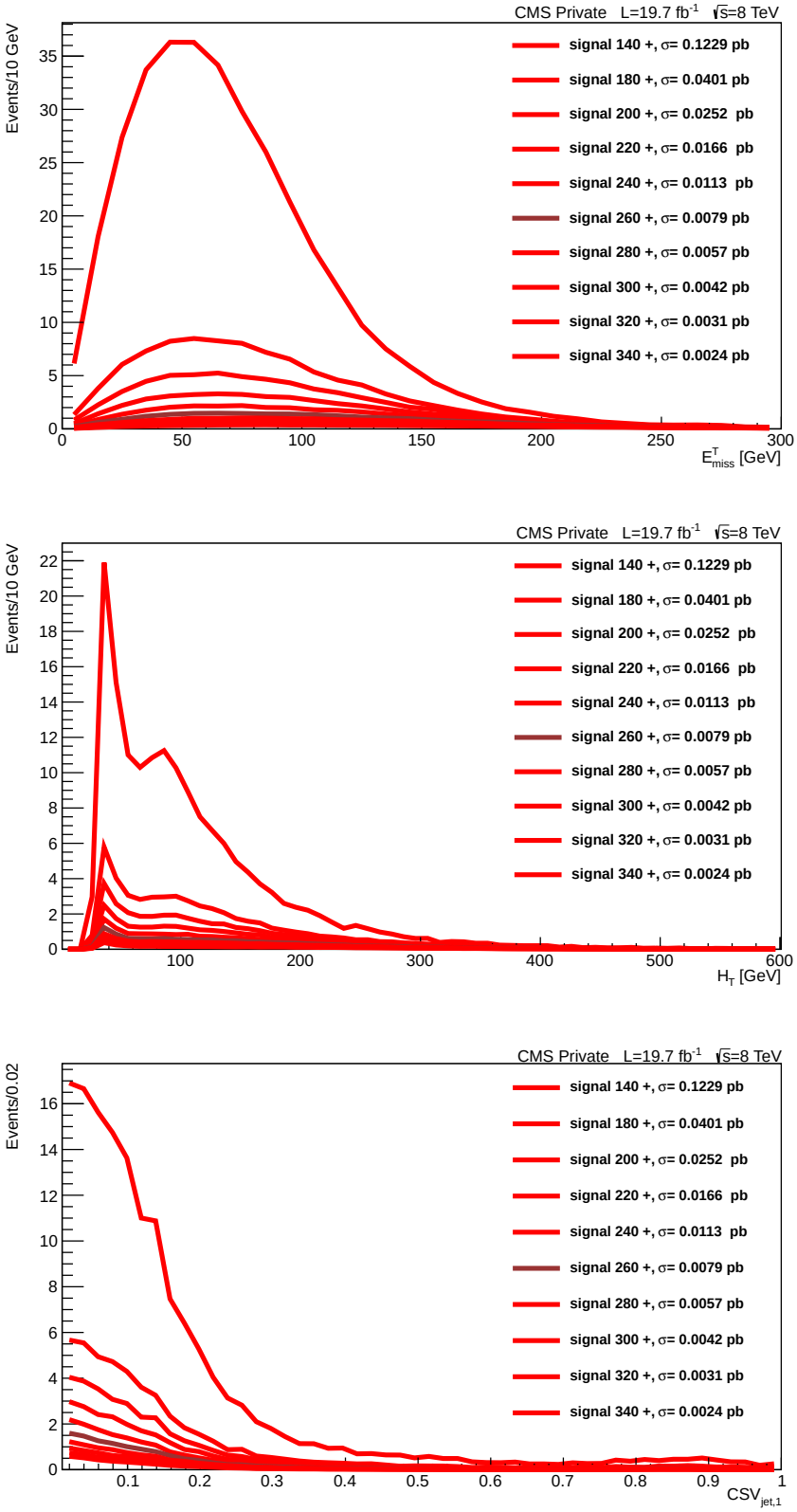

Figure 3.6: E_T^{miss}, H_T and Combined Secondary Vertex b tag for first jet in p_T distributions after request three charged leptons. Sign + signal of ten mass points are shown.

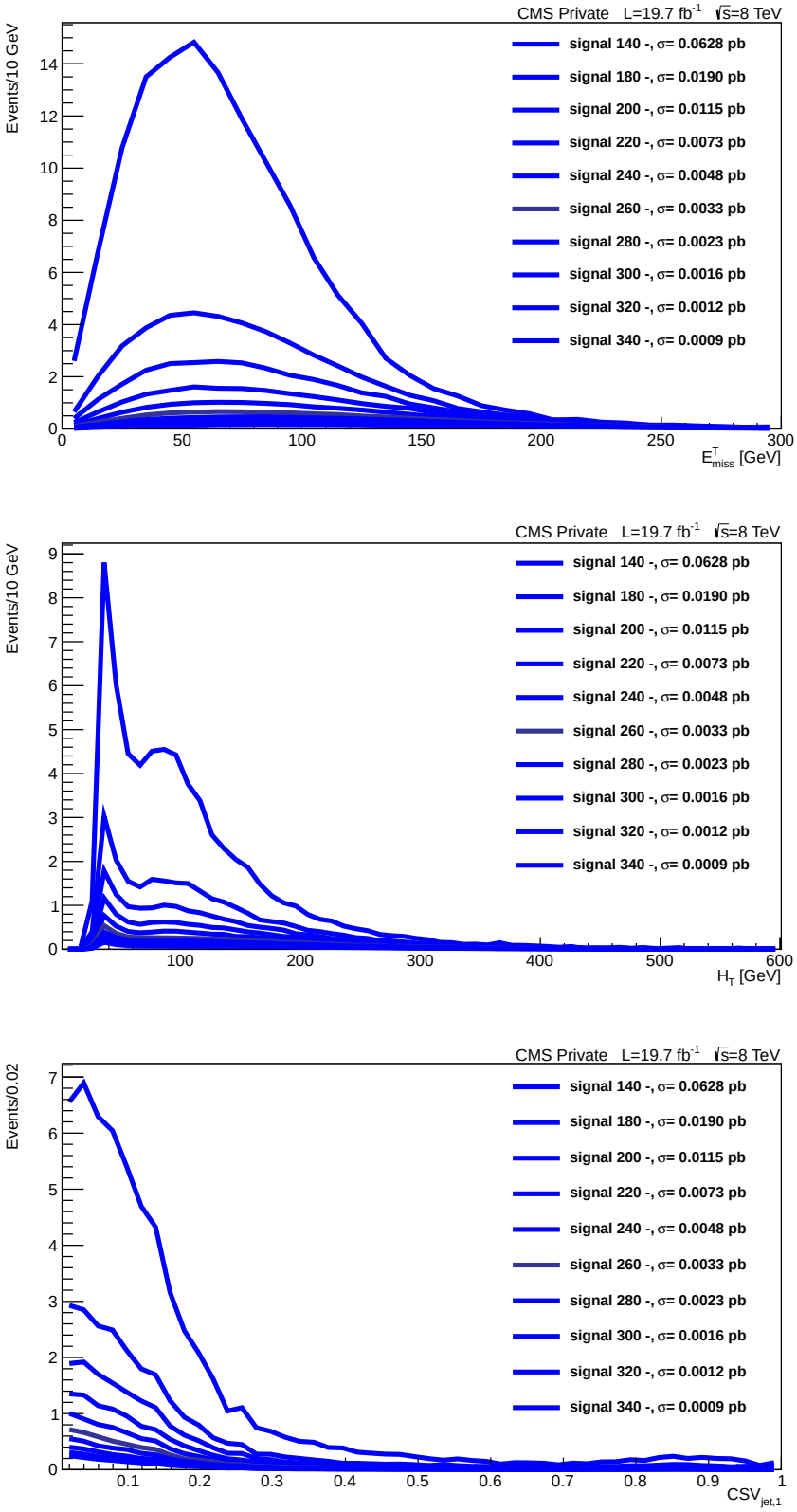

Figure 3.7: E_T^{miss}, H_T and Combined Secondary Vertex b tag for first jet in p_T distributions after request three charged leptons. Sign - signal of ten mass points are shown.

Chapter 4

LHC and CMS apparatus

4.1 LHC

The Large Hadron Collider (LHC) is located at the European Laboratory for Particle Physics CERN, near Geneva. Its structure crosses the border between Switzerland and France, going from Jura mountains in France to Leman lake in Switzerland. The circumference ring is 27 km long and it lies between 45 and 170 m below the surface. The tunnel is the same of the former Large Electron Positron (LEP) machine and it was build from 1983 to 1989. LHC first studies were performed still in 1982, before UA1 experiment's discovery of charged and neutral massive vector boson W, Z. In 1994 CERN council approved the LHC machine and in 1996 final decision to start the construction was taken. In 2000 LEP ended operation and in 2005 LHC hardware commissioning was in place. LHC commissioning with beams was performed in 2008 and 2009. Run I data taking with proton-proton, lead ion - lead ion, proton - lead ion beams covered the period from 2010 to February 2013.

Around the ring there are eight collision points: the experiments are located at four of them. The role of collisions points is listed below:

- Point 1, near CERN Meyrin (SUI): A Toroidal LHC ApparatuS experiment (ATLAS);
- Point 2: A Large Ion Collider Experiment (ALICE);
- Point 3, near Jura mountains: Momentum beam cleaning (machine service);
- Point 4: RadioFrequency (RF) and beam instrumentation (machine service);
- Point 5, near Cessy village (FRA): Compact Muon Solenoid experiment (CMS);
- Point 6: Beam dumping system (machine service);
- Point 7: Betatron beam cleaning (machine service);
- Point 8, near the border line: LHC-b experiment.

Beams injections points are near Point 1 and Point 8, in two opposite directions.

The following accelerators are part of the LHC injectors chain, sketched in Figure 4.1:

- Duoplasmatron proton source 90 keV, with a beam current of 500 mA;
- RadioFrequencyQuadrupole up to 750 keV;
- LINAC2 linear Alvarez accelerator which accelerates the proton up to 50 MeV, 180 mA (and 4.2 MeV/nucleon for lead beams);
- Proton Synchrotron (PS) Booster circular accelerator which accelerates the proton up to 1.4 GeV;

- Proton Synchrotron (PS), build in 1959, with a circumference of 628 m, which accelerates the proton up to 25 GeV and provides up to 5.9 GeV/nucleon for lead beams;
- Super Proton Synchrotron (SPS), build in 1981, with a circumference of 6.9 km, which accelerates the proton up to 450 GeV and provides up to 177 GeV/nucleon for lead beams.

Finally, LHC brings the beams energy up to 4 TeV for proton and 2.6 TeV/nucleon for lead in 2012. Table 4.1 summarizes the main LHC parameters.

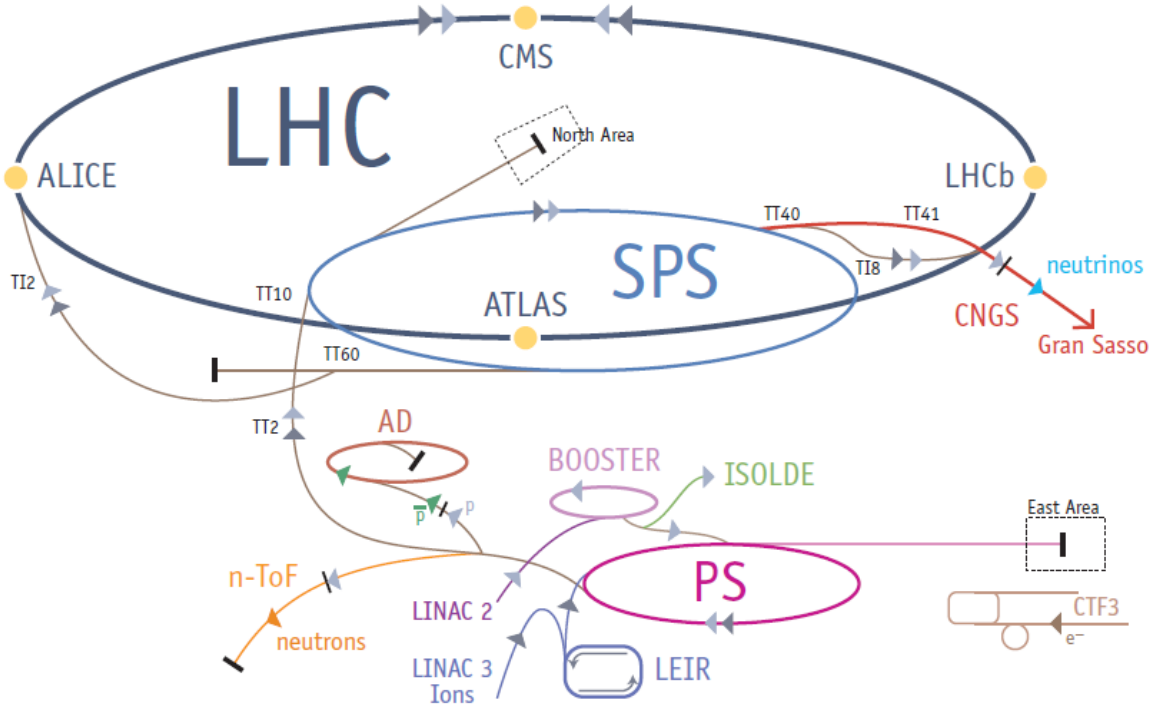

Figure 4.1: LHC injectors chain

4.2 LHC performance at 8 TeV pp collisions in 2012

The CERN machines operated from March 2012 to February 2013 without issues. Around seven months were dedicated to proton proton collisions at 8 TeV and two months in proton-ion mode. The pp collisions period was extended to reach the goal of delivered luminosity (~ 20 fb^{-1}). The LHC machine had some technical stops devoted to maintenance and few weeks in machine developments status related to test with different bunch spacing (move from 50 ns to 25 ns), beam energy, bunch schemes. The machine development studies are important for next Run II period. During technical stops, access to the experimental cavern and LHC tunnel was possible: experiments profit in repairing and replacing dead or not working electronic channels, where it was possible. LHC, as Figure 4.2 shows, delivered more than 24 fb^{-1} in pp collisions at 8 TeV. Table in Figure 4.3 summarizes some relevant features and records of LHC machine in 2012. Figure 4.4 shows the LHC working conditions during a stable beams period.

Experiments did not collect all the delivered luminosity: the detectors dead time and some unforeseen events caused looses. The integrated luminosity collected by CMS is about 20 fb^{-1}, as reported in Figure 4.5. The collected sub-section of a run during which the instantaneous luminosity is unchanging, is called "luminosity section". A luminosity section covers 220 orbits $\sim$

material	Value
Circumference	26659 m
Sectors	8
Experimental interaction points	4
Revolution time	88 μs
Magnetic field in dipoles	8.3 T
Current in dipoles	11850
Stored energy in dipoles	10 MJ
Dipoles	1232
Quadrupole	392
Multipole	3700
Cooling temperature	1.9 K (Helium)
Spot sizes	16 μm
Vacuum	10^{-11} bar
Operation luminosity	$10^{33} cm^{-2} s^{-1}$
Nominal luminosity	$10^{34} cm^{-2} s^{-1}$
Operation proton beams energy	3.5 TeV (2011 pp), 4 TeV (2012 pp)
Bunches number	2835
Proton per bunch	10^{11}
Time between bunches	50 ns

Table 4.1: LHC main parameters.

93 s, and it is an unit of accounting for integrated luminosity. The analysis picks up production data files with only the ”certified” luminosity sections. Some luminosity sections are rejected, due to detector performance below the quality standards.

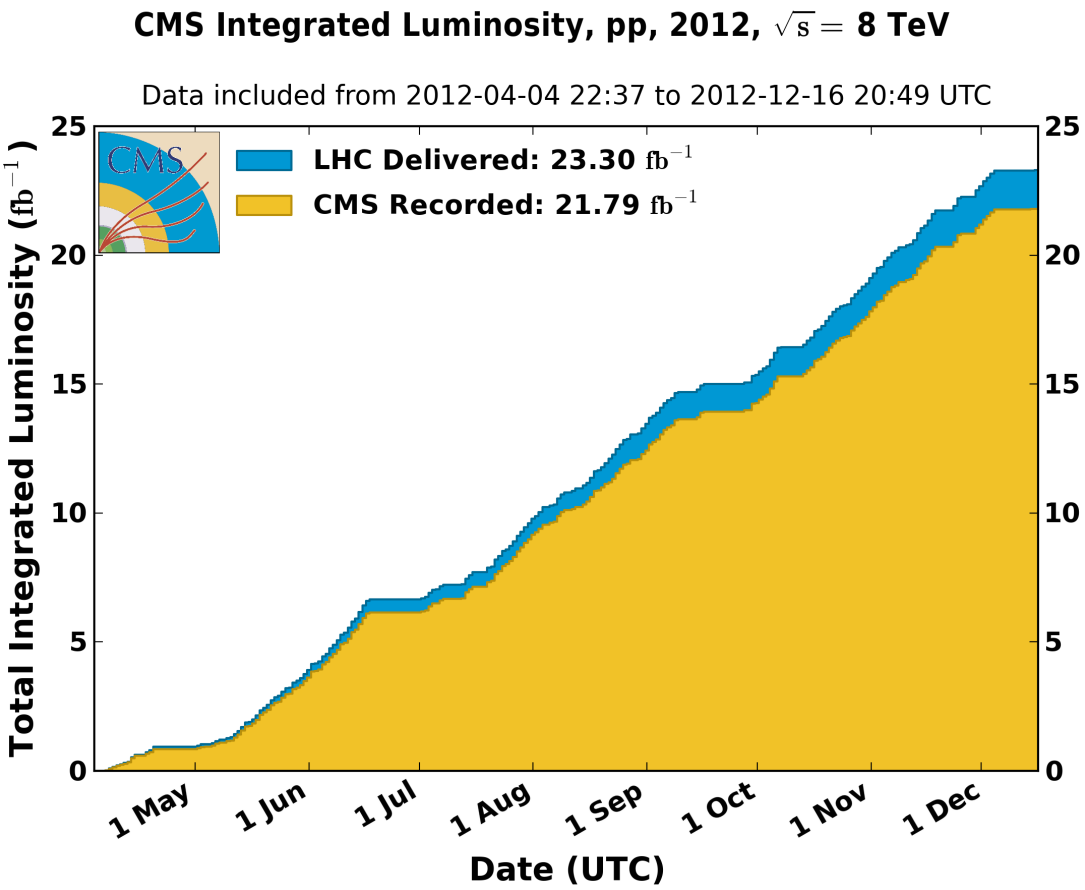

Figure 4.2: Delivered and recorded integrated luminosity for proton-proton collisions at $\sqrt{s}$ =8 TeV.

4.3 Compact Muon Solenoid experiment

The Compact Muon Solenoid (CMS) experiment [61] is a general purpose apparatus. The searches program is in common with LHC machine and in competition or collaboration with ATLAS. Higgs boson discovery in 2012 met one of the main goal of the machine, but more studies about this particle are required. Searches for physics beyond SM at 1 TeV scale, like super symmetry or extra dimensions, play a key role: next run period, as described in chapter 7.4 will achieve the design energy and potentially new particles will be found. Precision measurements about top quark properties, hadrons with bottom quark behaviors, W particles mass are also investigated subjects. Ion physics (lead-lead collisions, lead-proton collisions) studies related to Quark Gluon Plasma is an important part of CMS scientific program, too. Thus, physics requirements are related to the searches for the Higgs boson, super symmetric particles, new massive vector bosons, studies about extra dimensions, SM precision measurements and heavy ion physics.

The main detector requirements to meet the goals of the LHC program are listed below:

- trigger acceptance for rare events close to 100%;
- muon alignment better than 200 μm;
- muon charge determination up to transverse momentum p_T $\sim$1 TeV;
- dielectron and diphoton mass resolution of about 1 % at 100 GeV;

LHC and CMS Records Online in 2012 – Protons

Peak Instantaneous Stable Luminosity	7670.19×10³⁰cm⁻²s⁻¹	Fill 3347	2012.11.30 01:16:49
Maximum Interactions per Crossing (pileup)	34.55	Fill 3347	2012.11.30 01:16:49
Maximum Luminosity Delivered in one Fill	246.28 pb⁻¹	Fill 2692	2012.06.02 05:10:16
Maximum Luminosity Delivered in one Day	286.08 pb⁻¹	Day 280	2012.10.06
Maximum Luminosity Delivered in one Week	1300.54 pb⁻¹	Week 24	2012.06.10
Maximum Luminosity Delivered in one Month	3693.06 pb⁻¹	Month 10	2012.10.01
Maximum Colliding Bunches	1380	Fill 2660	2012.05.24 15:34:46
Longest Time in Stable Beams for one Fill	22.74 hours	Fill 2692	2012.06.02 05:10:16
Longest Time in Stable Beams for one Day	21.52 hours	Day 231	2012.08.18
Longest Time in Stable Beams for one Week	87.63 hours	Week 24	2012.06.10
Longest Time in Stable Beams for one Month	265.18 hours	Month 7	2012.07.01
Fastest Turnaround Time to Stable Beams	2.18 hours	Fill 2634 to 2635	2012.05.17 04:48:36
Best Recording Efficiency By Lumi for one Fill	98.93% [171.20 pb⁻¹]	Fill 2875	2012.07.24 15:45:40
Maximum Recorded Lumi one Fill	238.90 pb⁻¹	Fill 2692	2012.06.02 05:10:16
Maximum Recorded Lumi one Day	280.07 pb⁻¹	Day 330	2012.11.25
Maximum Recorded Lumi one Week	1172.08 pb⁻¹	Week 24	2012.06.10
Maximum Recorded Lumi one Month	3490.64 pb⁻¹	Month 10	2012.10.01

Figure 4.3: Machine performance for proton-proton collisions.

- jets energy resolution below 15 % for jet $p_T > 50$ GeV;
- geometric coverage $|\eta| < 2.5$.

Figure 4.6 shows a schematic view of the CMS detector.

CMS has a cylindrical central barrel closed by two end caps. Geometry covers almost the full solid angle. The overall dimensions of the detector are a length of 21.6 m, a diameter of 14.6 m and a weight of 12500 tons. CMS is composed by the following sub detectors, listed from interaction point to outside:

- tracker [62];
- electromagnetic calorimeter (ECAL) [63];
- hadronic calorimeter (HCAL) [64];
- muon chambers [65].

At the heart of CMS sits a 3.8 T superconducting solenoid, with 5.9 m of inner diameter and 13 m long. The flux of the solenoid is returned by a set of iron disks in the end caps and concentric cylinders in the barrel. The return field in the yoke is large enough to saturate 1.5 m of iron. The muon detectors are embedded inside the disks and the cylinders to ensure robustness and full geometric coverage. The core of the magnet is large enough to accommodate also the inner tracker and the calorimetry inside. The possibility of detection of the SM Higgs boson played a crucial role in the conceptual design of the CMS experiment as a benchmark to test the performance of the detector.

Since the SM Higgs boson mass was not predicted by theory and its production cross section and natural width vary widely over the allowed mass range, a search was envisaged over a large range of masses in different decay modes: pairs of photons, Z bosons, W bosons, τ leptons, and b quarks. Planning the analysis of all these channels ensured a detector capable of observing a Higgs boson over a broad mass range and able to detect most potential sig-

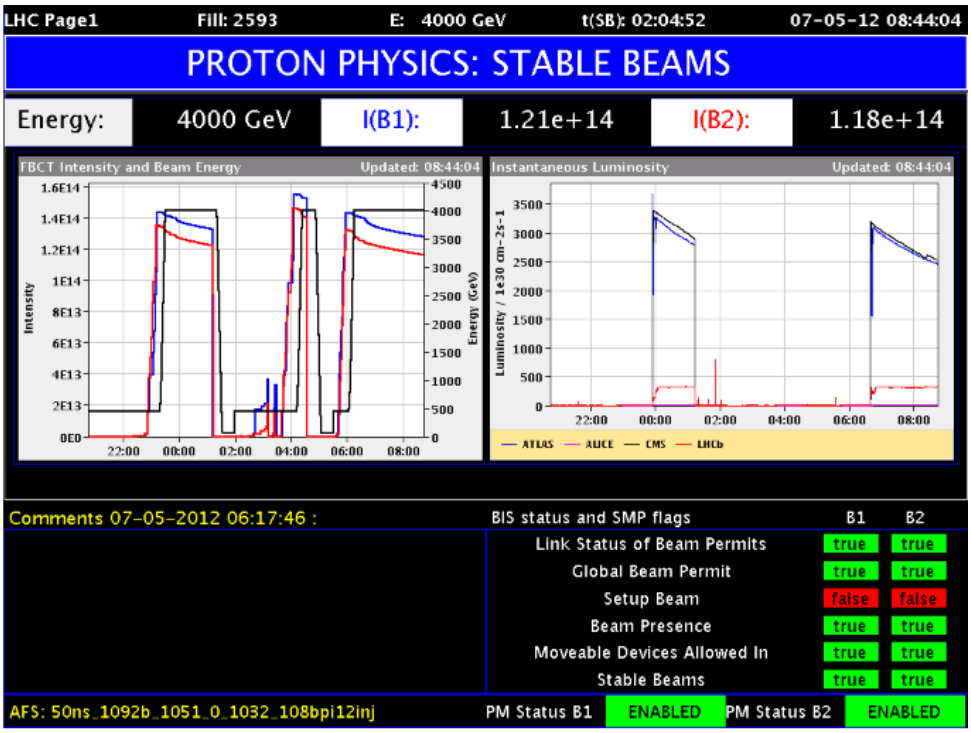

Figure 4.4: "LHC page 1" during stable beams in proton physics.

nals of new physics. Within the magnetic field volume are a silicon pixel and strip tracker, a lead tungstate crystal electromagnetic calorimeter, and a brass/scintillator hadron calorimeter. Muons are measured in gas-ionization detectors embedded in the steel flux-return yokes. Extensive forward calorimeters complement the coverage provided by the barrel and end cap detectors. Charged particles are tracked within the pseudo rapidity range $|\eta|$ <2.5, where $\eta = -ln[tan(\theta/2)]$, and θ is the particle polar angle measured from the positive z axis (along the anticlockwise beam direction).

The silicon pixel tracker comprises 66 million pixels with 100 $\times$ 150 μm^2 of size, arranged in three barrel layers and two disks at each end. The silicon strip tracker, organized in ten barrel layers and twelve disks at each end, comprises 9.3 millions strips with pitch between 80 and 180 μm, with a total silicon surface area of 198 m^2. The tracker has a track-finding efficiency larger than 99% for muons with transverse momentum p_T greater than 1 GeV and transverse momentum resolution between 1.5 and 2.5 % for charged tracks of p_T around 100 GeV in the central region ($|\eta|$ <1.5). Measurements of the impact parameters of charged tracks and secondary vertices are used to identify jets that are likely to contain the hadronization and decay products of b quarks (called b jets). A b jet tagging efficiency of more than 50 % is achieved with a rejection factor for light quark jet of around 200, as measured in $t\bar{t}$ events in data. The dimuon mass resolution at the Z mass, dominated by instrumental effects, is measured to be 0.6 % in the barrel region, consistent with the design goal.

The ECAL is a fine-grained hermetic calorimeter consisting of $\sim$ 76000 lead tungstate crystals, arranged in a quasi-projective geometry and distributed in a barrel region $|\eta|$ <1.48 and two end caps covering up to $|\eta|$ =3.0. The front-face cross section of the crystals is 22 $\times$ 22 mm^2 in the barrel region and 28.6 X 28.6 mm^2 in the end caps. Preshower detectors consisting of two planes of silicon sensors interleaved with a total of three radiation lengths of lead absorber are located in front of the end caps. Electromagnetic showers are very narrow in lead tungstate (Moliere radius of 21 mm), helping in particle identification and in the implementation of iso-

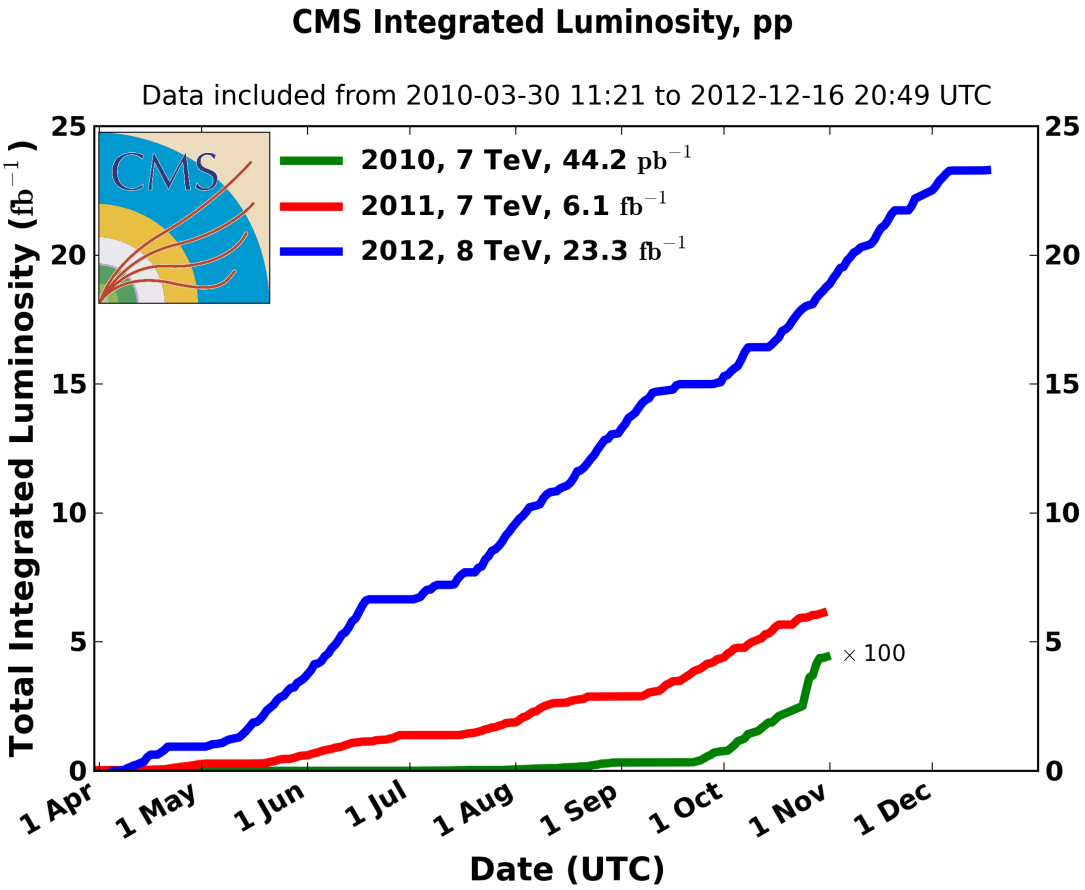

Figure 4.5: Delivered integrated luminosity for proton-proton collisions at $\sqrt{s}$ =7 TeV and $\sqrt{s}$ =8 TeV.

lation criteria. In the central barrel region the energy resolution of electrons that do not radiate substantially in the tracker material indicates that the resolution of unconverted photons is consistent with the design goals ($\frac{\sigma_E}{E} \sim 1\%$). For such photons the diphoton mass resolution is 1.1 GeV at a mass of 125 GeV.

The HCAL barrel and end caps are sampling calorimeters consisting of brass and scintillator plates, covering $|\eta|$ =3.0. Their thickness varies from 7 to 11 interaction lengths X_0, depending on η; a scintillator tail catcher placed outside the coil of the solenoid, just in front of the innermost muon detector, extends the instrumented thickness to more than 10 X_0 everywhere. Iron forward calorimeters with quartz fibers, read out by photo multipliers, extend the calorimeter coverage up to $|\eta|$ =5.0.

The muon spectrometer is composed of three types of gaseous muon detectors based on different technologies:

- the drift tubes (DT) in $|\eta|$ <1.2;
- the cathode strip chambers (CSC) for 0.9< $|\eta|$ <2.4;
- the resistive plate chambers (RPC) in $|\eta|$ <1.6.

The DTs and the CSCs provide a precise position measurement and together with RPCs operate within the first level trigger system, providing two independent and complementary sources of information. The muon system consists of four stations in the barrel and end caps, designed

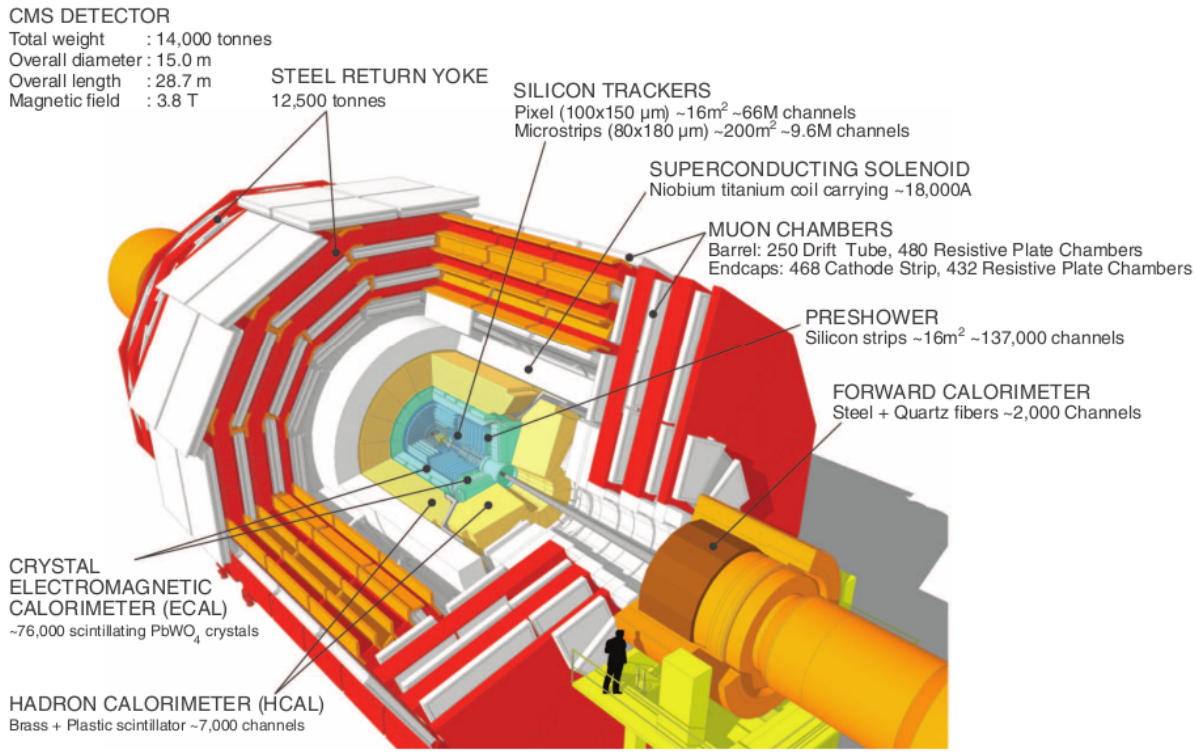

Figure 4.6: Sketch of the CMS detector.

to ensure robust triggering and detection of muon over a large angular range. In the barrel region each muon station consists of twelve drift-tube layers, except for the outermost station, which has eight layers. In the end caps, each muon station consists of six detection planes. The precision of r-ϕ position measurement is 100 μm in the drift tubes and varies from 60 to 140 μm in the cathode strip chambers.

The CMS trigger and data acquisition (DAQ) systems ensure that potentially interesting events are recorded with high efficiency. The first level (L1) trigger, comprising the calorimeter, muon, and the global trigger processors, uses coarse-granularity information to select the most interesting events in a time range of some μs. The detector data are pipe lined to ensure negligible dead time up to a L1 rate of 100 kHz. After L1 triggering, data are transferred from readout electronics of all sub detectors, through the readout network, to the high-level-trigger (HLT) processor farm, which operates offline-quality reconstruction algorithms to decrease the event rate to around 0.5 kHz, before data storage.

The CMS experiment employs a highly distributed, worldwide computing infrastructure for off line reconstruction and analysis, called GRID. It has a primary Tier 0 center at CERN, supplemented by seven Tier 1 as national centers, more than 50 Tier 2 as regional centers, and many Tier 3 centers at national laboratories and universities throughout the world. The CMS software running on this high-performance computing system executes numerous tasks, including the reconstruction and analysis of collected data, as well as the generation and detailed detector simulation of MC event samples. Storage and computing are resources located in all the world. More information about trigger, DAQ system, storage and computing are given in the next sections.

4.4 CMS Trigger

The LHC bunch crossing rate is around 40 MHz. Maximum data writing rate is $\sim$ 300 Hz. Thus, experiments must reject on the fly most of collisions. The mechanism to select which data could be relevant for further off lines physics analysis is the trigger process, embedded into the data acquisition (DAQ) system. CMS trigger and DAQ consists of four parts: the detector electronics, the level 1 trigger processors, the readout network, on line event filter system in the process farm that executes the algorithms for HLT reconstruction and selection. The size of the LHC detectors and the underground caverns imposes a minimum transit time for signals from the front-end electronics to reach the services cavern housing the level 1 trigger logic and return back to the detector front-end electronics. The total time allocated for the transit and for reaching a decision to keep or discard data from a particular beam crossing is 3.2 μs. During this time, the detector data must be held in buffers while the trigger data is collected from the front-end electronics and decisions taken discarding a large fraction of events while retaining the small fraction of interactions of interest (about 1 every 1000 events). The time allocated to level 1 trigger calculations is less than 1 μs. Custom hardware processors form the level 1 decision. The level 1 triggers involve the calorimetry and muon systems, as well as some correlation of information between these systems. The level 1 decision is based on the presence of trigger primitive objects such photons, electrons, muons, and jets above defined transverse energy or transverse momentum thresholds. It also employs global sums of transverse energy or missing transverse energy E^T_{miss}. Reduced-granularity and reduced-resolution data are used to form trigger objects. Level 1 trigger rate during 2012 data taking is limited to 100 kHz. Much of the logic in the trigger system is contained in custom Application Specific Integrated Circuits (ASICs), semi-custom and gate-array ASICs, Field Programmable Gate Arrays (FPGAs), Programmable Logic Devices (PLDs), and discrete logic such as Random Access Memories that are used for memory Look-Up Tables (LUTs). Upon receipt of a level 1 trigger, after a fixed time interval of 3.2 μs, the data from the pipelines are transferred to the front-end readout buffers. After signal processing, zero-suppression and data-compression, the data are placed in dual-port memories for access by the DAQ system. Each event, with a size of about 600 kB in proton-proton collisions, is contained in several hundred front-end readout buffers. Through the event building switch, data from a given event are transferred to a processor. Each processor runs the same high-level trigger software code to reduce the level 1 output rate of 100 kHz to less than 1 kHz for mass storage. The use of a processor farm for all selections beyond level 1 allows maximal benefit to be taken from the evolution of computing technology. Flexibility is maximized since there is complete freedom in the selection of the data to access, as well as in the sophistication of the algorithms. Various strategies guide the development of the HLT software code. The HLT code is written in the same high level language (based on C++) of the offline analysis, within the CMSSW dedicated software framework. Rather than reconstructing all possible objects in an event, whenever possible only those objects and regions of the detector that are actually needed are reconstructed. Partial reconstruction idea and notion of many virtual trigger levels are in place: calorimeter and muon systems information are used, followed by the use of the tracker pixel data and finally the use of the full event information (including tracking algorithm).

4.5 CMS Data Acquisition system

Figure 4.7 gives an example of the layout of the Function Manager in the central DAQ system. Function Manager (FM) modules merge the synchronized Trigger Throttle Signal for each partition. L1 Trigger receives and reacts on merged signals. Around 650 front end drivers, when

trigger fired, pick up data and, through the front readout links, the information go to the 72 read out units in the read out builder network (called ”slice”). CMS has eight independent DAQ slices. The Storage Manager (SM) keeps temporarily events accepted by HLT farm. The SM writes data to the local disk array; the closed files are then transferred to Tier 0. The SM maintain some information on stored data in a dedicated Database. The Run Control Monitor System (RCMS) is the master part for data taking. Monitoring information is provided by specific designed applications. Error information are handled by an automatic sentinel system. The sentinel routes all messages to a collecting application. Several tools are used in the on line operation, related to central DAQ system. RCMS Graphical User Interface (GUI) indicates subsystems status. ”DaqDoctor” application indicates clearly what is on going (including possible solution for errors). ”aDAQmon” is a powerful graphical monitoring of the DAQ system with diagnostics. ”Hotspot” displays errors in the XDAQ framework or applications and allows searching for specific errors. ”Storage Manager page 1” shows information on the data stored and informs about data transfer to Tier 0. ”Nagios” on line cluster monitors the status of computers and services.

The Run Control and Monitor System (RCMS) [66] is the set of hardware and software components responsible for controlling and monitoring the experiment during data taking. It provides users with a virtual counting room, enabling them to operate the experiment and monitor detector status and data quality from any point in the world. The architecture of the CMS DAQ system has roughly 10000 objects that need to be controlled. The RCMS architecture is scalable to control and monitor a large distributed system. The Internet applications face similar issues, so CMS adopts the web technologies and services, such as eXtensible Markup Language (XML) data format for data exchange and the Simple Object Access Protocol (SOAP) protocol for communication. As a component of the CMS on line software, the RCMS inter operates with the other on line software components, like the Detector Control System (DCS), and the XDAQ cross platform DAQ framework. The RCMS views the experiment as a collection of partitions. A partition is a configurable group of resources. Multiple partitions can be active concurrently, sharing resources, allowing several sections of the experiment to run independently. The RCMS performs actions on the partitions. Configuration and monitoring actions have timing constraints. Configuration and setup of partitions require a time period of the order of minutes, their control (status changes, commands execution) order of seconds. For examples, during 2012 data taking period sub system tracker configuration required around 3 minutes (the longest period), while the DT occupies around 30 seconds. Users have to be authorized and authenticated to get access to the RCMS functions. The logical layout consists of four types of elements: session managers, sub systems controllers, user interfaces, and a set of Services that are needed to support specific functions like security, logging, and resource management. A number of DAQ sub systems are involved in data taking. Any sub system is partitioned, and different partitions operated concurrently. The standard partition boundaries are the sub detectors. A hierarchy masters over sub system partitions: actions performed at the level propagates to components. Graphical User Interfaces are important to provide the user on shift with a set of intuitive functions to control and monitor the experiment.

4.6 Storage and Computing

In the distributed computing GRID, offline analysis is supported by a technological team. More than one Tier 2 can be involved during analysis tools running. For instance, the seesaw type III signal samples are stored in Tier 2 Legnaro-Padua and the code (analyzers, filters, root macros) runs on the special cluster of user interface (UI). Monitors tools are used during massive run of the analysis. The Legnaro-Padua Tier 2 is a computing facility [67], serving in particular

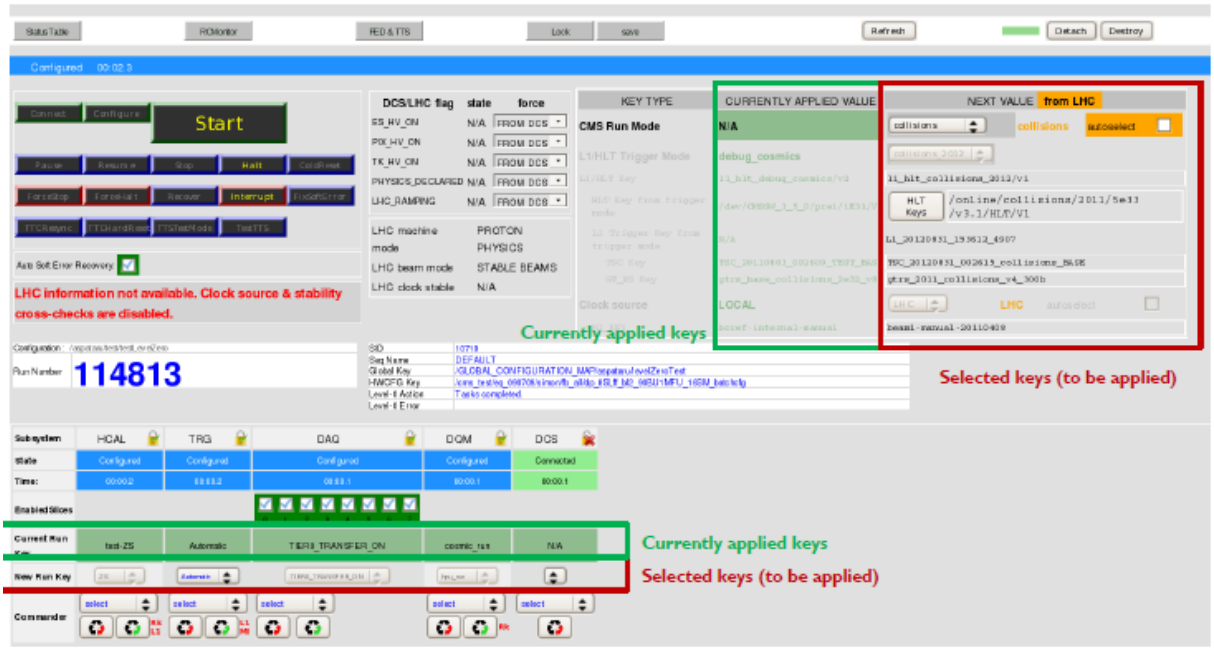

Figure 4.7: Central DAQ Level 0 Function Manager.

the ALICE and CMS LHC experiments. Its unique characteristic is its topology: the computational resources are spread in two different sites, about 15 km apart: the INFN Legnaro National Laboratories and the INFN Padua unit. Nevertheless these resources are integrated and are exposed as a single computing facility. The history of Legnaro-Padua Tier 2 goes back to 2001, when it started as a collaboration between INFN Legnaro National Laboratory and INFN Padua to setup a prototype computing farm, located in Legnaro, for CMS Monte Carlo productions. Since then the two sites have always been involved in several GRID related activities and in other computing activities of the LHC experiments, in particular ALICE and CMS. In 2008 a tighter integration of the two INFN units has been achieved exploiting a dedicated fiber link connecting the two sites, implementing therefore a distributed Tier 2: the services and resources, since then all located in Legnaro, have been deployed in both sites. The bulk of servers is composed of 190 worker nodes, which are split about equally between the sites and configured as a single cluster managed by batch system. These computing resources are accessible using a GRID interface providing a high level of scalability and reliability. The storage for the CMS Virtual Organizations (VO) is $\sim$ 1.1 PB on 16 disk servers. Along with the storage there are the services providing remote data access through different protocols and the CMS data set transfer agents (Phedex). One of the critical aspects in setting up the distributed Tier 2 was the networking. All the out bound traffic goes through the Legnaro router (at 2 $*$10 Gb/s). The core of the Tier 2 monitoring is based on three common tools, all with customized scripts and configurations:

- "Ganglia" is the main source providing the status and performance of the Tier 2 hardware resources, which are divided in two groups with different frequencies of metric collection: high (around 30 s) for the storage servers and all services, and lower (around 5 min) for less critical machines like the worker nodes;
- "Nagios" collects all the site health information not only of internal resources but also from external views;
- "Cacti" is used to monitor all the network switches and appliances. In addition to the monitoring there are several scripts and cron jobs developed to take corrective

actions for the more common issues, for example automatically killing memory consuming jobs when a server starts swapping or closing problematic worked nodes (e.g. low disk space, black hole nodes).

In Padua a special cluster of computers has been setup in order to provide an efficient system for the final stage of analysis activities of the local CMS community, with a total storage of about 30 TB. Despite the intrinsic complexity of its distributed architecture, the Legnaro-Padua Tier2 proved to be very reliable: it has always been among the top sites in the availability ranking measured by CMS and ALICE and in the official GRID Availability and Reliability Report the site averages for the last two years were respectively 99.7% and 99.2 %. The site contribution to the computing activities of the two VOs is usually larger than their quota of resources thanks to the dynamic sharing of worker nodes which allows the exploitation of extra slots whenever they are left unused by the other VO.

Chapter 5

Data analysis

5.1 Analysis strategy

The research strategy to investigate the seesaw with heavy fermion weak triplet mediators mechanism is based on the study of final states with exactly three charged leptons, missing transverse energy and low hadronic activity without b jets. The signal must have missing transverse energy, related to the $\Sigma^{\pm}$ and $W^{\pm}$ decays in final states with neutrinos. The total charge of three charged leptons must be ± 1, like the total charge of $\Sigma^{\pm}$ and Σ^{0}. The study of the MC signal shows the leptons can be selected with transverse momentum p_T greater than 10 GeV. The Z boson, coming from the $\Sigma^{\pm}$, decays into neutrinos or into jets are considered; anyway the jets activity of the signal is smaller than the jets activity of the background. Background contributions are classified in two groups:

- physical backgrounds: events coming from physical processes that have final states similar to the signal signature;
- non physical or instrumental backgrounds: events with misidentified objects (fake objects), events with missing objects due to the detectors inefficiencies, events with additional objects originated from other interactions in the same bunch crossing (PU), events with additional objects originated from secondary interactions and/or from decays in the detectors material.

The main physical background sources are diboson and triboson decay and events with a single heavy boson produced accompanied by an energetic photon that converts into a leptons pair (Dalitz pair). Instrumental backgrounds are events with one or two charged identified lepton(s) and the remaining one or two fake lepton(s); the most relevant contributions to these backgrounds come from $t\bar{t}$, $b\bar{b}$, WWjets, $c\bar{c}$, and DY production processes. Backgrounds are also classified as reducible and irreducible: if contribution is reducible a removal strategy is in place, in the other case an estimation, performed on suitable control region, takes into account how many events are expected in data. Strategies to reduce backgrounds invoke physics objects and impose thresholds on their physical quantities. Selections usually act at different analysis flow steps. To optimize discovery potential, events selected in the analysis are grouped into categories. The criteria to assign an event to a defined category are: number of electrons (or number of muons), opposite or same charge sign of the same flavor leptons pair (OSSF, SSSF), sign of the total charge of the three leptons. The twelve different categories are described in Table 5.1. At the end of analysis flow, the comparison between background and data gives the results, with uncertainties. Finally, results interpretations in theoretical model are performed.

In this chapter, the following items are addressed in details:

- event reconstruction and physics objects;

- data samples and triggers selection;
- events selection;
- signal and SM backgrounds;
- photon asymmetric conversion background determination;
- non prompt leptons background determination;
- total background estimation;
- data, MC signal and backgrounds comparison;
- systematic uncertainties.

Table 5.1: Categories of the selected events.

Category	μ	e	Symbol	Sign
SSSF	3	0	$\mu^+\mu^+\mu^-$	+
SSSF	0	3	$e^+e^+e^-$	+
SSSF	2	1	$\mu^+\mu^+e^-$	+
OSSF	2	1	$\mu^+e^+\mu^-$	+
SSSF	1	2	$e^+e^+\mu^-$	+
OSSF	1	2	$\mu^+e^+e^-$	+
SSSF	3	0	$\mu^-\mu^-\mu^+$	-
SSSF	0	3	$e^-e^-e^+$	-
SSSF	2	1	$\mu^-\mu^-e^+$	-
OSSF	2	1	$\mu^-e^-\mu^+$	-
SSSF	1	2	$e^-e^-\mu^+$	-
OSSF	1	2	$\mu^-e^-e^+$	-

5.2 Event reconstruction and relevant physics objects

Different detectors measure and identify particles using their peculiar features in interactions with materials, as depicted in Figure 5.1. Photons, mass less and neutral particles, go undetected through tracking detectors and produce shower in ECAL. Electrons and positrons, lightest charged leptons, leave curve tracks in the tracker and produce showers in ECAL. Muons go through all detectors and give signals in all of them, including the muon chambers. Charged hadrons -such as kaons, pions, protons - make tracks in the inner detectors and ECAL, then produce showers in HCAL. Neutral hadrons produce showers in HCAL. Neutrinos are not detected directly: they are associated to the missing transverse energy, because of the imbalance of energy in transverse plane.

Event reconstruction is the operation of constructing physics quantities from the raw data, the output from the sub-detectors, collected by the experiment. At the higher level reconstruction step, these physics quantities correspond to physics characteristics of particles produced in the LHC collisions. The reconstruction process is a collection of independent units, each one providing a set of corresponding reconstructed objects as output. Each reconstruction unit is implemented in the CMS framework (CMSSW software) as a "module", in which algorithms, that are able to process data from the Event, are implemented. The reconstructed quantities are then stored again in the Event being used in the data analysis. A used Event data reconstruction technique is the so called "particle flow" (PF) [68–71], which enhances the performance of the detector. Particle flow attempts to reconstruct all stable particles in an event by combining information from all sub-detectors. This way, an optimal determination of particle direction,

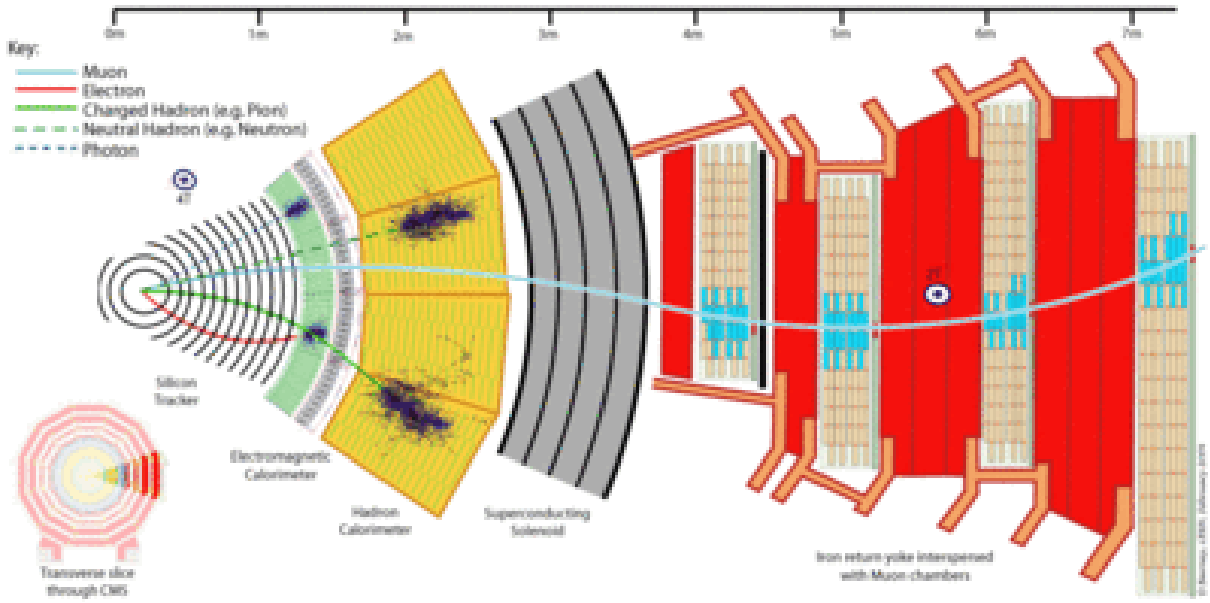

Figure 5.1: CMS Particle Identification.

energy and type is obtained. The algorithm categorizes all particles into the following five types: muons, electrons, photons, charged and neutral hadrons. Then, the resulting particles list is used to construct a variety of higher-level objects and observables such as jets, missing transverse energy E^T_{miss}, photon isolation variables, b-jet tagging discriminators. The research strategy to investigate seesaw type III invokes electrons, muons, E^T_{miss} and jets non b tagged. The reconstruction of the main physics quantities used in the analysis are briefly described in next sections.

5.2.1 Tracker track

The default reconstruction of charged particles tracks in the silicon tracker system is performed by the combinatorial track finder (CTF). Triplets or pairs of hits with an additional constraint from the beam spot or a vertex are used as initial estimates, or seeds, of tracks. The seeds are then propagated outward in a search for compatible hits. As hits are found, they are added to the seed trajectory and the track parameters and uncertainties are updated. This search continues until either the limit of the tracker is reached or no more compatible hits can be found, yielding the collection of hits that belong to the track. In the final step, this collection of hits is fit to obtain the best estimate of the track parameters. The ”generalTrack” collection is produced using rather loose track finding cuts. As a result, it has a very high efficiency to find tracks, but it contains quite a large fraction of fake tracks. Therefore, physics analysis uses only a subset of the tracks that satisfy quality criteria, selecting the proper quality flag associated to the track. The quality flag is based upon parameters like the number of hits on the track and its χ^2, and vertices compatibility. Track are defined ”high Purity”, ”tight”, ”loose”. Note that ”high Purity” tracks are a subset of ”tight” tracks.

5.2.2 Primary interaction vertex

The primary vertex (PV) identification starts from the reconstructed tracks, selected on the basis of their compatibility with the beam spot, number of hits and normalized tracks χ^2. The tracks are clustered into several primary vertex candidates, according to the z-coordinate of the point of closest approach of the tracks to the z-axis. Several primary interaction vertices can be

found in the same bunch crossing due to the occurrence of more than one pp collision, known as PileUp (see Section 3.2). A vertex fit is performed in (x, y, z) coordinates for each primary vertex candidate using the corresponding tracks. The primary vertex candidates compatible with the beam line are retained.

5.2.3 Jets

Quarks or gluons produced in the LHC collisions cannot be observed directly, but they fragment into stable hadrons, which can be detected in the tracking and calorimeter systems. These hadrons generated from a parton produce a roughly collimated flow of particles called jet. The identification and measurement of physics quantities related to jets is performed by different kind of algorithms, which assembles a collection of objects (calorimetric towers, particles) to obtain the final jet. These algorithms provide a good measurement of the initial parton energy and direction. Beside this, they should be collinear safe, such that the result is unchanged if e.g. the energy carried by a single particle is instead distributed among two collinear particles, and infrared safe, such that the result of the jet finding is stable against the addition of soft particles. Jet algorithms which do not satisfy one of the two conditions yield ambiguous results and lead to unnecessary uncertainties when applied to calculations in perturbation theory. Many jet algorithms are implemented in the CMS framework. In the analysis, jet reconstruction algorithm chosen is the anti-k_T [72], a variation of the k_T algorithm. The "inclusive k_T" method is a cluster-based jet algorithm. The cluster procedure starts with a list of input objects, stable particles or calorimeter cells. For each object i and each pair (i, j) the following distances are calculated:
$d_i = p_{T,i}^2$
$d_{ij} = min(p_{T,i}^2, p_{T,j}^2)[(\eta_i\eta_j)^2 + (\phi_i\phi_j)^2]/R^2$
where R^2 is a dimensionless parameter normally set to unit. The algorithm searches for the smallest d_i and d_{ij} , and call it d_{min} . If d_{min} is a d_{ij}, the objects i and j are merged into a new object with momentum the sum of the momentum of i and j. If a distance of type d_i is the smallest, then the corresponding object i is removed from the list of input objects and filled into the list of final jets. The procedure is repeated until all objects are included in jets. This algorithm is both collinear- and infrared-safe to all orders of perturbation QCD. The "anti-k_T" follows the same repetition as the "inclusive k_T" but distance definitions are:
$d_i = \frac{1}{p_{T,i}^2}$
$d_{ij} = min(\frac{1}{p_{T,i}^2}, \frac{1}{p_{T,j}^2})[(\eta_i\eta_j)^2 + (\phi_i\phi_j)^2]/R^2$
The energy measurement obtained by jet algorithms does not match the energy of the initial parton originating the jet. The jets at this level are so called raw jets. The bias in jet energy reconstruction is caused by different reasons, among which the most important are: non-linear response of the calorimeters, detector segmentation, presence of material in front of calorimeters, electronic noise, noise due to physics (PU of interactions from same bunch crossing). Many levels of correction [73] are applied to the raw jets in order to obtain the energy value that is closer to the true energy of the initial parton. In the analysis, three corrections are in place:

- Offset (L1): the PU and electronic noise effects are removed. This correction can be estimated using events collected by a random trigger, without any preconditions except a beam crossing, and referred to as zero bias events. The offset contribution is evaluated as the average calorimeter energy deposited inside a cone of radius R, and depends on the η of its axis;
- Relative (η) (L2): the variation in jet response with η is flattened, using the dijet imbalance method applied on collision data. This method is based on the principle

of transverse momentum conservation: considering a two partons final state, the resulting particle jets have equal transverse momentum, in an ideal case. The unbalance between the jets transverse momentum that is observed on average, is due to the variation of the jet response across the detector versus η;

- Absolute (p_T) (L3): the calorimetric energy response to a particle level jet is smaller than unity and varies as a function of the jet p_T . The absolute correction removes these variations and make the response equal to unity at all p_T. This corrections is obtained from simulation using the MC truth, and from real data exploiting γ + jets and Z + jets events.

Selected physical variables that describe PF jets are used to differentiate between a physics jets and a noise or noise-enhanced one. HCAL noise tends to populate high values of neutral hadron fraction, and ECAL noise tends to populate high values of neutral electromagnetic fraction. Jet properties requirements are neutral hadron fraction to be much less than one, neutral electromagnetic fraction to be much less than one, charged hadron fraction to be greater than zero, charged electromagnetic fraction to be less than one (reject electrons). In addition, other requests on particles constituents come from simulated events studies: they recognize regions, in the PF jet variable phase-space, where mismatched jets tend to populate and determine efficiency of jet identification.

In the analysis, the object jet has the following features:

- the fraction of jet energy carried by neutral hadron is < 0.99;
- the fraction of jet energy carried by neutral electromagnetic (photon) is < 0.99;
- the fraction of jet energy carried by charged hadron fraction is > 0;
- the fraction of jet energy carried by charged electromagnetic fraction is < 0.99;
- particles constituents are more than one;
- at least one charged particle constituent is present;
- jet pseudo rapidity η is inside the geometrical regions covered by detectors: $|\eta| < 2.4$;
- the jet transverse momentum p_T is above 30 GeV.

5.2.4 b quark jets

The jets produced by b-quark hadronization are characterized by quantities that allow to identify them (b tagging), discriminating jets from gluons (g), light flavor quarks (u, d, s) and c-quark. Especially the b-quark long lifetime with respect to the other quarks and its semileptonic decay properties is exploited for the b tagging. The impact parameter of a track with respect to the primary vertex is used to distinguish the decay products of a b hadron from other tracks. A sign is associated to the impact parameter, which is given by the scalar product of the vector pointing from the primary vertex to the point of closest approach of the track with the jet direction. Tracks originating from the decay of particles traveling along the jet axis will tend to have positive impact parameter values. In contrast, the impact parameters of prompt tracks can have positive or negative values. A good discrimination variable for b tagging is the impact parameter significance σ_{IP} defined as the ratio of the signed impact parameter to its estimated uncertainty. In CMS an algorithm based on σ_{IP} is used for b tagging, called Track Counting (TC). It sorts the tracks in a jet by decreasing values of impact parameter significance. The probability to have several tracks with high positive value of the σ_{IP} is low for light-flavor jets. Another powerful way to discriminate b-jets from other jets is to look for the presence

of a secondary vertex inside the jet. Variables associated to a secondary vertex that are useful in b tagging are: the flight distance and direction, defined by the vector between the primary and secondary vertex, track multiplicity and invariant mass associated to the secondary vertex. The Simple Secondary Vertex (SSV) algorithm uses the significance of the flight distance as discriminating variable. By using additional variables, a discrimination is provided even in cases where the secondary vertex is not reconstructed, increasing the efficiency with respect to the SSV algorithms. This is a more complex approach and involves the use of secondary vertices (when reconstructed) together with track-based lifetime variables, leading to the Combined Secondary Vertex (CSV) algorithm. Two likelihood ratios are built from these variables. They are used to discriminate between b and c jets and between b and light-flavor jets. Loose selections corresponding to 10% of misidentification probability for light flavor jets lead to a b-jet tagging efficiency of 80-85%, whereas tight selections corresponding to 0.1% of misidentification probability for light flavor jets lead to a b-jet tagging efficiency of 45-55%. In the analysis, the CSV b tagging algorithm is used at "loose working point". The b tagging veto on first jet in p_T is fixed at CSV threshold value of 0.244.

5.2.5 Isolation

A powerful variable used to determine whether a lepton is inside or outside a jet is the isolation (Iso). This quantifies the amount of energy of the particles detected in a region around the track of the reconstructed lepton. The region where the isolation variable is computed is a cone in the (η, ϕ) plane:
$\Delta R = \sqrt{\Delta\eta^2 + \Delta\phi^2} = \sqrt{(\eta - \eta_0)^2 + (\phi - \phi_0)^2}$
where η_0 and ϕ_0 identify the cone axis, which is the direction of the inner lepton track at the vertex position. The vertex is defined as the point of closest approach of the track to the beam line on a plane perpendicular to the beam. In the analysis, the cone radius chosen is $\Delta R = 0.3$. The particle flow isolation variable (pfIso) is the ratio between the sum of transverse momentum (or transverse energy) of the objects in the cone of radius ΔR and the lepton transverse momentum. The charged and neutral hadrons and photons are taken in account. In the algebraic sum (numerator), a correction for the PU is also present.

$$pfIso(lepton) = [\sum^{chargedhadrons} p_T + max(\sum^{neutralhadrons} p_T + \sum^{photons} p_T - 0.5\sum^{PileUp} p_T)]/p_T^{lepton}$$

5.2.6 Missing Transverse Energy

Neutral weakly interacting particles, such as neutrinos, escape from typical collider detectors without producing any direct response in the detector elements. The presence of such particles must be inferred from the unbalance of total momentum. The vector momentum imbalance in the plane perpendicular to the beam direction is particularly useful in pp and p$\bar{p}$ colliders, and is known as missing transverse momentum. Its magnitude is called missing transverse energy (MET), denoted E^T_{miss}. As for jet, the energy measurement obtained requires corrections. In the analysis, the so called "Type1" correction algorithm is applied on PF E^T_{miss}. This correction is a propagation of the jet energy corrections; the algorithm replaces the vector sum of transverse momenta of particles which is clustered as jets with the vector sum of the transverse momenta of the jets to which jet energy correction is applied.

5.2.7 Muons

The reconstruction of muons originated by pp collisions starts independently in the silicon tracker (tracker track) and in the muon spectrometer (standalone muon track). A complete muon reconstruction in the whole CMS volume, matching the information of the tracker and muon system, is achieved following two different approaches:

- Global Muon reconstruction (from outside to inside): starting from a standalone muon, a matching tracker track is found and a global muon track is fitted combining hits from tracker and standalone muon tracks. The greater is the muon p_T, the more the global fit can improve the momentum resolution with respect only the tracker track, since the level arm is bigger;
- Tracker Muon reconstruction (from inside to outside): all tracker track with $p_T >$ 0.5 GeV and p$>$ 2.5 GeV are considered as possible muon candidates. They are extrapolated toward the muon system, taking into account the energy loss in the material, the magnetic field and the uncertainty due to multiple scattering. If at least a muon segment (inside a DT or CSC, depending on which part of the CMS volume is involved in the extrapolation) matches the extrapolated track, the corresponding tracker track is classified as a tracker muon track. The matching is performed looking at the spatial distance between the extrapolation and the segment inside the muon chamber.

At low momentum the tracker muon is more efficient than the global muon reconstruction. In fact, as the muon p_T drops, the penetration inside the muon system is less deep. This results in higher probability for low p_T muons to produce just one segments in the first muon station layer. For about 1% of the muons from collisions, it happens that only a standalone muon track is reconstructed, and both of the above approaches fail. The failing rate is very low thanks to the high tracker track efficiency. In the CMS framework, the results of these algorithms are merged in a single collection of muon candidates. A physics analysis achieves the balance between identification efficiency and purity by applying a selection based on the muon identification variables. Three basic selections are:

- soft muon selection, where the muon is a tracker muon, with additional requirements on the spatial matching of the segment in the muon chambers;
- tight muon selection, where the muon is global, with additional requirements, such as cut on the normalized χ^2 of the track fit, at least one muon chamber hit included in the final track fit, segments matched in at least two muon stations, the corresponding tracker track with more than 10 silicon tracker hits (including at least one pixel hit) and a small distance between the closest point of the track to the primary vertex (impact parameter);
- particle flow muon selection, a selection is performed on all the muon candidates reconstructed with the standard algorithms. This selection has been optimized to identify muons in jets with high efficiency, keeping low the fake rate from misidentified charged hadrons.

Global muons with tight selection coming from Z boson decay have a fake rate probability of the order of 3.6% and 4%, in the forward and central region of the detector. Four muon identification variables are defined:

- Tracker Iso: is the sum of the transverse momenta of tracker tracks within the isolation cone. Only tracks with $p_T > 1$ GeV , $\Delta z < 0.2$ cm and $\Delta r < 0.1$ cm are considered, where Δz and Δr are the minimum distances from the tracker track to the cone vertex;
- Ecal Iso: is the sum of the transverse energies deposited in the electromagnetic calorimeter by particles passing through it. Only crystals with E$>$ 0.25 GeV are considered;
- HCAL Iso: is the sum of the transverse energies deposited in the hadron calorimeter

by particles passing through it; no cuts are applied on the calorimetric towers;

- Combined Iso: is the linear sum of the Tracker, Ecal and HCAL Isolation.

The identification variable Combined Iso with cone size ΔR <0.3 is used in the analysis. Charged particles from vertices other than the primary vertex in the cone contribute to the isolation value of the object. With particle flow, these PU particles can be sorted out and just not be counted. There are also neutral particles from PU but they do not produce tracks, so it is not possible to assign neutral particles to vertices. The neutral particles from PU are taken in account with an algorithm, called "Delta Beta PU correction": they are estimated to give a contribution equal to an half of charged particle from PU, that are found in the cone of radius ΔR. The efficiency to select an isolated muon is defined as the fraction of the muons that pass a given combined isolation threshold over all the muons in a sample of muon candidates originating from Z decays.

In the analysis, the object muon has the following features:

- the muon track is globally reconstructed in all detectors;
- the muon pseudo rapidity is inside the geometrical regions covered by muon detectors ($|\eta| < 2.4$);
- the χ^2 over number of degree of freedom (normalized χ^2) of the global muon track fit is $\chi^2/\text{ndof} < 10$;
- the number of silicon layers activated is > 5;
- the number of Valid Stand Alone Pixel Hits is > 0;
- the number of matched muon stations is > 1;
- the number of muon chamber hit in global fit is > 0;
- the impact parameter with respect to the primary vertex in the transverse plane is $|d_{0,pv}| < 0.005$ cm;
- the impact parameter is $|d_{z,pv}| < 0.5$ cm;
- the isolation with Delta Beta PU correction in cone size 0.3 is Iso$<$ 0.10.

These conditions optimize the selection efficiency with respect to the purity.

5.2.8 Electrons

The reconstruction of electrons originated by pp collisions uses the combination of tracking and calorimetric information, so it starts in the pixel detector, the silicon strip tracker and the electromagnetic calorimeter. The measurement of the electron energy in the ECAL is hampered by the amount of tracker material which is distributed in front of the ECAL, and by the presence of a magnetic field aligned with the collider beam axis, called z axis. Electrons passing through the silicon layers of the tracker radiate bremsstrahlung photons and the energy reaches the ECAL with a significant spread in the azimuthal direction ϕ. The so called "ECAL clustering" procedure, and in particular the building of "superclusters" (clusters of clusters) is in place to take in account the ϕ spread and collect the bremsstrahlung energy. The electromagnetic showers initiated by electrons deposit their energy in several ECAL crystals. For a single electron reaching the ECAL, most of the energy is collected in a small number of crystal ($\sim$ 25). The cluster is the fixed size arrays of crystals that contains the electromagnetic shower. To obtain a measurement of the electron energy at primary interaction vertex and minimize the cluster containment variations, bremsstrahlung photons are collected using more complex algorithms of superclustering. The "Hybrid algorithm" attempts to profit from the simple geometry of the

ECAL barrel and exploit the properties of the lateral shower shape in the transverse direction while dynamically searching for separated bremsstrahlung energy in the ϕ direction. In the language of the hybrid superclustering, the "seed" cluster is a collection over ϕ of contiguous dominoes made of 3 to 5 crystals in η and separated by other such collections by a valley where less than 100 MeV is observed in a domino. The "Island algorithm" in the end cap builds clusters by connecting rows of crystals containing energies decreasing monotonically when moving away from the highest energy crystal of the seed cluster, called "seed crystal". Then, superclusters are built by collecting other island clusters in a ϕ road in both directions around each island clusters, starting from a list of clusters ordered in transverse energy, in a procedure called bremsstrahlung recovery. In the language of Island algorithm, the "seed" cluster is a cluster that initiates a bremsstrahlung recovery procedure. Supercluster driven pixel seed finding is then used to initiate the building of trajectories in the inner tracker (initial track). The electron track reconstruction relies on a dedicated "Gaussian sum filter" (GSF), using a specific energy loss modeling. The electron track reconstruction is decomposed into four modular components:

- initial tracks called "seeds" are looked for with a seed generator. A seed is created when two hits compatible with a given beam spot are found in the pixel detector, in order to build a track outward. The search of seeds is restricted to a region compatible with a supercluster in ECAL (supercluster-driven limitation);
- the "trajectory builder" constructs outward all the possible trajectories for a given seed;
- the ambiguities among the possible trajectories are solved by the "trajectory cleaner" and a maximum number of track candidates is kept;
- the final fit of the track is performed with the "trajectory smoother", which uses all the collected hits to estimate the track parameters at each layer through a backward fit.

The bremsstrahlung emission introduces, in general, non Gaussian contributions to the event by event fluctuations of the calorimetry and tracking measurements. Additional electron tracks from conversion of secondary photons, actually the first stages of an "electromagnetic showering", contribute to the energy lost in front of the ECAL. More elaborate reconstruction procedures, involving recognition of distinct track supercluster patterns are in general needed to better disentangle the sources of partial energy containment in the supercluster, adapt the energy scale corrections and estimate associated errors. The electron direction is obtained from the associated primary track. The main background for isolated primary electrons in CMS comes from "fake" electrons from hadron overlaps in jets, but also prompt electrons from semileptonic decays of mostly c or b quarks, and possibly electrons from early photon conversions in the tracker material. The bremsstrahlung emission and secondary conversions which accompany real electrons complicate the identification strategy. Whether the electron measurements are compatible with a small amount of bremsstrahlung or, on the contrary, characterized by considerable ϕ spread and secondary conversions, is likely to affect electron identification and background rejection performance. The definition of variables for electron identification profits from the classification of electron patterns.

The classification groups electrons in four classes:

- golden electrons: electrons least affected by radiation emission, with a reconstructed track well matching the supercluster and well behaved in supercluster pattern;
- big brem electrons: electrons with a good track supercluster geometrical matching, a

well behaved supercluster pattern, and no evidence of energy loss effects from secondary photon conversion despite a very large measured bremsstrahlung fraction;

- narrow electrons: electrons have significantly large bremsstrahlung fraction but not as high as for big brem, a rather well behaved supercluster, a relaxed track supercluster geometrical matching;
- showering electron: remaining electrons, failed other prescriptions ("bad" electrons).

Electrons identification makes use of a complete set of estimators. The estimators are combined to establish full compatibility of observations with the expectations from single electrons. The performance (efficiency, rejection power, purity) of this identification depends of course on the degree of isolation imposed on the electron candidates and on the nature of the considered background. It also depends on the quality requirements imposed on the electron objects themselves. In general, the "well measured" and the "badly measured" electrons are likely to be differently affected by possible fake background sources. Finally, the distinction between multi clusters and single cluster electron patterns is expected to play an important role in the separation of electron from "fake" electrons in QCD jets formed by overlapping particles. A dedicated study shows that jet from the QCD jet background is found to have a probability of 18.5% to give a "fake" reconstructed electron with p_T in the range from 5 to 50 GeV. The jet background is discriminated by a precise matching in energy and position between the calorimeter cluster and the track and by the use of shower shape variables. Indeed, hadron showers are longer and broader, and subject to larger fluctuations, than electromagnetic showers. The bremsstrahlung, however, affects the electron identification capability. The electron shower shape, in particular in the ϕ projection, appears distorted. On the other hand, the emission of radiation in the tracker volume is a characteristic almost exclusive to electrons.

Some variables coming from classification improve the electron identification procedure:

- the ratio of energy deposited in the HCAL tower just behind the electromagnetic seed cluster over the energy of the seed cluster H/E;
- the ratio between the energy sums over 3X3 crystal matrices and the energy sums over 5X5 crystal matrices Σ_9/Σ_{25}, these clusters are centered on the highest energy crystal (seed crystal) of the seed cluster;
- the shape variable $\sigma_{i\eta i\eta}$ defined from the crystals i and the seed crystal s of the seed cluster $\sigma_{i\eta i\eta} = \sum_{crystals}(\eta_i - \eta_s)^2 \frac{E_i}{E_{seedcluster}}$;
- the shape variable $\sigma_{i\phi i\phi}$ defined from the crystals i and the seed crystal s of the seed cluster $\sigma_{i\phi i\phi} = \sum_{crystals}(\phi_i - \phi_s)^2 \frac{E_i}{E_{seedcluster}}$;
- the energy-momentum matching obtained by matching the corrected supercluster energy E_{corr} with the track momentum p_{in} taken at the closest position from the nominal vertex;
- the geometrical matching is performed taking the track parameters at interaction vertex (η_{in}, ϕ_{in}) extrapolating to the ECAL assuming a perfect helix, and matching the resulting $(\eta_{extrap}, \phi_{extrap})$to the energy weighted position of the supercluster (η_{sc}, ϕ_{sc}): $|\Delta\eta_{in}|$ and $|\Delta\phi_{in}|$;

In the analysis, the object electron has the following features (selections for end cap are in brackets):

- the electron pseudo rapidity is inside the geometrical regions covered by ECAL detector: $|\eta| < 2.4$, $\notin [1.4442, 1.566]$;

- the first defined matching variable is $|\Delta\phi_{in}| < 0.15(0.10)$;
- the second defined matching variable is $|\Delta\eta_{in}| < 0.007(0.009)$;
- the defined cluster shape covariance variable is $\sigma_{i\eta i\eta} < 0.01(0.03)$;
- the energy ratio variable is $H/E < 0.12(0.1)$;
- the conversion rejection parameters is applied to solve electron-photon disambiguation;
- the impact parameter with respect to the primary vertex in the transverse plane is $|d_{0,pv}| < 0.01(0.01)$ cm;
- the impact parameter is $|d_{z,pv}| < 0.2(0.2)$ cm;
- the difference between the inverse defined quantities E_{corr} and p_{in} is $|\frac{1}{E_{corr}} - \frac{1}{p_{in}}| < 0.05(0.05)$;
- the isolation with Delta Beta PU correction in cone size 0.3 is Iso$< 0.15(0.15)$.

These conditions optimize the selection efficiency with respect to the purity.

5.2.9 Variables from objects quantities

Some variables are build from objects quantities.

The hadron activity variable H_T is the N jets p_T sum in the events:
$H_T = \sum_{jets=0}^{N} p_T$

The lepton activity variable is the N leptons p_T sum (in the seesaw type III analysis N=3):
$L_T = \sum_{lepton=0}^{N} p_T$

The transverse mass is the relationship between lepton and E_T^{miss}:
$M_T = \sqrt{(2. * p_T[E_T^{miss}] * p_T[lepton] * (1 - cos(\phi[lepton] - \phi[E_T^{miss}])))}$

The sum of all objects activity is:
$S_T = H_T + L_T + E_T^{miss}$

5.3 Standard Model background samples

In the analysis, the SM processes are physical backgrounds. The dominant contribution comes from WZ production (diboson class). ZZ production (diboson class) and triboson class, mainly WWW production give background events. Other SM processes are taken in account in analysis flow: WW (diboson class), $t\bar{t}$, W+jet, Z+jet and DY. Contributions coming from diboson production are irreducible background.

The WZ sample of $\sim$ 10 M events is produced with PYTHIA generator [56]. All the leptonic final states were simulated for the Z and W bosons decays. For the final states into taus, the tau-lepton decays are simulated using the TAUOLA package [74]. The CMS measured cross section is (24.6 $\pm$ 1.7) pb [75].

The ZZ sample of $\sim$ 10 M events is produced with PYTHIA generator [56]. All the leptonic final states were simulated for the Z bosons decays. For the final states into taus, the tau lepton decays are simulated using the TAUOLA package [74]. The CMS measured cross section is (8.4 $\pm$ 1.3) pb [76]. ZZ is a background source when the Z bosons both decay in l^+l^-, but one of the four leptons is missing due to the detector inefficiencies.

The WW sample of $\sim$ 10 M events is produced with PYTHIA generator [56]. All the leptonic final states were simulated for the W bosons decays. For the final states into taus, the tau lepton decays are simulated using the TAUOLA package [74]. The CMS measured cross section is (69.9 $\pm$ 7.0) pb [76].

The WWW sample of $\sim$ 221 k events is produced with MADGRAPH generator [55]. The calculated cross section at NLO is 0.08 pb.

The $t\bar{t}$ sample of $\sim$ 12 M events is produced with MADGRAPH generator. The tau lepton decays are simulated using the TAUOLA package [74]. The CMS measured cross section is (25.32 $\pm$ 1.34)pb [77].

The W+jet sample of $\sim$ 58 M events is produced with MADGRAPH generator. The CMS measured cross section is (35,640 $\pm$ 560) pb [78].

The Z+jet sample (leptons invariant mass above 50 GeV) of $\sim$ 30 M events is produced with MADGRAPH generator. The CMS measured cross section is (3,503 $\pm$ 171) pb [78].

The "DY" sample (leptons invariant mass between 10 and 50 GeV) of $\sim$ 38 M events is produced with MADGRAPH generator. The calculated cross section at LO is 11,050 pb.

Table 5.2 recaps information about SM MC sample investigating in the analysis flow. The luminosity equivalent (L) is the ratio number of generated MC events in the sample over production cross section σ. The ratio integrated luminosity (data) over equivalent luminosity gives the luminosity scale factor to be applied as weight on each background. MC background, MC signal and data events are reconstructed and processed using the same CMS tools. More details about MC background samples are in the Appendix D.

Table 5.2: MC background samples information at $\sqrt{s}$ =8 TeV.

Background	σ (pb)	equivalent L (fb^{-1})	Reference
WZ	24.6	406.35	measured SMP-12-006 [75]
ZZ	8.4	1,165.27	measured SMP-12-024 [76]
WWW	0.08	2,684.29	generator MC@NLO at NLO
WW	69.9	143.07	measured SMP-12-024 [76]
$t\bar{t}$	25.32	504.68	measured TOP-12-007 [77]
W+jet	35,640	1.54	measured SMP-12-011 [78]
Z+jet	3,503	8.69	measured SMP-12-011 [78]
DY	11,050	3.43	generator MADGRAPH at LO

5.4 Data samples and triggers selection

The analysis is performed on a data sample collected during the 2012 pp collisions data taking period (Table 5.3). The data sets called "DoubleEle" (DE), "DoubleMu" (DM), and "MuE" (ME) contain the events selected by the dilepton HLT algorithms. For the analysis, the selected HLT paths are described in Table 5.4. The events are triggered by a two leptons (electrons or muons) exceeding defined p_T thresholds at 17 GeV and 8 GeV. On line reconstructed electrons pass quality checks about calorimetric and track quantities, too. A triggered event could be present in different data sets, so a dedicated logic does not allow the double counting event. More details about data samples are in the Appendix D.

Table 5.3: Data taking run periods in 2012 pp collisions at 8 TeV, and the corresponding integrated luminosity.

Run period	Run range number	DE Lumi (fb^{-1})	DM Lumi (fb^{-1})	ME Lumi (fb^{-1})
Run A	190456 - 193621	0.876	0.876	0.876
Run B	193833 - 196531	4.412	4.412	4.412
Run C	198022 - 203742	7.055	7.017	7.055
Run D	203777 - 208686	7.369	7.369	7.360
Total	190456 - 208686	19.710	19.674	19.703

Table 5.4: The selected HLT paths.

HTL paths	Version
HLT_Ele17_CaloIdT_CaloIsoVL_TrkIdVL_TrkIsoVL_Ele8_CaloIdT_CaloIsoVL_TrkIdVL_TrkIsoVL	15,16,17,18,19
HLT_Mu17_Mu8	16,17,18,19,21,22
HLT_Mu17_Ele8_CaloIdT_CaloIsoVL_TrkIdVL_TrkIsoVL	4,5,6,7,8,9
HLT_Mu8_Ele17_CaloIdT_CaloIsoVL_TrkIdVL_TrkIsoVL	4,5,6,7,8,9

The trigger efficiencies, measured using events collected with hadronic triggers at $\sqrt{s} = 8\ TeV$ in 2012, are derived according to Reference [79], and reported in Table 5.5.

Table 5.5: Trigger efficiencies for low p_T selection ($p_T > 10$ GeV) and high p_T selection ($p_T > 20$ GeV).

Note	$\mu\mu$	ee	μe
two leptons low p_T	0.94±0.06	0.93±0.06	0.93±0.06
two leptons high p_T	0.90±0.05	0.92±0.06	0.93±0.06

The minimum of the two lepton trigger efficiencies reduced by 1 σ is 85%, the maximum increased by 1 σ is 100%. The worst case scenario is the $\sim$ 15% loose of the dilepton events using the dilepton triggers. Looking for three leptons events, it is realistic to suppose that the third lepton could fire the dilepton trigger at least with one of the first two leptons. The additional trigger probability due to the third lepton will be 85% times 15%, equal to 13%. The total trigger probability will be 85% plus 13%, equal to 98%. In the analysis, a conservative value of dilepton triggers efficiency for three leptons events is considered: (98±2)%.

5.5 Events selection

The reconstructed events with the following physics objects in final state are selected, according with expected signature:

- exactly three charged isolated leptons (electrons or muons);
- the leptons transverse momentum p_T above 20, 10, 10 GeV thresholds, respectively;
- three leptons charge sum $= \pm 1$.

The event cleanup and vertex selection procedures are applied on interesting triggered events at analysis PAT step. During each bunch crossing, many vertices are produced (PU). Each event has a vertex collection associated to it that is ordered by the sum of squared track p_T. The triggered events are cleaned up by requiring:

- beam background removal:

  if $N_{tracks} \geq 10$, require at least 25% of them to be high purity (see Section 5.2.1);
- at least one good vertex with:

  distance from the center of the detector in z direction: $|z| < 24\ cm$;

  distance from the center of the detector in the transverse plane: $|\rho| < 2\ cm$;

  number of degrees of freedom: $N(dof) > 4$;
- hadronic calorimeter barrel and end caps sections noise filtering.

5.6 Signal and SM backgrounds

The signal and SM backgrounds characterization drives the choice about thresholds on physical quantities and variables. The goal is background reduction and signal preservation and the significance, defined by the Formula 5.1, is used:

$$S = \frac{N_{Signal}}{\sqrt{N_{Backgrounds} + N_{Signal}}} \tag{5.1}$$

The thresholds set is common to all signals, because the optimization process for each mass points does not really improve results. Signal at 180 GeV sign + is selected, as delegate, to perform study, because it corresponds to the upper limit value fixed by CMS with 2011 data [51].

Figure 5.6 shows E_T^{miss} distribution on selected events, and, in the lower plot, the significance as a function of E_T^{miss}. The choice for the E_T^{miss} selection gives about the maximum of significance: E_T^{miss} >50 GeV.

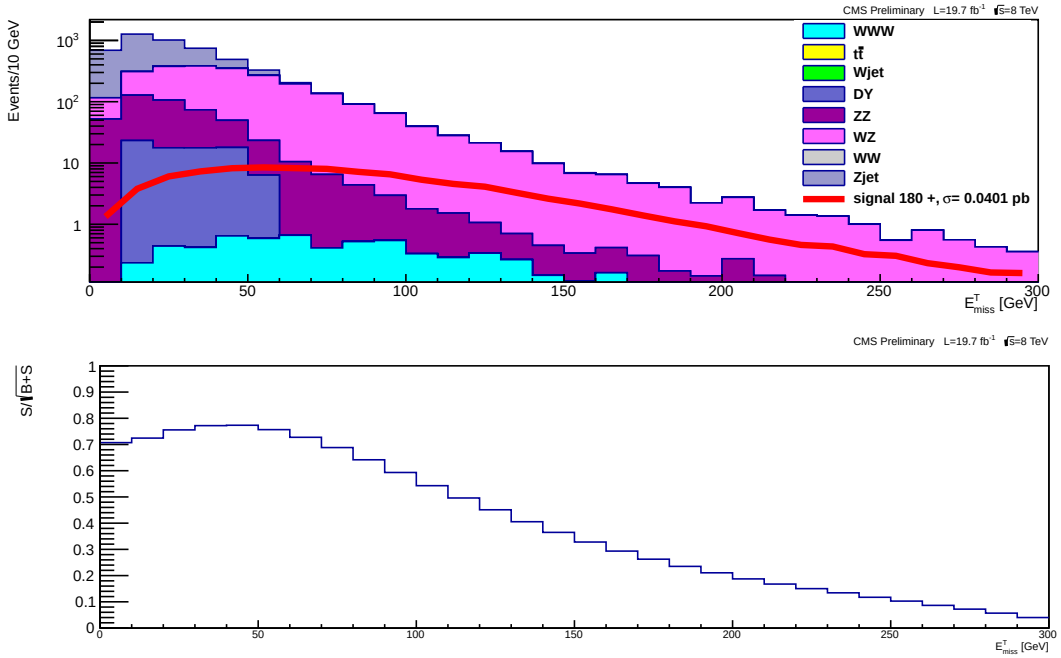

Figure 5.2: E_T^{miss} distribution on selected events. In the lower plot the significance as a function of E_T^{miss}. Reference signal is mass 180 sign +.

Figures 5.3 and 5.4 show H_T distribution on selected events and after E_T^{miss} selection, respectively. There is a background tail for high H_T values without a clear evidence in the significance distribution of the best H_T selection. The selection H_T <150 GeV has defined as one optimization with the full set of cuts. Figures 5.5 and 5.6 and 5.7 show b tag CSV variable distribution for the jet with the highest p_T in the event at three levels of selection: on selected events, and after E_T^{miss} step, and after $E_T^{miss} + H_T$ step, respectively.

E_T^{miss} lower threshold reduces SM background because V+jets and the dibosons events have less E_T^{miss} respect to the signal. The selections on H_T and on first jet in p_T b tag CSV value reduce the SM backgrounds, too. No request on total number of jets is applied.

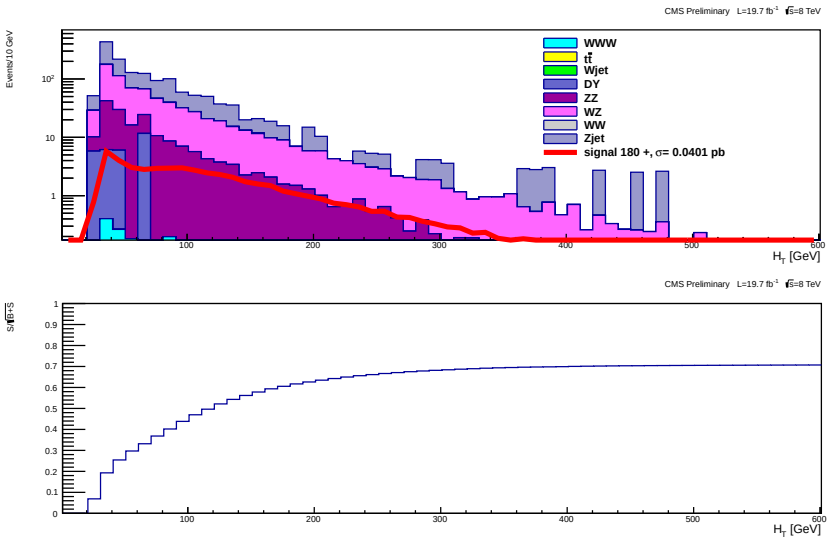

Figure 5.3: H_T distribution on selected events. In the lower plot the significance as a function of H_T. Reference signal is mass 180 sign +.

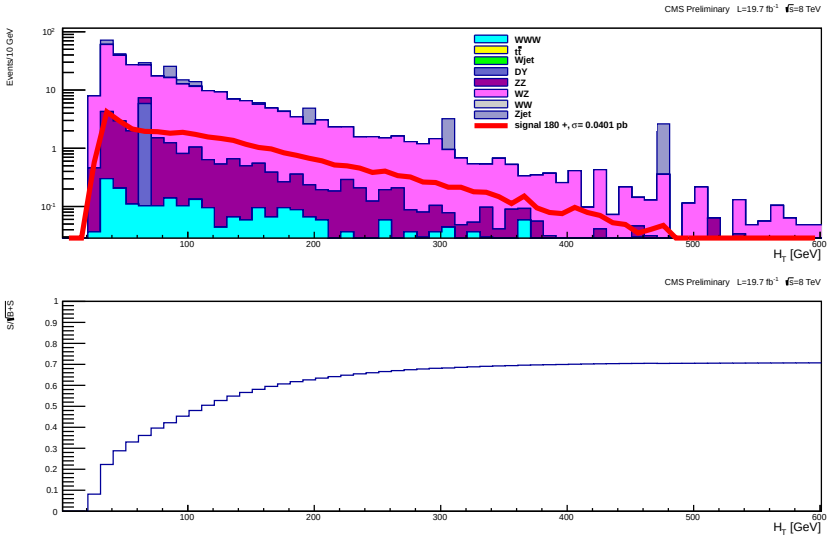

Figure 5.4: H_T distribution on selected events, and E_T^{miss} selection. In the lower plot the significance as a function of H_T. Reference signal is mass 180 sign +.

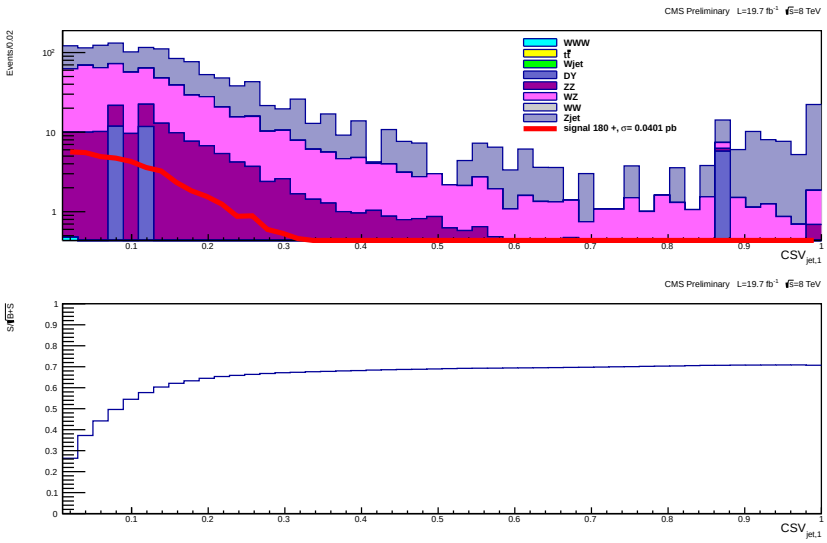

Figure 5.5: First jet in p_T Combined Secondary Vertex b tag distribution on selected events. In the lower plot the significance as a function of first jet in p_T CSV b tag. Reference signal is mass 180 sign +.

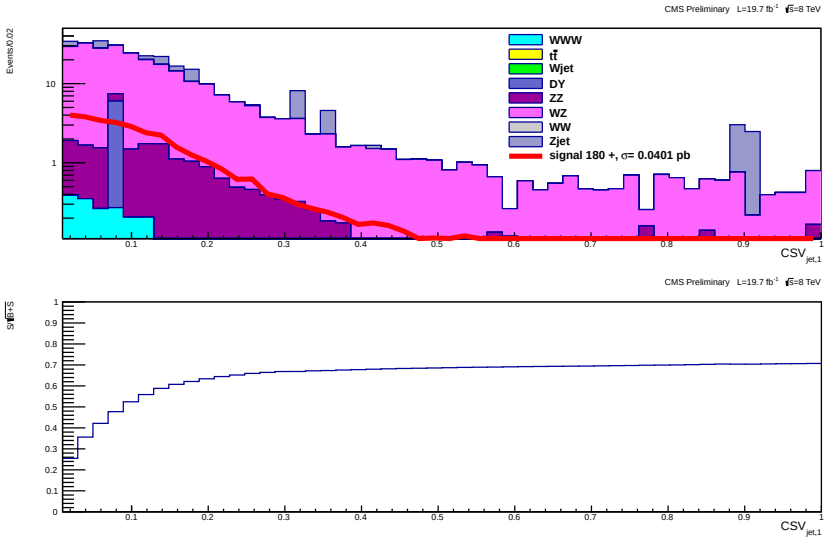

Figure 5.6: First jet in p_T Combined Secondary Vertex b tag distribution on selected events and E_T^{miss} selection. In the lower plot the significance as a function of first jet in p_T CSV b tag. Reference signal is mass 180 sign +.

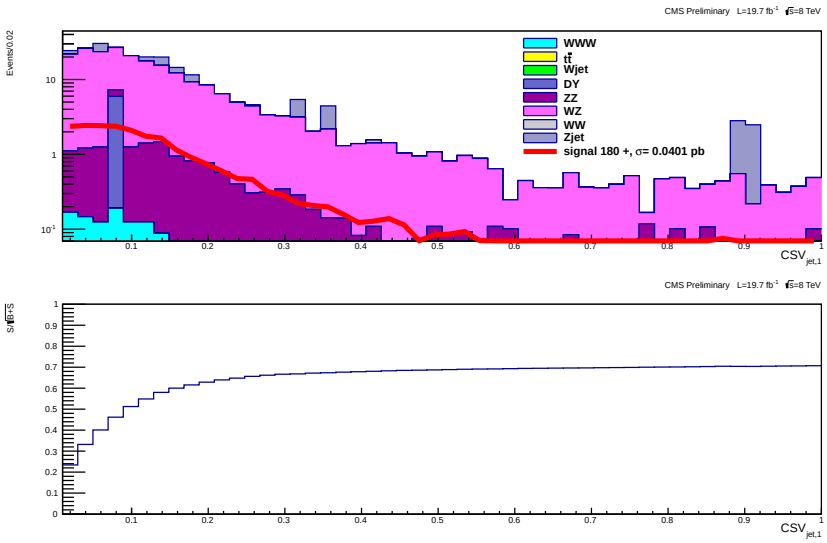

Figure 5.7: First jet in p_T Combined Secondary Vertex b tag distribution on selected events and E_T^{miss} and H_T selections. In the lower plot the significance as a function of first jet in p_T CSV b tag. Reference signal is mass 180 sign +.

The invariant mass for the OSSF leptons is required to be outside the Z mass peak $|m(Z) - M(ll)| < 15$ GeV to reduce the Z+jet background contribution, and to be larger than 12 GeV to remove the leptonic decay of small mass resonances. Figures 5.8 and 5.9 show the Z peak of the OSSF invariant mass for electrons and muons, before the Z mass cut.

The asymmetric conversions for Z+γ events (Dalitz) are not properly simulated in MC. The most important contributions, related to the four categories $e^{\pm}e^{\pm}e^{\mp}$ and $\mu^{\pm}e^{\pm}\mu^{\mp}$ are removed with the three lepton invariant mass selection: $|m(Z) - M(lll)| < 15$ GeV. The Dalitz contributions in the other categories are estimated with the data driven method described in the Section 5.7.

Finally, the following requests have effects on the triggered and selected events:

- $E_T^{miss} > 50$ GeV;
- $H_T < 150$ GeV;
- first jet in p_T CSV b tag value < 0.244;
- if OSSF pair, $M_{ll} > 12$ GeV;
- if OSSF pair, $M_{ll} < 76$ GeV or $M_{ll} > 106$ GeV (Z veto);
- if OSSF pair, $M_{lll} < 76$ GeV or $M_{lll} > 106$ GeV only for categories $e^{\pm}e^{\pm}e^{\mp}$ and $\mu^{\pm}e^{\pm}\mu^{\mp}$ (Z Dalitz veto).

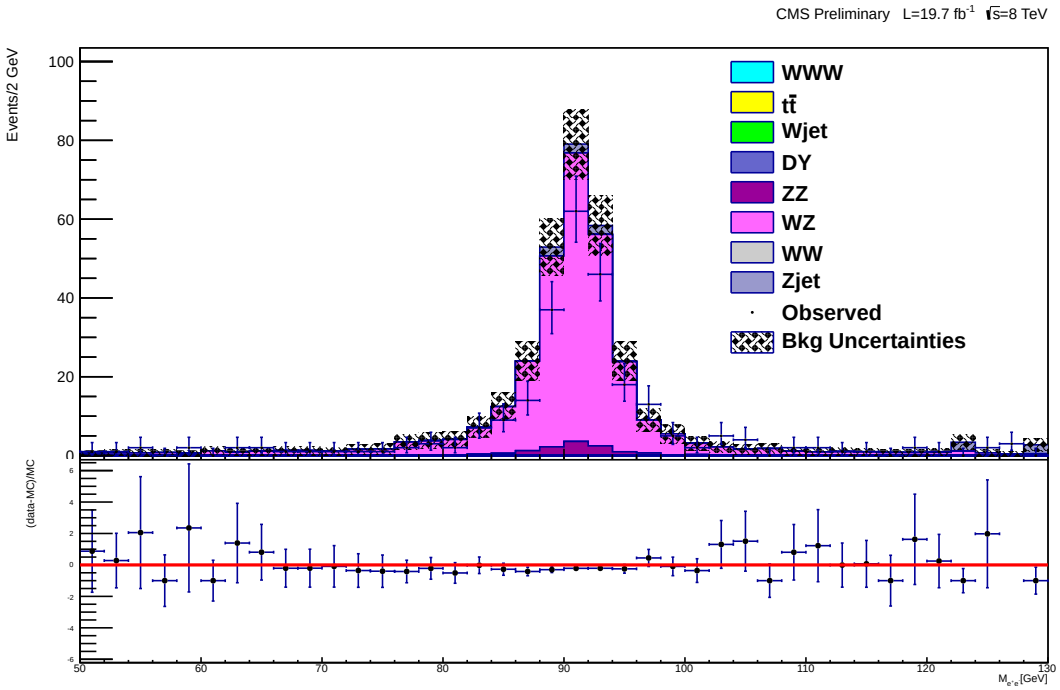

Figure 5.8: Z mass peak in electrons decay on selected events and after selections on E_T^{miss}, H_T, first jet in p_T CSV b tag value.

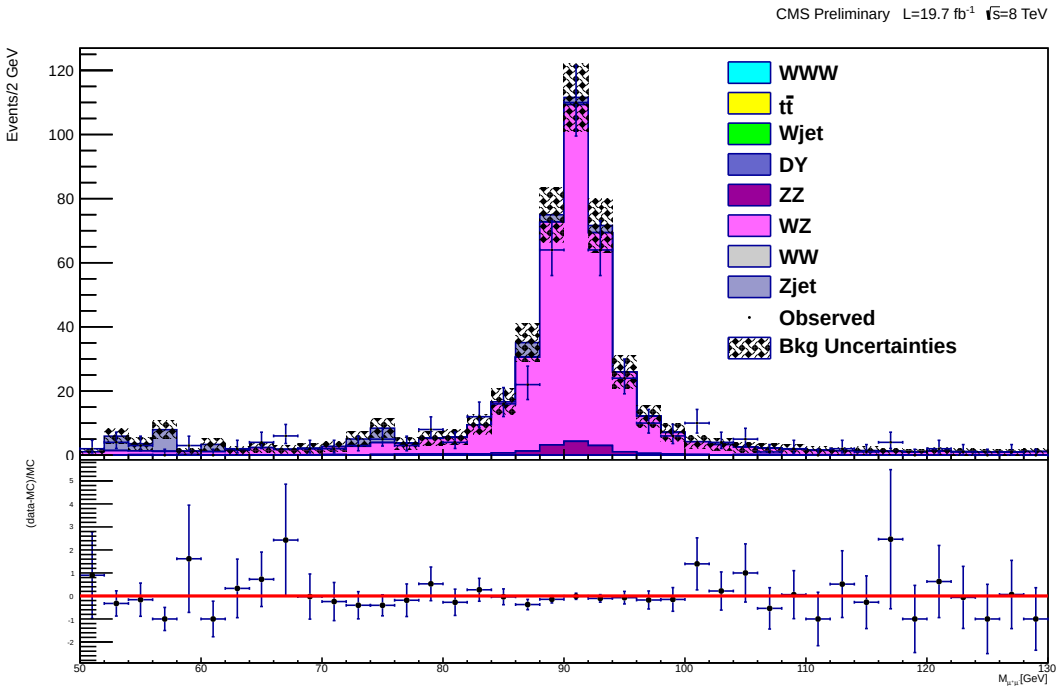

Figure 5.9: Z mass peak in muons decay on selected events and after selections on E_T^{miss}, H_T, first jet in p_T CSV b tag value.

5.7 Photon asymmetric conversion background determination (Dalitz)

Photon conversions contributions, in presence of W or Z boson (Vγ), are physical backgrounds. There are two different types of photon conversions:

- external conversions: a photon radiates in the external magnetic field of the detector or interacts with the material in the detector and generates an opposite sign same flavor lepton pair (primarily, e^+e^- pair). The ratio of the rate of external conversions from this final state radiation to e^+e^- versus $\mu^+\mu^-$ is between 6.0 $*10^4$ and 2.0 $*10^5$ [80].
- internal or asymmetric conversions: virtual photon γ^* decays and one lepton takes almost the photon energy and the other lepton is soft and not detected. Electrons and muons have almost the same probability to be involved.

The FSR contribution is dominated by radiation from electrons in Z boson decay (Figure 5.10 from reference [80]). Events exhibit a three bodies invariant mass of l^+l^-l close to the Z mass, as expected from the dominance of asymmetric conversions, so one of the leptons from the converted photon has a low energy and escapes detection. A selection on the OSSF invariant mass reduces the external conversion contribution. MC generators simulate internal conversion of emitted photon, but they have a cut off on the momentum of the converted lepton, therefore the contribution from this process is not properly accounted.

The estimation of the background contribution due to internal photon conversion is done with a data driven method. The number of $l^+l^-\gamma^*$ with external conversion is estimated with the number of events where the two leptons invariant mass is inside the Z mass peak with 15 GeV of tolerance. The number of $l^+l^-\gamma^*$ with internal conversion is estimated with the number of events where the three leptons invariant mass is inside the Z mass peak with 15 GeV of tolerance. The overlap between the two categories is removed with the selection described in Figures 5.13 and 5.14. The external conversions are ~ 100 times more abundant with respect to the internal ones, and they can be estimated also with the full selection chain. The assumption is that the ratio between these two numbers calculated at the pre selection step remains the same after the full selection. The ratios evaluated for electrons and muons are called conversion factors C. The measured C_e is (2.1 ± 0.3)%; the measured C_μ is (0.7 ± 0.1)% (see Reference [81]).

Figure 5.11 from Reference [80] shows the three-bodies $l^+l^-e^\pm$ peak where OSSF pair does not make a Z candidate.

Figure 5.12 from Reference [80] shows the three-bodies $\mu^+\mu^-\mu^\pm$ peak where OSSF pair does not make a Z candidate. The 3μ plot is interesting because there is essentially no contributions from external conversions, and the peak shown is entirely from internal conversions.

Figures 5.13 and 5.14 show the three leptons invariant mass versus the two leptons invariant mass for muons and electrons OSSF pairs.

Figures 5.15 and 5.16 depict the three bodies invariant mass $l^+l^-\gamma^*$, where the mass l^+l^- is outside the Z peak mass with 15 GeV of tolerance, in 2012 data concerning the analysis.

After the analysis flow selections, events that have an invariant mass $l^+l^-\gamma^*$ in Z mass peak [76;106] GeV, are counted. The measured conversion factors C_e and C_μ are applied on number of Dalitz events. In the four categories where Dalitz contribution is the most relevant, the events is removed with the three leptons invariant mass selection, in the categories $\mu^\pm\mu^\pm e^\mp$ and $\mu^\pm e^\pm e^\mp$ the Dalitz contribution is estimated. Table 5.6 (Table 5.7) shows the numbers of Dalitz events (with errors). The symbol "na" stays for not applicable because SSSF leptons are

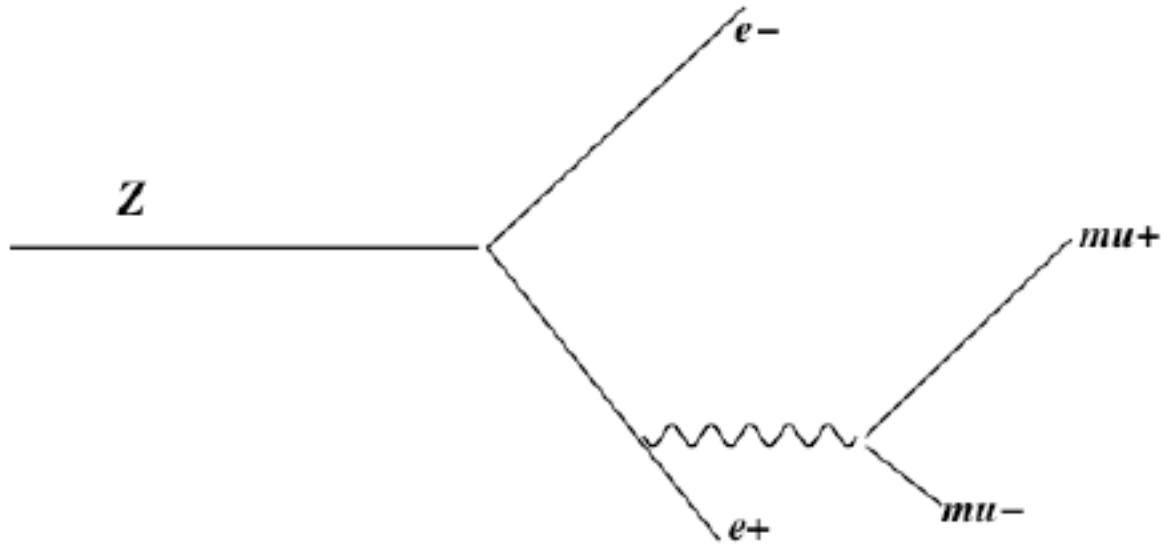

Figure 5.10: A Feynman diagram showing a Z decay to electrons, and an asymmetric FSR decay to muons (indicated by length of the muon legs).

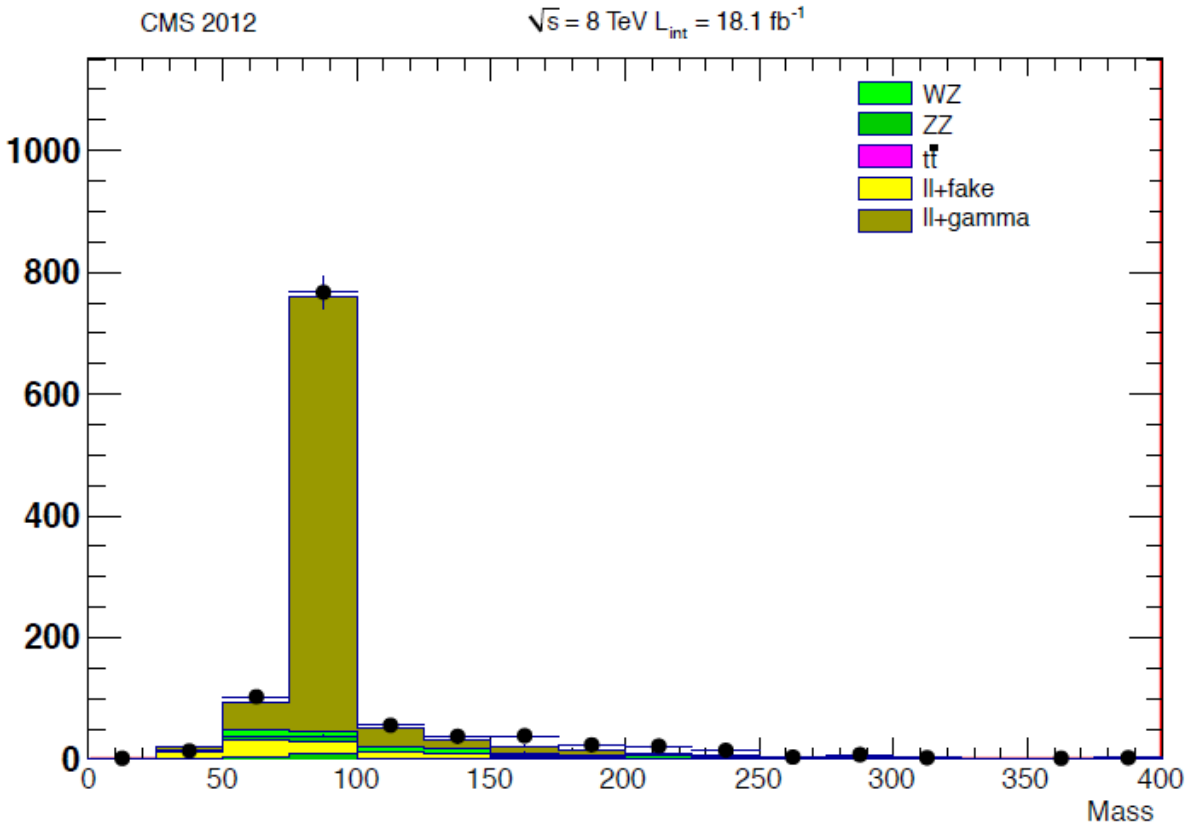

Figure 5.11: M($l^+l^-e^\pm$) where M(l^+l^-) is either < 75 GeV or > 105 GeV. Note that most external conversions to electrons have already been removed in the electron identification requirements.

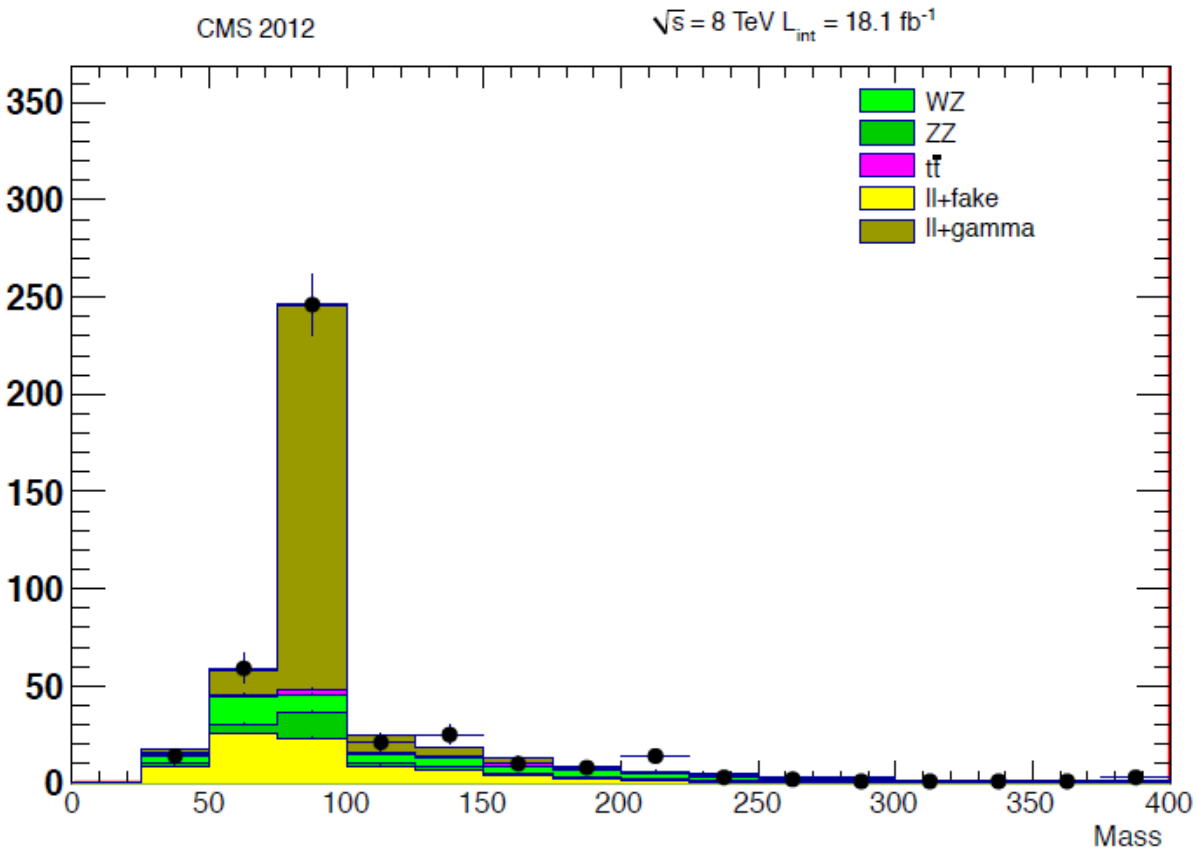

Figure 5.12: M($\mu^+\mu^-\mu^\pm$) where M($\mu^+\mu^-$) are either < 75 GeV or > 105 GeV.

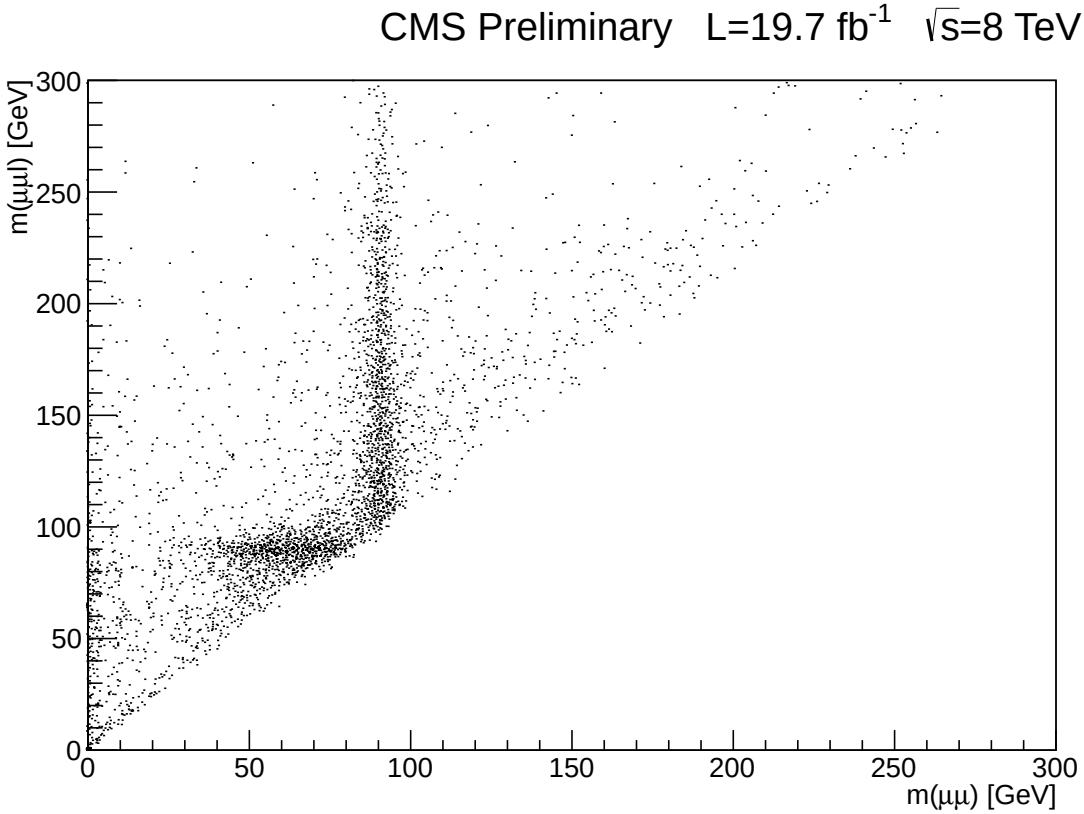

Figure 5.13: Dalitz events in data for $\mu^+\mu^+\mu^-$ and $\mu^-\mu^-\mu^+$ categories. Third lepton carries out almost all γ^* energy.

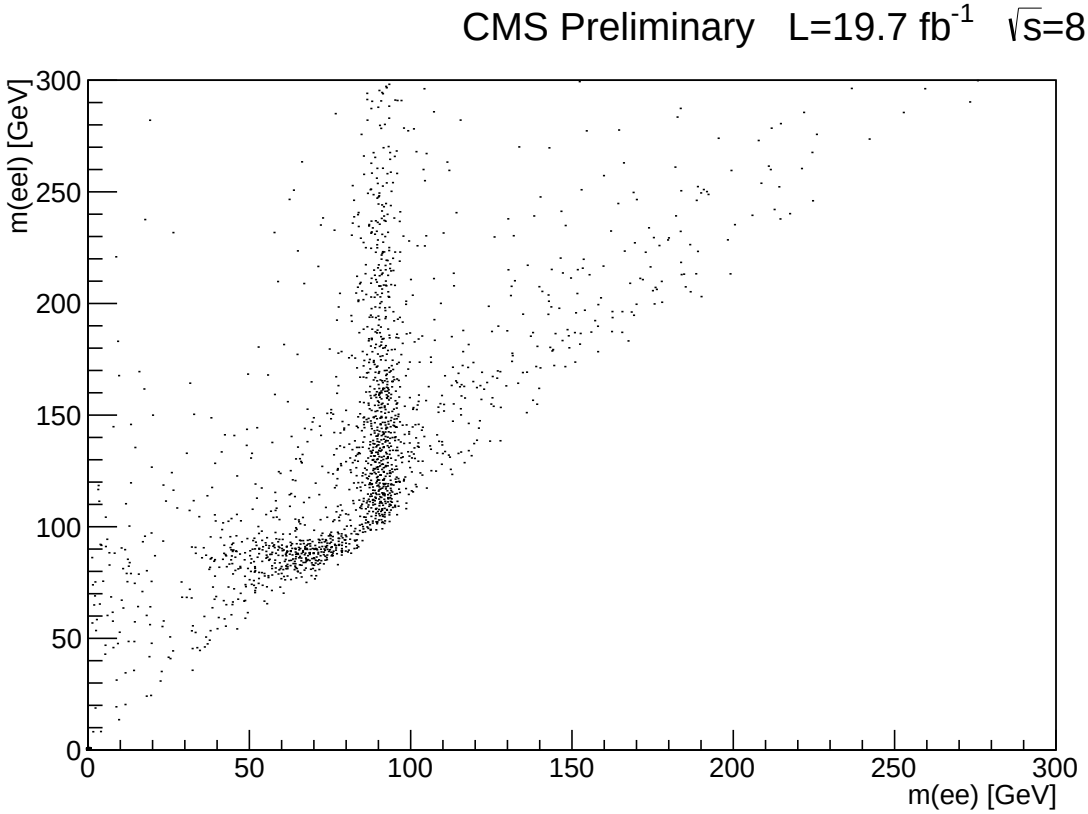

Figure 5.14: Dalitz events in data for $\mu^+e^+e^-$ and $\mu^-e^-e^+$ categories. Third lepton carries out almost all γ^* energy.

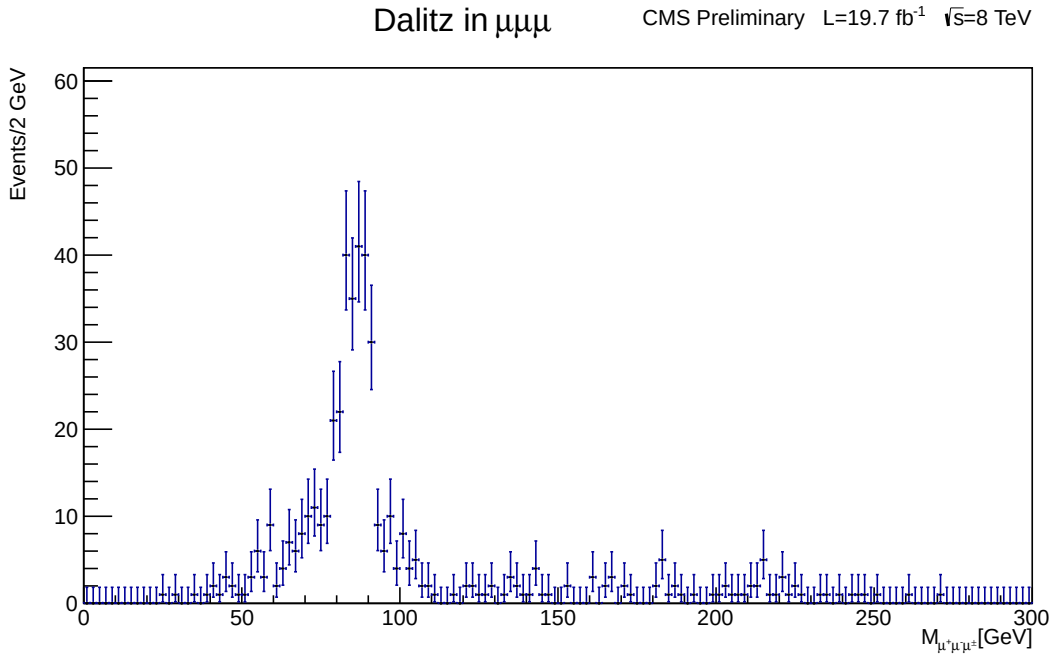

Figure 5.15: Invariant mass spectrum in data for $\mu^+\mu^+\mu^-$ and $\mu^-\mu^-\mu^+$ categories.Third lepton carries out almost all γ^* energy.

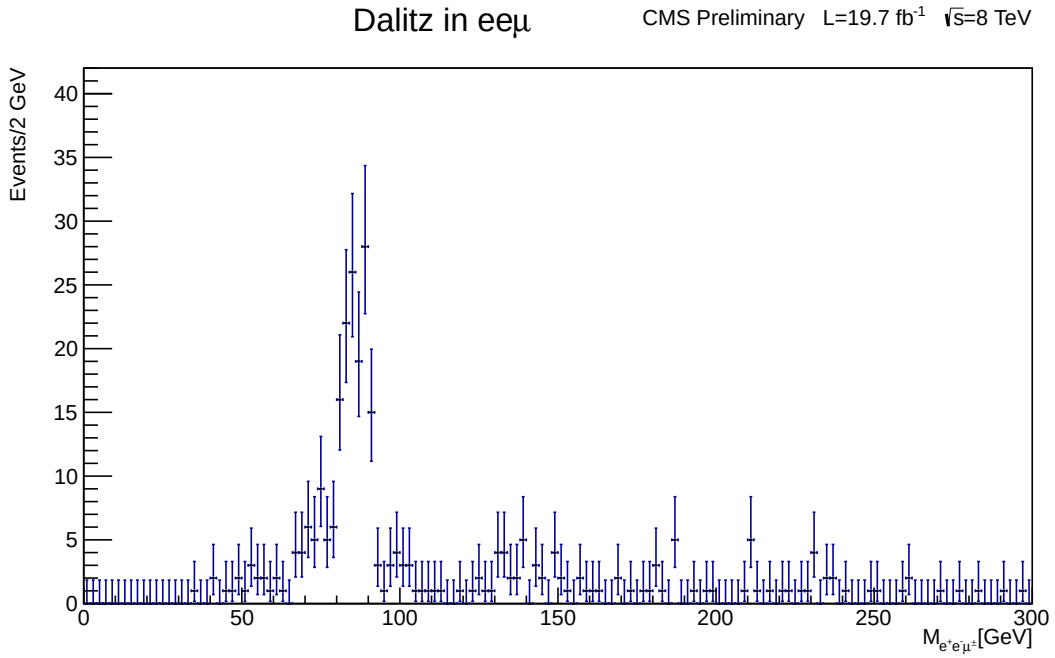

Figure 5.16: Invariant mass spectrum in data for $\mu^+e^+e^-$ and $\mu^-e^-e^+$ categories. Third lepton carries out almost all γ^* energy.

present, the words "not used" are related to Z asymmetric conversions selection.

Systematic error on Dalitz contribution is 50%, considered the data driven evaluation method.

Table 5.6: Number of Dalitz events.

Category	Events in Z peak	C factor	Dalitz	Dalitz event per cat
$\mu^\pm\mu^\pm\mu^\mp$	391	0.007	2.74	1.37
$e^\pm e^\pm e^\mp$	360	0.021	7.56	not used
$\mu^\pm\mu^\pm e^\mp$	na	na	na	na
$\mu^\pm e^\pm\mu^\mp$	1626	0.007	11.38	not used
$e^\pm e^\pm\mu^\mp$	na	na	na	na
$\mu^\pm e^\pm e^\mp$	298	0.021	6.26	3.13

Table 5.7: Number of Dalitz events with errors.

Category	Events in Z peak	C factor	Dalitz	Syst	Dalitz event per cat
$\mu^{\pm}\mu^{\pm}\mu^{\mp}$	391	0.007±0.001	2.74 ±0.42 (15%)	50%	1.37±0.72 (52%)
$e^{\pm}e^{\pm}e^{\mp}$	360	0.021±0.003	7.56 ±1.15 (15%)	50%	not used
$\mu^{\pm}\mu^{\pm}e^{\mp}$	na	na	na	na	na
$\mu^{\pm}e^{\pm}\mu^{\mp}$	1626	0.007±0.001	11.38 ±1.65 (15%)	50%	not used
$e^{\pm}e^{\pm}\mu^{\mp}$	na	na	na	na	na
$\mu^{\pm}e^{\pm}e^{\mp}$	298	0.021±0.003	6.26 ±0.97 (15%)	50%	3.13±1.63 (52%)

5.8 Non prompt leptons background determination (Fake)

Instrumental background is due to leptons that do not come from primary interaction vertex. Non prompt isolated leptons from W, Z, γ or other SM processes are defined "fake leptons". For example, muons from kaons and pions decaying in flight, electrons or muons from heavy flavor decays are "fake leptons". Possible "fake leptons" sources are:

- $t\bar{t}$ where $t \to Wb$. Three leptons in final state come from two W bosons decay $W \to l\nu$ and one b quark semileptonic decay;
- $b\bar{b}$ where $b \to Wc \to W(Wd)$ and three W bosons decay $W \to l\nu$;
- WW+jets where a third lepton is fake;
- $t\bar{t}W^{\pm}$jets, $t\bar{t}$WW,$t\bar{t}$Z where the presence of one or two bosons in addition to $t\bar{t}$ gives three leptons in final state, if t decays semileptonically;
- Drell-Yan (γ^* and Z) and QCD.

Analysis reconstructed objects features and the selections on events reduce contributions from the non prompt leptons sources. Leptons isolation criteria act on $t\bar{t}$, $b\bar{b}$, WW+jets, and QCD processes. Moreover, the invariant mass of two leptons coming from the same parent b quark is below 12 GeV, and selection on the OSSF invariant mass has impact on $b\bar{b}$. The $t\bar{t}$V(V) cross sections are smaller than other processes, so contributions are not relevant.

The background contribution due to fake leptons is estimated with a data driven method. The procedure is in two steps: first, the average fake rate is determined using control samples. Secondly, the fake rate is applied to the events selected by the analysis. The Fake Rate FR is defined as the probability for a loose lepton to pass the tight identification selection in samples where the presence of prompt isolated leptons is suppressed, and therefore almost all leptons are candidate fakes. The tight selection picks out the "A leptons" (A stays for Analysis leptons). The loose selection picks out the "F leptons" (F stays for Fake leptons). So the FR formula is $FR = \frac{N(A)}{N(F)}$.

The tight lepton is defined in Sections 5.2.7 and 5.2.8.

In the analysis, the loose muon has the following features (selections for tight muon are in square brackets):

- the χ^2 over number of degree of freedom (normalized χ^2) of the global muon track fit is $\chi^2/\text{ndof} < 50$ [$\chi^2/\text{ndof} < 10$];
- the impact parameter with respect to the primary vertex in the transverse plane is $|d_{0,pv}| < 0.2$ cm [$|d_{0,pv}| < 0.005$ cm];
- the isolation with Delta Beta PU correction in cone size 0.3 is Iso< 0.40 [Iso< 0.10].

In the analysis, the loose electron has the following features (selections for tight electron are in square brackets):

- the impact parameter with respect to the primary vertex in the transverse plane is not present [$|d_{0,pv}| < 0.01(0.01)$ cm];
- the isolation with Delta Beta PU correction in cone size 0.3 is Iso$< 0.60(0.60)$ [Iso$< 0.15(0.15)$].

The main difference between A and F objects is the isolation variable.

The Fake Rate is measured in a sample dominated by non-prompt (fake) leptons, passing the denominator requirements:

- selection events with at least one lepton using single lepton loose triggers;
- suppression contamination from prompt leptons.

The chosen data sample to calculate FR values is called "JetHT": events are triggered by HLT algorithms, where jet has $p_T > 60GeV$ or $H_T > 200GeV$. JetHT samples contains almost all integrated luminosity available in 2012 pp data, as reported in Table 5.8. In addition to the hadronic trigger, a single lepton loose trigger is required with the p_T threshold (17 GeV) corresponding to the highest value in the dilepton triggers used in the analysis.

Table 5.8: Data samples and triggers used in fake leptons procedure.

Info	Name	Note
Data set	$/JetHT/Run2012B-22Jan2013-v1/AOD$	L=4.88 fb^{-1}
Data set	$/JetHT/Run2012C-22Jan2013-v1/AOD$	L=7.21 fb^{-1}
Data set	$/JetHT/Run2012D-22Jan2013-v1/AOD$	L=7.63 fb^{-1}
Trigger	HLT_Mu17_vX	
Trigger	HLT_Ele17_CaloIdL_CaloIsoVL_vX	

On the selected events coming from "JetHT" data set, the following requests are applied:

- one lepton and one jet with opposite direction ($\Delta R(l, jet) > 1.0$);
- the jet $p_T > 60$ GeV;
- $E_T^{miss} < 20$ GeV;
- $M_T(E_T^{miss}, p_T^l) < 20$ GeV;
- if OSSF leptons pair is present, its invariant mass is outside the Z peak mass region defined as [76;106] GeV.

The requests reduce the contamination from prompt leptons due to electroweak processes, such as W or Z production. FR factors depend on A and F object definitions and lepton p_T threshold. A scan in leptons p_T thresholds for five fixed values at two fixed values of isolation is performed both for electrons and muons. Figures 5.17 and 5.18 show the FR factors results for electron and muon, respectively.

Table 5.9 summarizes the Fake Rate calculations. The considered FR is the value resulting with the analysis selections: p_T >10 GeV and Iso<0.10 (0.15) for muons (electrons). Numerator and denominator in FR ratio count hundreds events, so statistical errors are below the systematic uncertainty estimated to be 50% [82].

Table 5.9: Fake Rate factors calculations for electrons and muons.

lepton	p_T [GeV]	Iso	Numerator	Denominator	FR	stat err FR
Electron	>10	0.15	92	303	0.30	0.04
Muon	>10	0.10	284	1902	0.15	0.01

Finally, in the analysis, FR factors are (0.30 $\pm$ 0.04) for electron, (0.15 $\pm$ 0.01) for muon. The arithmetic mean value is used in categories where leptons have different flavors, and it is (0.225 $\pm$ 0.02).

In the analysis context, there are four possible combinations of objects:

- FFF: QCD multilepton events produce all non isolated leptons, but the contribution is negligible due to the selection requirements;

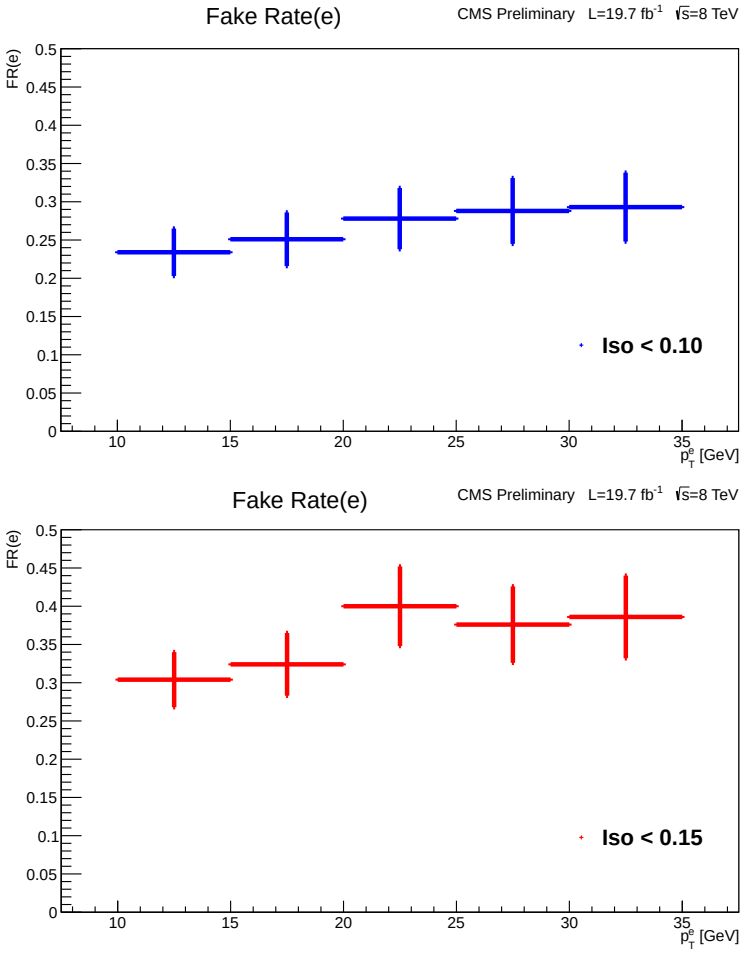

Figure 5.17: FR factors for electrons with statistical error. Five points with p_T above 10, 15, 20, 25, 30 GeV are shown.

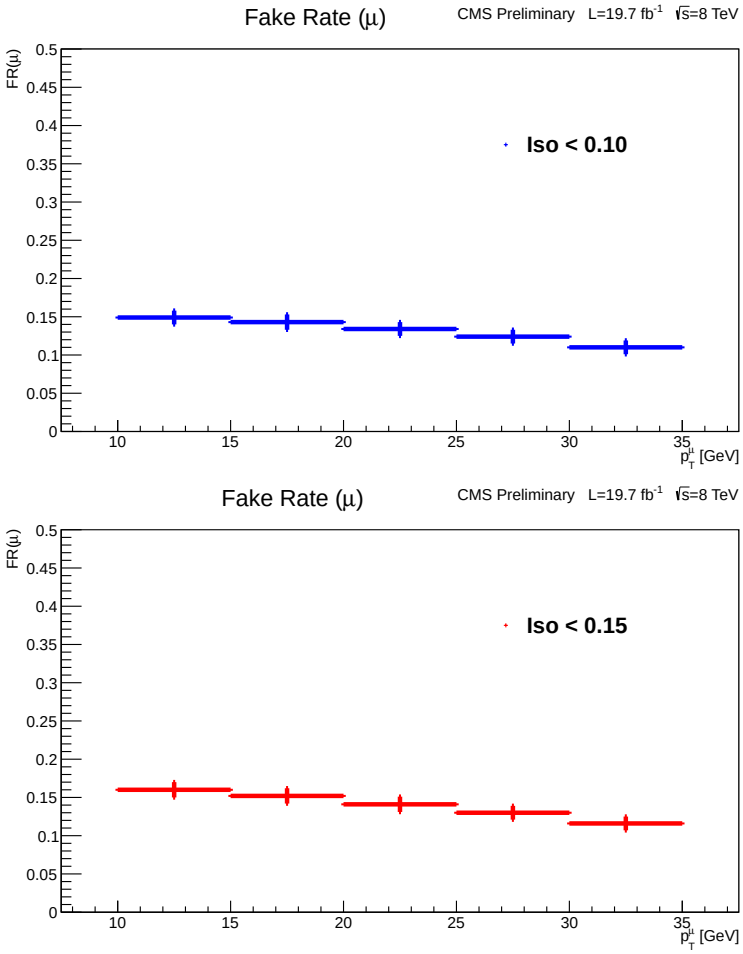

Figure 5.18: FR factors for muons with statistical error. Five points with p_T above 10, 15, 20, 25, 30 GeV are shown.

- AFF: W+jets events produce one isolated lepton and two non isolated leptons, the probability for two fake leptons to pass selection requirements is lower than case of only one F object;
- AAF: Drell Yan+jets, with virtual photon γ^* and Z boson, and WW+jets events produce two isolated leptons and one non isolated lepton, this is the most populate class;
- AAA: analysis events.

To simplify the issue, some assumptions are in place: the probability of a lepton to be fake is independent from the presence of another lepton, and no correlation is included for the fake-fake lepton case (AFF). Assuming case AFF is dominated by QCD where both leptons are fake, a calculation leads function f(FR), neglecting much smaller terms. The contribution from events with one true and one fake lepton ($t\bar{t}$, single top, Wjets) case AAF is determined by function g(FR). Functions f and g are:

- f(FR)= $FR^2 * (1 - FR)^{-2}$ to be applied on AFF combination;
- g(FR)= $FR * (1 - FR)^{-1}$ to be applied on AAF combination.

The fake contribution prediction is given by the difference $g(FR) * N(AAF) - f(FR) * N(AFF)$ events, as reported in Table 5.10, to account for both single and double fakes. The error propagation derivative method assigns the absolute error on the function output. The number of the fake events with errors is reported in Table 5.11 for all the categories.

Table 5.10: Number of the fake events for all the categories.

Category	AAF	AFF	Fake events
$\mu^+\mu^+\mu^-$	25	5	4.26
$e^+e^+e^-$	10	4	3.55
$\mu^+\mu^+e^-$	23	8	6.00
$\mu^+e^+\mu^-$	27	20	6.15
$e^+e^+\mu^-$	15	10	3.51
$\mu^+e^+e^-$	31	16	7.65
$\mu^-\mu^-\mu^+$	13	5	2.14
$e^-e^-e^+$	14	3	5.45
$\mu^-\mu^-e^+$	18	6	4.72
$\mu^-e^-\mu^+$	27	7	7.25
$e^-e^-\mu^+$	21	9	5.34
$\mu^-e^-e^+$	27	17	6.12

Table 5.11: Number of the fake events with errors for all the categories.

Category	AAF	AFF	Fake events±stat	Syst	Fake events
$\mu^+\mu^+\mu^-$	25	5	4.26 ±0.48 (11%)	50%	4.26 ±2.18 (51%)
$e^+e^+e^-$	10	4	3.55 ±0.88 (25%)	50%	3.55 ±1.98 (56%)
$\mu^+\mu^+e^-$	23	8	6.00 ±0.68 (11%)	50%	6.00 ±3.08 (51%)
$\mu^+e^+\mu^-$	27	20	6.15 ±0.72 (12%)	50%	6.15 ±3.16 (51%)
$e^+e^+\mu^-$	15	10	3.51 ±0.67 (19%)	50%	3.51 ±1.88 (54%)
$\mu^+e^+e^-$	31	16	7.65 ±0.72 (9%)	50%	7.65 ±3.89 (51%)
$\mu^-\mu^-\mu^+$	13	5	2.14 ±0.47 (22%)	50%	2.14 ±1.17 (55%)
$e^-e^-e^+$	14	3	5.45 ±0.90 (16%)	50%	5.45 ±2.87 (53%)
$\mu^-\mu^-e^+$	18	6	4.72 ±0.67 (14%)	50%	4.72 ±2.45 (52%)
$\mu^-e^-\mu^+$	27	7	7.25 ±0.69 (9%)	50%	7.25 ±3.69 (51%)
$e^-e^-\mu^+$	21	9	5.34 ±0.68 (13%)	50%	5.34 ±2.75 (52%)
$\mu^-e^-e^+$	26	17	6.12 ±0.71 (12%)	50%	6.12 ±3.14 (51%)

5.9 Total backgrounds estimation

SM processes, Dalitz events, Fake Leptons events are the three background contributions in the seesaw type III search.

Table 5.12 recaps SM background events contribution with only statistical error, and percent error in brackets. Systematic errors are added in square sum, as reported in Table 5.13.

Table 5.12: Number of selected events for SM backgrounds with only statistical errors.

Category	WZ	ZZ	WWW	Total SM
$\mu^+\mu^+\mu^-$	7.47±0.60 (8%)	0.88±0.12 (14%)	0.18±0.04 (20%)	8.53±0.62 (7%)
$e^+e^+e^-$	3.15±0.39 (12%)	0.22±0.06 (28%)	0.13±0.03 (24%)	3.50±0.40 (11%)
$\mu^+\mu^+e^-$	0.49±0.15 (32%)	0.12±0.04 (38%)	0.30±0.05 (16%)	0.90±0.17 (18%)
$\mu^+e^+\mu^-$	9.55±0.68 (7%)	0.42±0.09 (20%)	0.54±0.06 (12%)	10.52±0.69 (6%)
$e^+e^+\mu^-$	0.78±0.19 (25%)	0.14±0.05 (35%)	0.31±0.05 (15%)	1.22±0.21 (17%)
$\mu^+e^+e^-$	6.06±0.54 (9%)	0.69±0.11 (16%)	0.43±0.06 (13%)	7.19±0.56 (8%)
$\mu^-\mu^-\mu^+$	4.61±0.47 (10%)	0.68±0.11 (16%)	0.10±0.03 (27%)	5.39±0.49 (9%)
$e^-e^-e^+$	2.47±0.35 (14%)	0.19±0.06 (30%)	0.05±0.02 (38%)	2.71±0.35 (13%)
$\mu^-\mu^-e^+$	0.53±0.16 (30%)	0.05±0.03 (58%)	0.11±0.03 (26%)	0.69±0.17 (24%)
$\mu^-e^-\mu^+$	4.41±0.46 (10%)	0.41±0.08 (20%)	0.22±0.04 (18%)	5.04±0.47 (9%)
$e^-e^-\mu^+$	0.87±0.21 (24%)	0.03±0.02 (71%)	0.09±0.03 (29%)	1.00±0.21 (21%)
$\mu^-e^-e^+$	4.36±0.46 (10%)	0.64±0.10 (16%)	0.26±0.04 (17%)	5.27±0.47 (9%)

Table 5.13: Number of selected events for SM backgrounds with total errors. The systematic contributions are 6.0% for WZ [11], 12.0% for ZZ [11], and 50% for WWW.

Category	WZ	ZZ	WWW	Total SM
$\mu^+\mu^+\mu^-$	7.47±0.75 (10%)	0.88±0.16 (18%)	0.18±0.10 (54%)	8.53±0.77 (9%)
$e^+e^+e^-$	3.15±0.43 (14%)	0.22±0.07 (30%)	0.13±0.07 (55%)	3.50±0.45 (13%)
$\mu^+\mu^+e^-$	0.49±0.16 (32%)	0.12±0.05 (40%)	0.30±0.16 (52%)	0.90±0.23 (25%)
$\mu^+e^+\mu^-$	9.55±0.89 (9%)	0.42±0.10 (23%)	0.54±0.28 (51%)	10.52±0.94 (9%)
$e^+e^+\mu^-$	0.78±0.20 (26%)	0.14±0.05 (37%)	0.31±0.16 (52%)	1.22±0.26 (21%)
$\mu^+e^+e^-$	6.06±0.65 (11%)	0.69±0.14 (20%)	0.43±0.22 (52%)	7.19±0.70 (10%)
$\mu^-\mu^-\mu^+$	4.61±0.55 (12%)	0.68±0.13 (20%)	0.10±0.06 (57%)	5.39±0.57 (10%)
$e^-e^-e^+$	2.47±0.38 (15%)	0.19±0.06 (33%)	0.05±0.03 (63%)	2.71±0.38 (14%)
$\mu^-\mu^-e^+$	0.53±0.16 (31%)	0.05±0.03 (59%)	0.11±0.06 (56%)	0.69±0.18 (26%)
$\mu^-e^-\mu^+$	4.41±0.53 (12%)	0.41±0.10 (24%)	0.22±0.12 (53%)	5.04±0.55 (11%)
$e^-e^-\mu^+$	0.87±0.21 (24%)	0.03±0.02 (72%)	0.09±0.05 (58%)	1.00±0.22 (22%)
$\mu^-e^-e^+$	4.36±0.53 (12%)	0.64±0.13 (20%)	0.26±0.14 (53%)	5.27±0.56 (11%)

Table 5.14 gives the total background events number, to be used in comparison with data.

Table 5.14: Total background contribution with total errors.

Category	SM	Fake	Dalitz	Total background
$\mu^+\mu^+\mu^-$	8.53	4.26	1.37	14.2±2.4 (17%)
$e^+e^+e^-$	3.50	3.55	not used	7.1±2.0 (28%)
$\mu^+\mu^+e^-$	0.90	6.00	na	6.9±3.1 (45%)
$\mu^+e^+\mu^-$	10.52	6.15	not used	16.7±3.3 (19%)
$e^+e^+\mu^-$	1.22	3.51	na	4.7±1.9 (39%)
$\mu^+e^+e^-$	7.19	7.65	3.13	18.0±4.3 (23%)
$\mu^-\mu^-\mu^+$	5.38	2.14	1.37	8.9±1.5 (16%)
$e^-e^-e^+$	2.71	5.45	not used	8.2±2.9 (35%)
$\mu^-\mu^-e^+$	0.69	4.72	na	5.4±2.4 (46%)
$\mu^-e^-\mu^+$	5.04	7.25	not used	12.3±3.7 (30%)
$e^-e^-\mu^+$	1.00	5.34	na	6.3±2.8 (43%)
$\mu^-e^-e^+$	5.27	6.12	3.13	14.5±3.6 (24%)

5.10 SM background and data comparison

Figures from 5.19 up to 5.29 show the distribution of the following variables (see Section 5.2.9 for definitions):

- E_T^{miss};
- H_T;
- the first jet in p_T CSV b tag value;
- L_T;
- $M_{T,1}$ where 1 stay for first lepton in p_T;
- $M_{T,2}$ where 2 stay for second lepton in p_T;
- S_T;
- the leptons p_T (first, second and third);
- the first jet p_T.

These eleven distributions are obtained with the full selection, except the Z veto and the Z asymmetric conversion veto, to preserve significant statistics in the plots. After all selection step, the surviving events are grouped into categories.

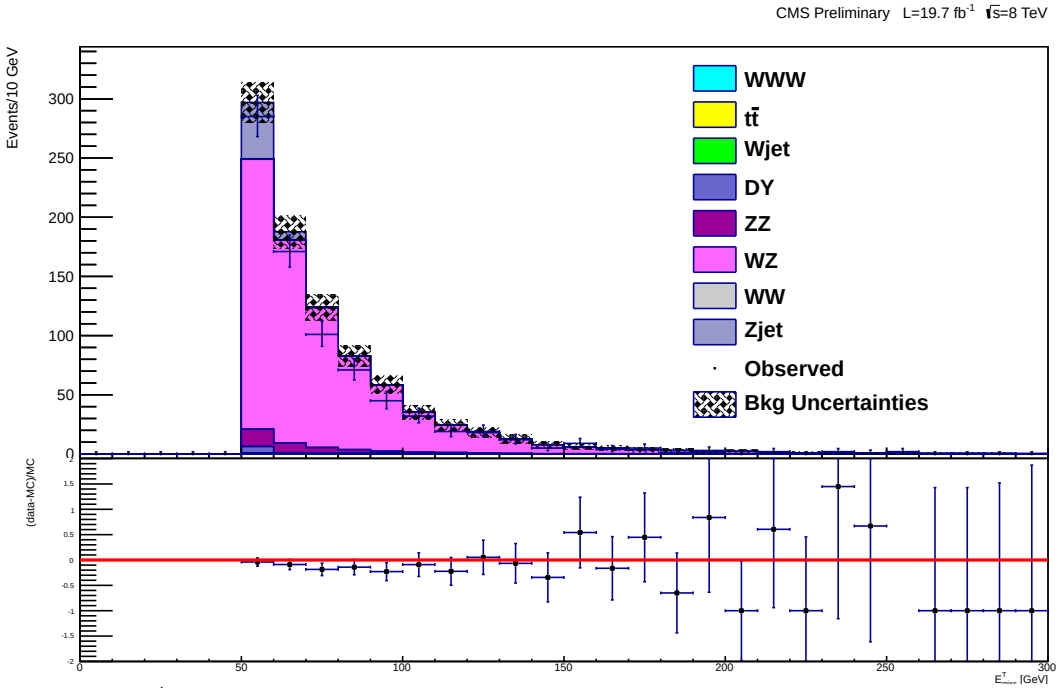

Figure 5.19: E_T^{miss} distribution with the full selection, except the Z veto and the Z asymmetric conversion veto.

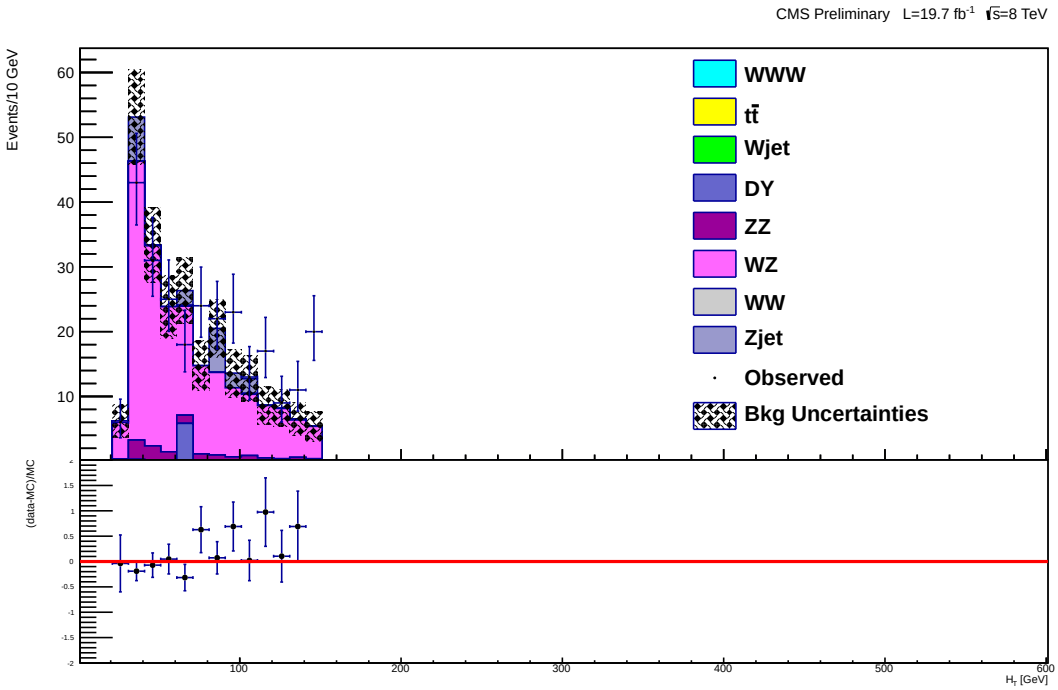

Figure 5.20: H_T distribution with the full selection, except the Z veto and the Z asymmetric conversion veto.

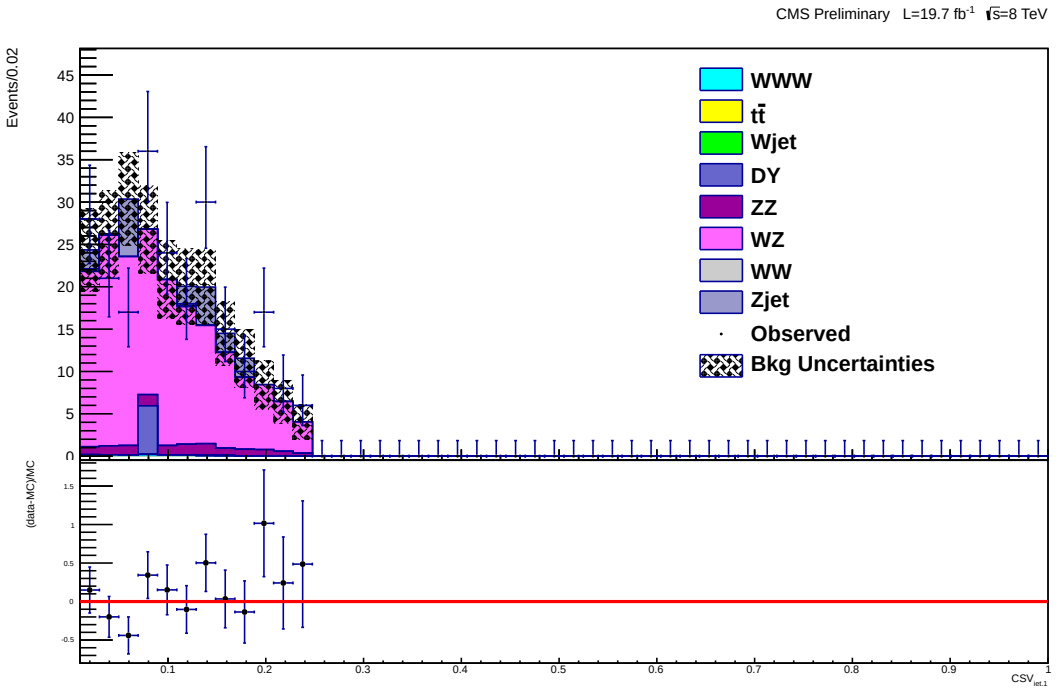

Figure 5.21: First jet in p_T CSV b tag distribution with the full selection, except the Z veto and the Z asymmetric conversion veto.

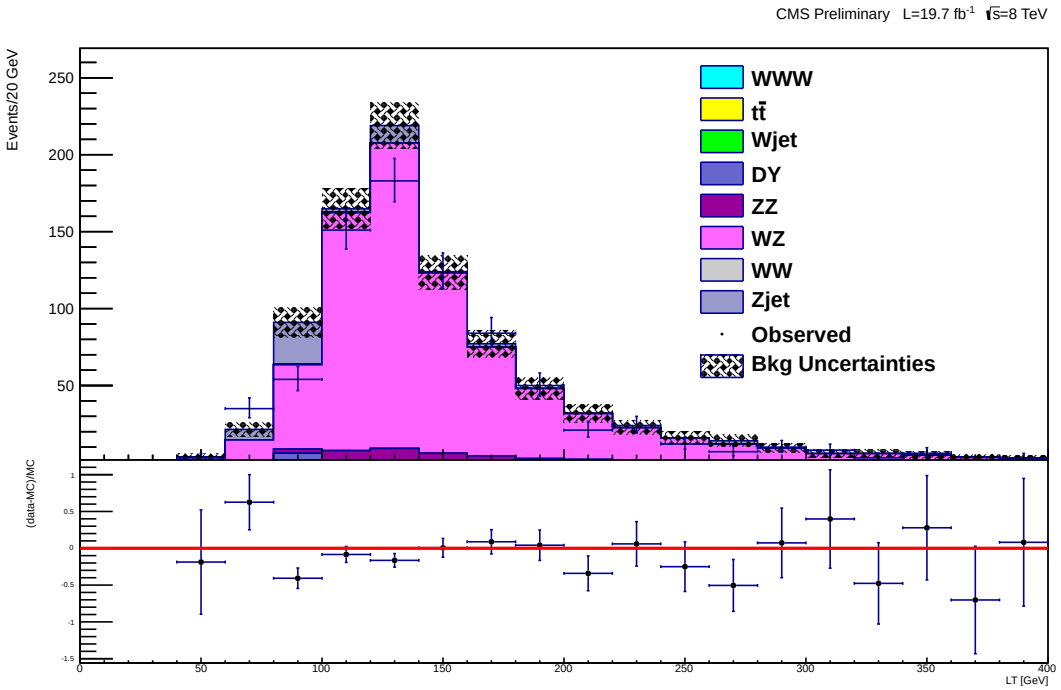

Figure 5.22: L_T distribution with the full selection, except the Z veto and the Z asymmetric conversion veto.

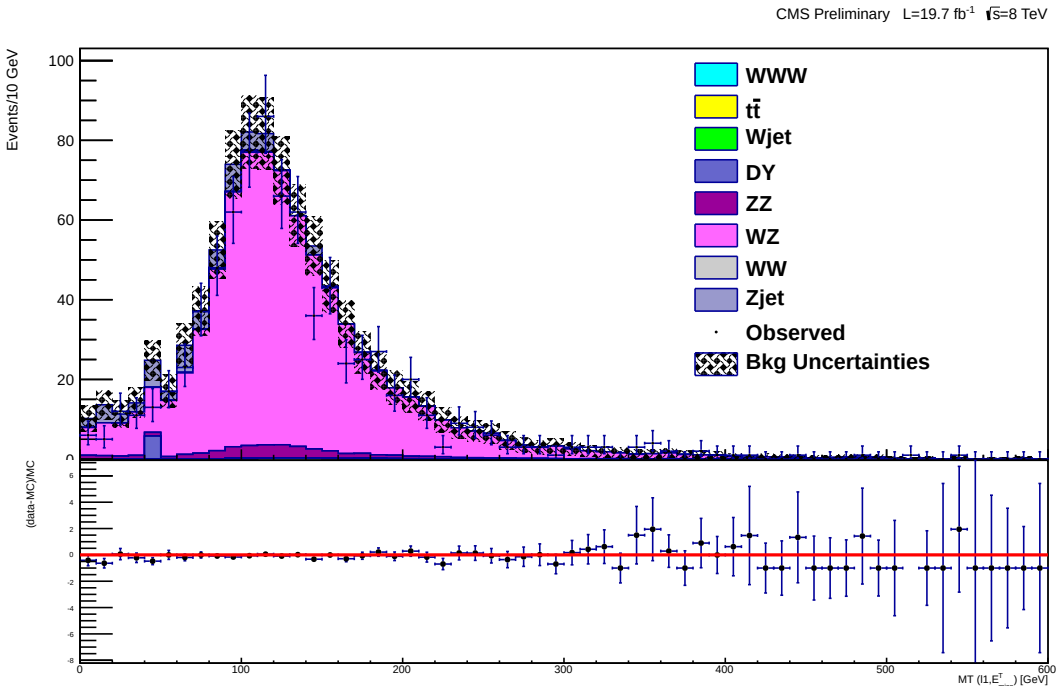

Figure 5.23: $M_{T,1}$ distribution with the full selection, except the Z veto and the Z asymmetric conversion veto.

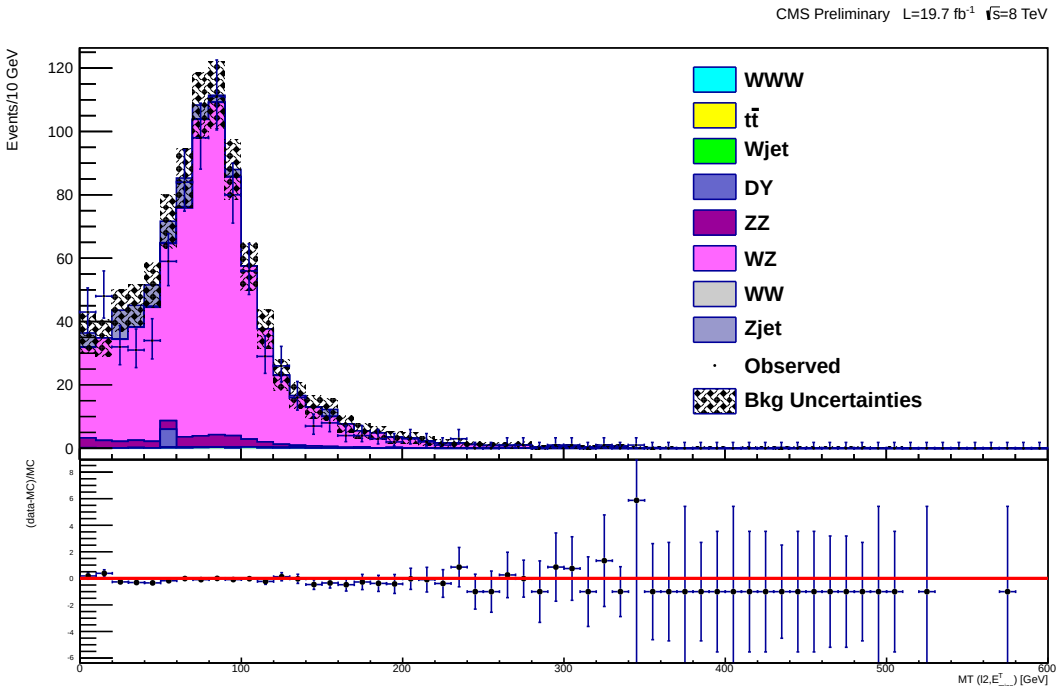

Figure 5.24: $M_{T,2}$ distribution with the full selection, except the Z veto and the Z asymmetric conversion veto.

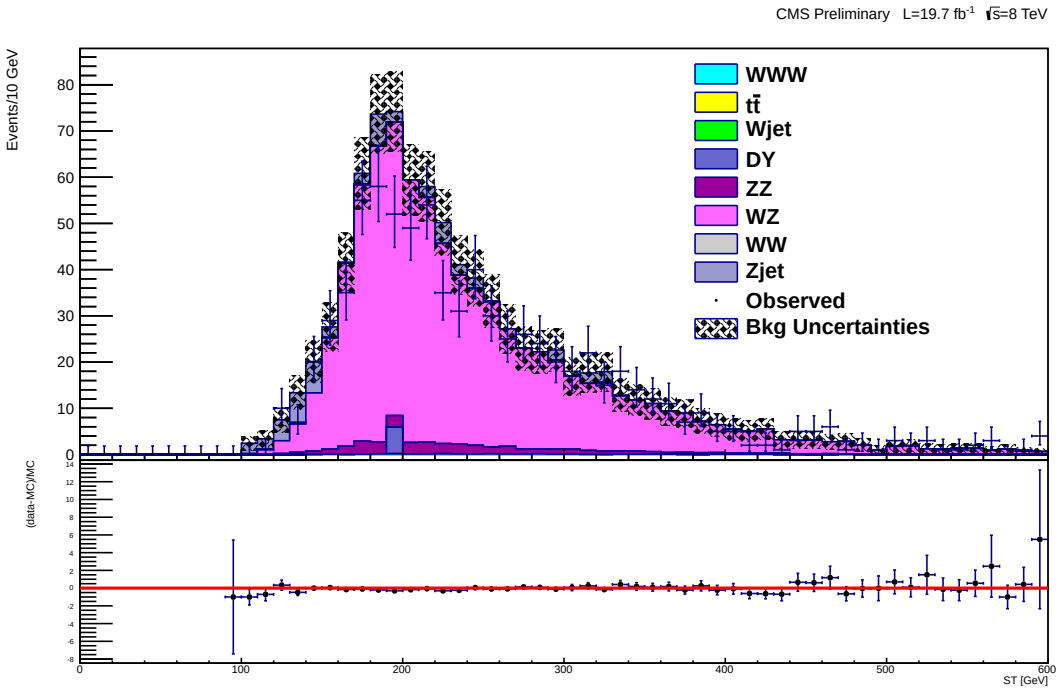

Figure 5.25: S_T distribution with the full selection, except the Z veto and the Z asymmetric conversion veto.

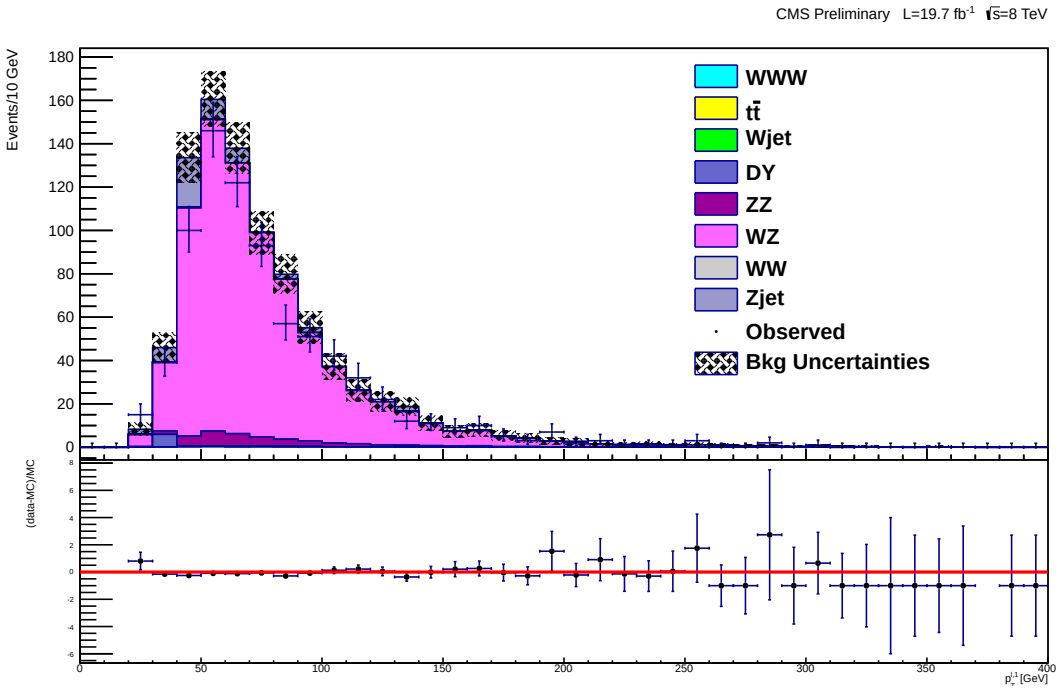

Figure 5.26: First lepton p_T with the full selection, except the Z veto and the Z asymmetric conversion veto.

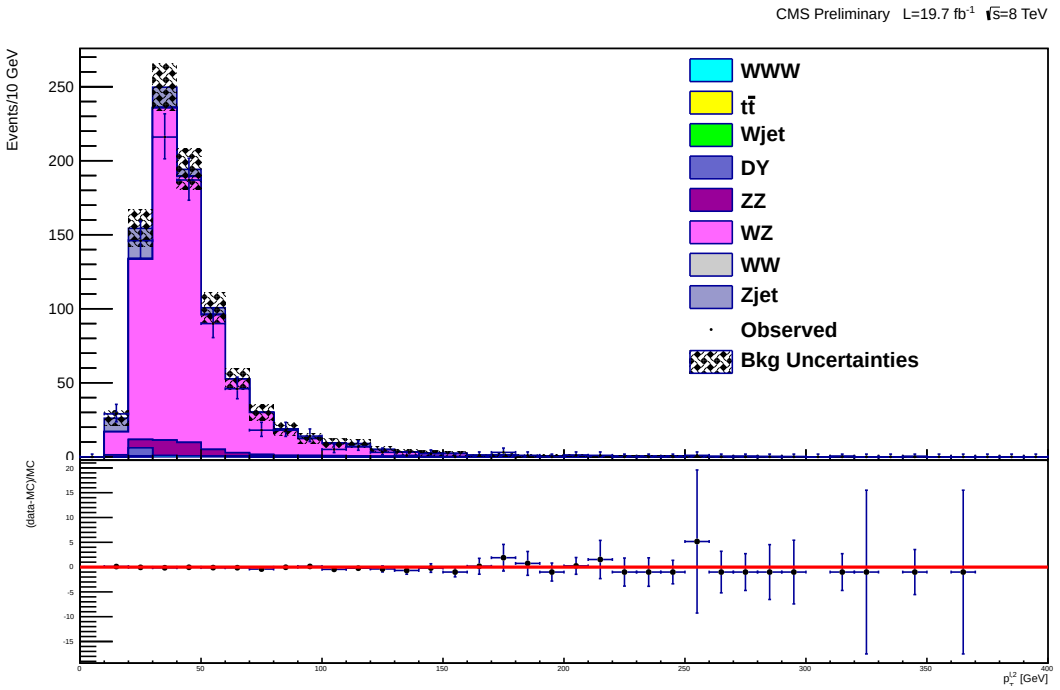

Figure 5.27: Second lepton p_T distribution with the full selection, except the Z veto and the Z asymmetric conversion veto.

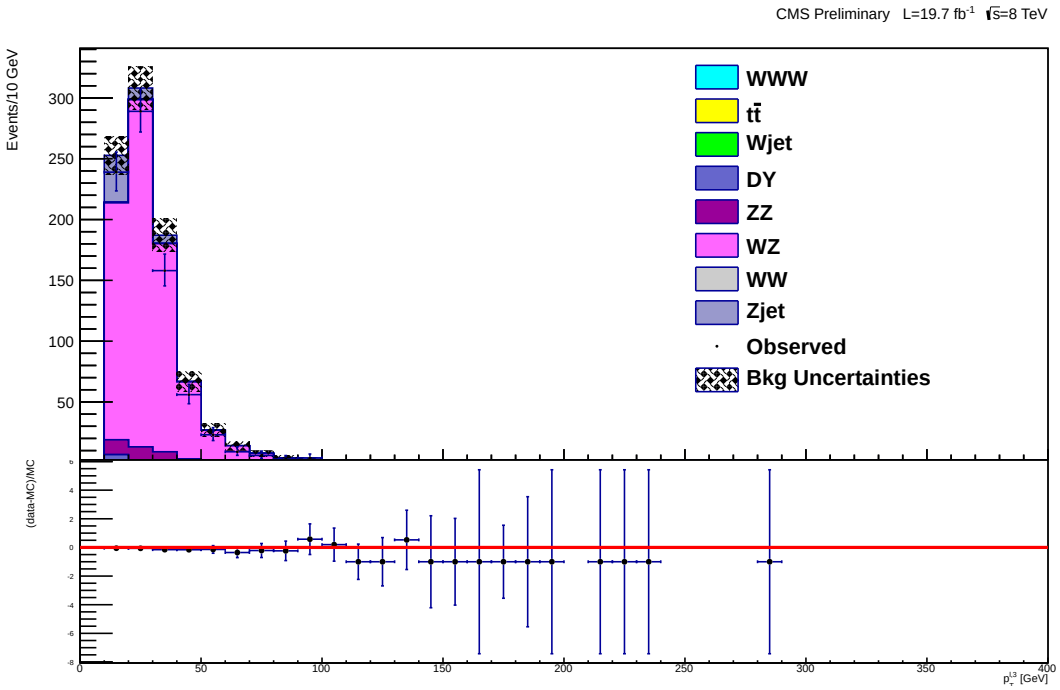

Figure 5.28: Third lepton p_T distribution with the full selection, except the Z veto and the Z asymmetric conversion veto.

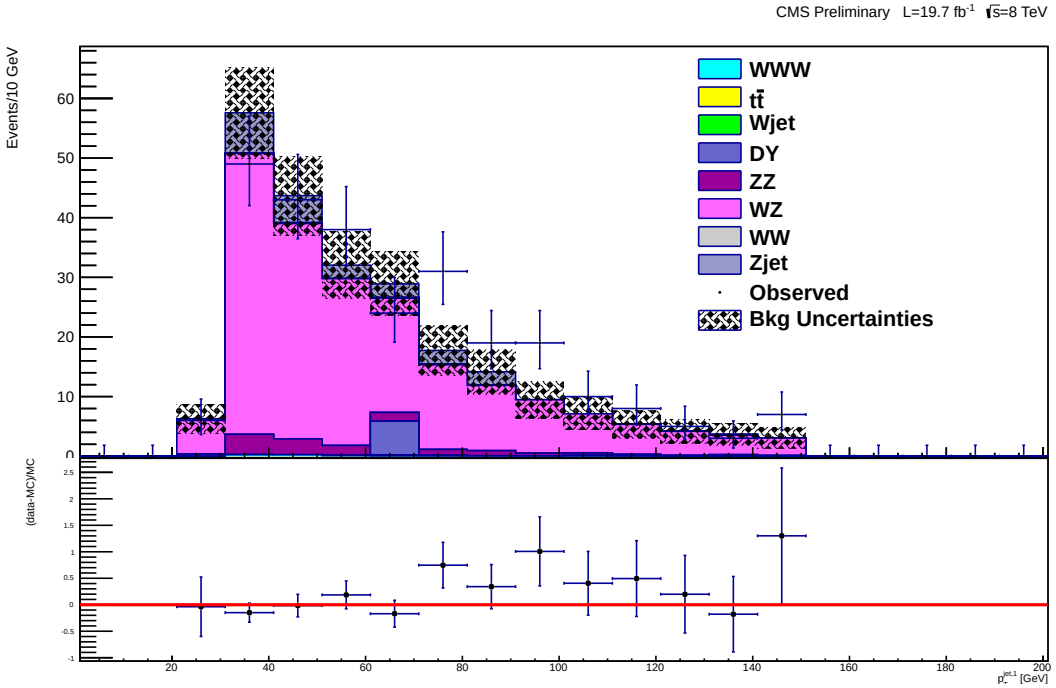

Figure 5.29: First jet p_T distribution with the full selection, except the Z veto and the Z asymmetric conversion veto.

5.11 MC signal events

Events selection is applied on MC signal samples, generated by CMS collaboration with full simulation tools on Padua group's request (see in Appendix D Table D.4 for details).

Tables 5.15 and 5.16 summarize surviving signal events involving Σ^+ mediator.

Tables 5.17 and 5.18 summarize surviving signal events involving Σ^- mediator.

Categories related to Σ^- mediator have less events than ones to Σ^+ mediator, following the production cross sections trend.

The errors consider the statistics and the total uncertainty due to trigger and object efficiency (Table 5.19). The total uncertainty for each category is almost constant in all mass points.

Table 5.15: Events involving Σ^+ mediator at ten mass points, grouped in categories. Statistics errors are reported.

Cat	140	180	200	220	240
$\mu\mu\mu$	14.9 ± 0.3 (1.9%)	5.0 ± 0.1 (1.9%)	3.6 ± 0.1 (1.7%)	2.9 ± 0.1 (1.6%)	2.1 ± 0.1 (1.5%)
eee	6.6 ± 0.2 (2.8%)	2.9 ± 0.1 (2.4%)	2.3 ± 0.1 (2.2%)	1.8 ± 0.1 (2.0%)	1.4 ± 0.1 (1.9%)
$\mu\mu e$	24.4 ± 0.4 (1.5%)	7.6 ± 0.1 (1.5%)	5.1 ± 0.1 (1.5%)	3.5 ± 0.1 (1.4%)	2.5 ± 0.1 (1.4%)
$\mu e\mu$	28.8 ± 0.4 (1.4%)	10.5 ± 0.1 (1.3%)	7.8 ± 0.1 (1.2%)	5.6 ± 0.1 (1.1%)	4.2 ± 0.1 (1.1%)
eeμ	20.8 ± 0.3 (1.6%)	6.4 ± 0.1 (1.7%)	4.4 ± 0.1 (1.6%)	3.0 ± 0.1 (1.5%)	2.2 ± 0.1 (1.5%)
μee	28.5 ± 0.4 (1.4%)	9.6 ± 0.1 (1.4%)	6.9 ± 0.1 (1.3%)	5.2 ± 0.1 (1.2%)	3.8 ± 0.2 (1.1%)
Cat	260	280	300	320	340
$\mu\mu\mu$	1.6 ± 0.1 (1.5%)	1.2 ± 0.02 (1.4%)	0.93 ± 0.01 (1.4%)	0.72 ± 0.01 (1.4%)	0.54 ± 0.01 (1.4%)
eee	1.1 ± 0.1 (1.7%)	0.84 ± 0.01 (1.7%)	0.65 ± 0.01 (1.7%)	0.50 ± 0.01 (1.6%)	0.39 ± 0.01 (1.7%)
$\mu\mu e$	1.8 ± 0.1 (1.4%)	1.35 ± 0.02 (1.4%)	0.97 ± 0.01 (1.4%)	0.75 ± 0.01 (1.3%)	0.56 ± 0.01 (1.4%)
$\mu e\mu$	3.2 ± 0.1 (1.0%)	2.39 ± 0.02 (1.0%)	1.77 ± 0.02 (1.0%)	1.37 ± 0.01 (1.0%)	1.04 ± 0.01 (1.0%)
eeμ	1.6 ± 0.1 (1.5%)	1.18 ± 0.03 (1.5%)	0.87 ± 0.01 (1.5%)	0.65 ± 0.01 (1.4%)	0.51 ± 0.01 (1.4%)
μee	2.8 ± 0.1 (1.1%)	2.08 ± 0.2 (1.1%)	1.59 ± 0.02 (1.1%)	1.25 ± 0.01 (1.0%)	0.96 ± 0.01 (1.0%)

Table 5.16: Events involving Σ^+ mediator at ten mass points, grouped in categories. Total errors are reported.

Cat	140	180	200	220	240
$\mu\mu\mu$	14.9 ± 0.6 (3.6%)	5.0 ± 0.2 (3.6%)	3.6 ± 0.1 (3.6%)	2.9 ± 0.1 (3.5%)	2.1 ± 0.07 (3.5%)
eee	6.6 ± 0.5 (8.1%)	2.9 ± 0.2 (8.0%)	2.3 ± 0.2 (7.9%)	1.8 ± 0.1 (7.8%)	1.4 ± 0.1 (7.8%)
$\mu\mu e$	24.4 ± 0.9 (3.6%)	7.6 ± 0.3 (3.7%)	5.1 ± 0.2 (3.6%)	3.5 ± 0.1 (3.6%)	2.5 ± 0.09 (3.6%)
$\mu e\mu$	28.8 ± 1.0 (3.6%)	10.5 ± 0.4 (3.6%)	7.8 ± 0.3 (3.5%)	5.6 ± 0.2 (3.5%)	4.2 ± 0.1 (3.5%)
eeμ	20.8 ± 1.1 (5.4%)	6.4 ± 0.4 (5.4%)	4.4 ± 0.2 (5.4%)	3.1 ± 0.2 (5.4%)	2.2 ± 0.1 (5.4%)
μee	28.5 ± 1.6 (5.4%)	9.6 ± 0.5 (5.4%)	6.9 ± 0.4 (5.3%)	5.2 ± 0.3 (5.3%)	3.8 ± 0.2 (5.3%)
Cat	260	280	300	320	340
$\mu\mu\mu$	1.6 ± 0.06 (3.5%)	1.2 ± 0.04 (3.5%)	0.93 ± 0.03 (3.4%)	0.72 ± 0.03 (3.4%)	0.54 ± 0.02 (3.4%)
eee	1.1 ± 0.09 (7.8%)	0.84 ± 0.06 (7.8%)	0.65 ± 0.05 (7.8%)	0.50 ± 0.04 (7.7%)	0.39 ± 0.03 (7.7%)
$\mu\mu e$	1.8 ± 0.07 (3.6%)	1.4 ± 0.05 (3.6%)	0.97 ± 0.04 (3.6%)	0.75 ± 0.03 (3.6%)	0.56 ± 0.02 (3.6%)
$\mu e\mu$	3.2 ± 0.1 (3.5%)	2.4 ± 0.09 (3.5%)	1.77 ± 0.06 (3.5%)	1.37 ± 0.05 (3.5%)	1.04 ± 0.04 (3.5%)
eeμ	1.6 ± 0.09 (5.4%)	1.2 ± 0.06 (5.4%)	0.87 ± 0.05 (5.4%)	0.65 ± 0.04 (5.4%)	0.51 ± 0.03 (5.4%)
μee	2.8 ± 0.1 (5.3%)	2.1 ± 0.1 (5.3%)	1.59 ± 0.09 (5.3%)	1.25 ± 0.07 (5.3%)	0.96 ± 0.05 (5.3%)

Table 5.17: Events involving Σ^- mediator at ten mass points, grouped in categories. Statistics errors are reported.

Cat	140	180	200	220	240
$\mu\mu\mu$	5.8 $\pm$0.1 (2.2%)	2.48 $\pm$ 0.05 (1.8%)	1.81 $\pm$ 0.03 (1.7%)	1.33 $\pm$ 0.02 (1.6%)	0.98 $\pm$ 0.01 (1.5%)
eee	2.4 $\pm$0.1 (3.3%)	1.4 $\pm$ 0.03 (2.4%)	1.14 $\pm$ 0.02 (2.1%)	0.86 $\pm$ 0.02 (1.9%)	0.65 $\pm$ 0.01 (1.8%)
$\mu\mu e$	9.8 $\pm$0.2 (1.7%)	3.8 $\pm$ 0.06 (1.5%)	2.46 $\pm$ 0.03 (1.4%)	1.62 $\pm$ 0.02 (1.4%)	1.12 $\pm$ 0.02 (1.4%)
$\mu e\mu$	11.0 $\pm$0.2 (1.6%)	5.4 $\pm$ 0.07 (1.2%)	3.8 $\pm$ 0.04 (1.1%)	2.67 $\pm$ 0.03 (1.1%)	1.90 $\pm$ 0.02 (1.1%)
eeμ	8.3 $\pm$0.2 (1.8%)	3.2 $\pm$ 0.05 (1.6%)	2.1 $\pm$ 0.03 (1.6%)	1.41 $\pm$ 0.02 (1.5%)	0.98 $\pm$ 0.01 (1.5%)
μee	11.2 $\pm$0.2 (1.6%)	4.9 $\pm$ 0.06 (1.3%)	3.5 $\pm$ 0.04 (1.2%)	2.37 $\pm$ 0.03 (1.2%)	1.74 $\pm$ 0.02 (1.1%)
Cat	260	280	300	320	340
$\mu\mu\mu$	0.71 $\pm$ 0.01 (1.4%)	0.54 $\pm$ 0.01 (1.4%)	0.39 $\pm$ 0.01 (1.4%)	0.29 $\pm$ 0.01 (1.4%)	0.23 $\pm$ 0.01 (1.3%)
eee	0.48 $\pm$ 0.01 (1.7%)	0.38 $\pm$ 0.01 (1.7%)	0.27 $\pm$ 0.01 (1.6%)	0.20 $\pm$ 0.01 (1.6%)	0.17 $\pm$ 0.01 (1.5%)
$\mu\mu e$	0.78 $\pm$ 0.01 (1.4%)	0.60 $\pm$ 0.01 (1.3%)	0.42 $\pm$ 0.01 (1.3%)	0.31 $\pm$ 0.01 (1.3%)	0.24 $\pm$ 0.01 (1.3%)
$\mu e\mu$	1.39 $\pm$ 0.01 (1.0%)	1.06 $\pm$ 0.01 (1.0%)	0.76 $\pm$ 0.01 (1.0%)	0.57 $\pm$ 0.01 (1.0%)	0.46 $\pm$ 0.01 (1.0%)
eeμ	0.70 $\pm$ 0.01 (1.4%)	0.52 $\pm$ 0.01 (1.4%)	0.37 $\pm$ 0.01 (1.4%)	0.27 $\pm$ 0.01 (1.4%)	0.22 $\pm$ 0.01 (1.4%)
μee	1.23 $\pm$ 0.01 (1.1%)	0.95 $\pm$ 0.01 (1.0%)	0.69 $\pm$ 0.01 (1.0%)	0.51 $\pm$ 0.01 (1.0%)	0.41 $\pm$ 0.01 (1.0%)

Table 5.18: Events involving Σ^- mediator at ten mass points, grouped in categories. Total errors are reported.

Cat.	140	180	200	220	240
$\mu\mu\mu$	5.8 $\pm$0.2 (3.8%)	2.48 $\pm$ 0.09 (3.6%)	1.81 $\pm$ 0.07 (3.5%)	1.33 $\pm$ 0.05 (3.5%)	0.98 $\pm$ 0.04 (3.5%)
eee	2.4 $\pm$0.2 (8.3%)	1.4 $\pm$ 0.1 (7.9%)	1.14 $\pm$ 0.09 (7.9%)	0.86 $\pm$ 0.07 (7.8%)	0.65 $\pm$ 0.05 (7.8%)
$\mu\mu e$	9.8 $\pm$0.4 (3.7%)	3.8 $\pm$ 0.1 (3.6%)	2.46 $\pm$ 0.09 (3.6%)	1.62 $\pm$ 0.06 (3.6%)	1.12 $\pm$ 0.04 (3.6%)
$\mu e\mu$	11.0 $\pm$0.4 (3.7%)	5.4 $\pm$ 0.2 (3.6%)	3.8 $\pm$ 0.1 (3.5%)	2.67 $\pm$ 0.1 (3.5%)	1.90 $\pm$ 0.07 (3.5%)
eeμ	8.3 $\pm$0.5 (5.5%)	3.2 $\pm$ 0.2 (5.4%)	2.1 $\pm$ 0.1 (5.4%)	1.41 $\pm$ 0.08 (5.4%)	0.98 $\pm$ 0.05 (5.4%)
μee	11.2 $\pm$0.6 (5.4%)	4.9 $\pm$ 0.3 (5.4%)	3.5 $\pm$ 0.2 (5.3%)	2.37 $\pm$ 0.1 (5.3%)	1.74 $\pm$ 0.09 (5.3%)
Cat.	260	280	300	320	340
$\mu\mu\mu$	0.71 $\pm$ 0.03 (3.5%)	0.54 $\pm$ 0.02 (3.4%)	0.39 $\pm$ 0.01 (3.4%)	0.29 $\pm$ 0.01 (3.4%)	0.23 $\pm$ 0.01 (3.4%)
eee	0.48 $\pm$ 0.04 (7.8%)	0.38 $\pm$ 0.03 (7.7%)	0.27 $\pm$ 0.02 (7.7%)	0.20 $\pm$ 0.02 (7.7%)	0.17 $\pm$ 0.01 (7.7%)
$\mu\mu e$	0.78 $\pm$ 0.03 (3.6%)	0.60 $\pm$ 0.02 (3.6%)	0.42 $\pm$ 0.01 (3.6%)	0.31 $\pm$ 0.01 (3.6%)	0.24 $\pm$ 0.01 (3.6%)
$\mu e\mu$	1.39 $\pm$ 0.05 (3.5%)	1.06 $\pm$ 0.04 (3.5%)	0.76 $\pm$ 0.03 (3.5%)	0.57 $\pm$ 0.02 (3.5%)	0.46 $\pm$ 0.01 (3.5%)
eeμ	0.70 $\pm$ 0.04 (5.4%)	0.52 $\pm$ 0.03 (5.4%)	0.37 $\pm$ 0.02 (5.4%)	0.27 $\pm$ 0.01 (5.4%)	0.22 $\pm$ 0.01 (5.4%)
μee	1.23 $\pm$ 0.07 (5.3%)	0.95 $\pm$ 0.05 (5.3%)	0.69 $\pm$ 0.04 (5.3%)	0.51 $\pm$ 0.03 (5.3%)	0.41 $\pm$ 0.02 (5.3%)

5.12 Systematic uncertainties

The sensitivity of the analysis is affected by uncertainties that limit the precision with which the signal and background are known. The systematic uncertainties include the imperfect knowledge of detector effects, such as energy scales, resolution, PU, the processes production at generator level and the absolute normalization to data integrated luminosity. In general, systematic uncertainties are grouped in three classes related to:

- simulation: PDF knowledge, leptons momentum scale and resolution, jets selection with JEC, E_T^{miss} scale and resolution, PU effects;
- data versus simulation correction factors: trigger efficiencies, objects reconstruction and identification, selection efficiencies;
- background: background yields from simulation and data driven method, integrated luminosity.

Systematic uncertainties related to simulation are negligible respect to the other classes contributions. In the second class, dilepton triggers efficiency value is 2%. The systematic uncertainties on leptons reconstruction and identification and isolation are common with other CMS analysis: values, which include the acceptance, are 2.5% for electron and 1.0% [83]. Details about muon and electron identification and isolation efficiency are in the Appendix B of the Reference [80]. Seesaw type III search investigates final states with three charged leptons: the assumptions to evaluate uncertainties are the sum for identical leptons and the square sum for different flavor leptons. Finally, the sum in square of contributions is the total systematic uncertainties in second class for each category (Table 5.19).

Table 5.19: Total uncertainty due to trigger and object efficiency. The object efficiency is calculated from [78].

Category	Trigger	Objects efficiency	Total
$\mu\mu\mu$	0.02	0.030	0.036
eee	0.02	0.075	0.078
$\mu\mu e$	0.02	0.032	0.038
$\mu e\mu$	0.02	0.032	0.038
eeμ	0.02	0.051	0.055
μee	0.02	0.051	0.055

In the third class, the uncertainty on integrated luminosity is 2.5% for 2012 pp collisions data.

Table 5.20 recaps systematic uncertainty contributions related to backgrounds relevant to final yield [11].

Table 5.20: Systematic uncertainties on backgrounds.

Source	Value
WZ	0.06
ZZ	0.12
WWW	0.50
Fakes	0.50
Dalitz	0.50
Luminosity	0.025

Chapter 6

Analysis results

The research strategy to investigate the seesaw with heavy fermion weak triplet mediators mechanism is based on the study of final states with exactly three charged leptons, missing transverse energy and low hadronic activity without b jets. Background sources are diboson and triboson decay, and events with a single heavy boson produced accompanied by an energetic photon that converts into a leptons pair (Dalitz pair), and events with one or two charged identified lepton(s) and the remaining two or one lepton(s) fake. Selected events are grouped into categories. At the end of analysis flow, the comparison between background and data in a "cut and count" experiment gives the results. Finally, results interpretations in theoretical model are performed and explained in next chapter.

6.1 Events yield

Table 6.1 shows the selected events observed in 2012 data.

Table 6.1: Selected events observed in 2012 data.

Category	Data
$\mu^+\mu^+\mu^-$	22
$e^+e^+e^-$	8
$\mu^+\mu^+e^-$	4
$\mu^+e^+\mu^-$	17
$e^+e^+\mu^-$	4
$\mu^+e^+e^-$	12
$\mu^-\mu^-\mu^+$	11
$e^-e^-e^+$	7
$\mu^-\mu^-e^+$	2
$\mu^-e^-\mu^+$	11
$e^-e^-\mu^+$	1
$\mu^-e^-e^+$	9

Table 6.2 compares the number of selected events observed in 2012 data and the number of total expected background events, with detailed contributions list.

Table 6.2: Background and data comparison, with detailed contributions list.

Category	SM	Fake	Dalitz	Total back	Data
$\mu^+\mu^+\mu^-$	8.53	4.26	1.37	14.2±2.4 (17%)	22
$e^+e^+e^-$	3.50	3.55	not used	7.1±2.0 (28%)	8
$\mu^+\mu^+e^-$	0.90	6.00	na	6.9±3.1 (45%)	4
$\mu^+e^+\mu^-$	10.52	6.15	not used	16.7±3.3 (19%)	17
$e^+e^+\mu^-$	1.22	3.51	na	4.7±1.9 (39%)	4
$\mu^+e^+e^-$	7.19	7.65	3.13	18.0±4.3 (23%)	12
$\mu^-\mu^-\mu^+$	5.38	2.14	1.37	8.9±1.5 (16%)	11
$e^-e^-e^+$	2.71	5.45	not used	8.2±2.9 (35%)	7
$\mu^-\mu^-e^+$	0.69	4.72	na	5.4±2.4 (46%)	2
$\mu^-e^-\mu^+$	5.04	7.25	not used	12.3±3.7 (30%)	11
$e^-e^-\mu^+$	1.00	5.34	na	6.3±2.8 (43%)	1
$\mu^-e^-e^+$	5.27	6.12	3.13	14.5±3.6 (24%)	9

6.2 Seesaw type III search results

Table 6.3 reports the expected event yield from background, the number of observed events, the expected seesaw signal event yield for flavor democratic scenario, in each of the six categories for two signs. The number of data events observed in all the categories is consistent with the number of predicted background events. The larger difference is the smaller number of real events in the $e^-e^-\mu^+$ category; the difference with respect to the expected events is $\sim 1.8\,\sigma$.

No signal is found in the data within the sensitivity of the analysis. The results are interpreted (see Chapter 7) giving the cross sections times the branching ratio of the Σ mediators needed to obtain the exclusion limits at 95 % confidence level. The mass region where the expected cross section is larger gives the mass exclusion limit.

Limit is an update of what CMS obtained at 7 TeV with 2011 data [51] for Σ^+. For the first time, limit is set on Σ^-, too.

Table 6.3: Background and data and signal events.

Category	Total back	Data	140	180	200	220	240	260	280	300	320	340
$\mu^+\mu^+\mu^-$	14.2±2.4 (17%)	22	14.9	5.0	3.6	2.8	2.1	1.6	1.2	0.9	0.7	0.6
$e^+e^+e^-$	7.1±2.0 (28%)	8	6.6	2.9	2.3	1.8	1.4	1.1	0.8	0.7	0.5	0.4
$\mu^+\mu^+e^-$	6.9±3.1 (45%)	4	24.4	7.6	5.1	3.5	2.5	1.8	1.3	1.0	0.7	0.6
$\mu^+e^+\mu^-$	16.7±3.3 (19%)	17	28.8	10.5	7.8	5.6	4.2	3.2	2.4	1.8	1.4	1.0
$e^+e^+\mu^-$	4.7±1.9 (39%)	4	20.8	6.4	4.4	3.0	2.2	1.6	1.2	0.9	0.7	0.5
$\mu^+e^+e^-$	18.0±4.3 (23%)	12	28.5	9.6	6.9	5.2	3.8	2.8	2.1	1.6	1.3	1.0
$\mu^-\mu^-\mu^+$	8.9±1.5 (16%)	11	5.8	2.5	1.8	1.3	1.0	0.7	0.5	0.4	0.3	0.2
$e^-e^-e^+$	8.2±2.9 (35%)	7	2.4	1.4	1.1	0.9	0.7	0.5	0.4	0.3	0.2	0.2
$\mu^-\mu^-e^+$	5.4±2.4 (46%)	2	9.8	3.8	2.5	1.6	1.1	0.8	0.6	0.4	0.3	0.2
$\mu^-e^-\mu^+$	12.3±3.7 (30%)	11	11.0	5.4	3.8	2.7	1.9	1.4	1.1	0.8	0.6	0.5
$e^-e^-\mu^+$	6.3±2.8 (43%)	1	8.3	3.2	2.1	1.4	1.0	0.7	0.5	0.4	0.3	0.2
$\mu^-e^-e^+$	14.5±3.6 (24%)	9	11.2	4.9	3.5	2.4	1.7	1.2	1.0	0.7	0.5	0.4

6.3 Event display

A CMS dedicated tool, called "cmsShow", shows the reconstructed objects for one selected event of the category $\mu^+e^+\mu^-$ (Figure 6.1).

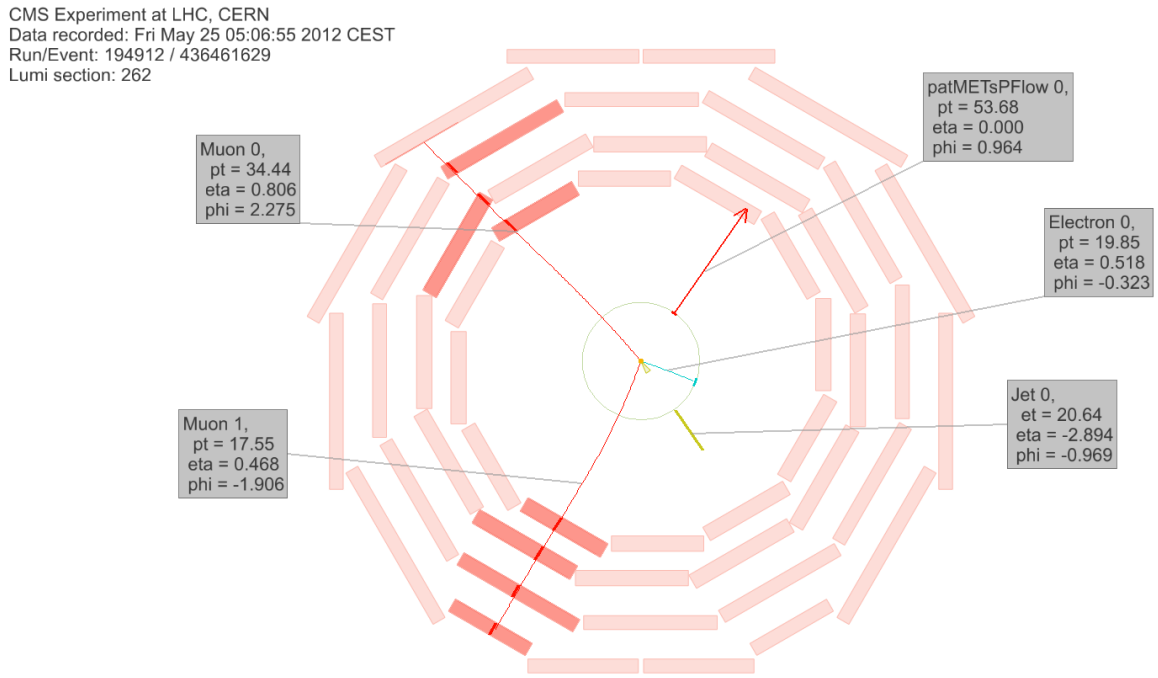

Figure 6.1: One selected event observed by CMS in 2012.

6.4 Summary of results about seesaw type III search

ATLAS (A Toroidal LHC ApparatuS) [84] and CMS search seesaw type III signatures in different ways. The results are interpreted by theoreticians and the theoretic community suggests new possible signatures. Table 6.4 summarizes the knowledge status up to now.

Table 6.4: Seesaw type III search status.

Way	ATLAS at 8 TeV [85]	CMS at 7 TeV [51]	CMS at 8 TeV [86]
final state	at least 4 charged leptons	3 charged leptons	3 charged leptons
total charge	not defined	$+1$	± 1
channel	only Z to ll	several diagrams	several diagrams
mass range	(120-500) GeV	(120-200) GeV	(140-340) GeV
tau coupling	negligible	valued	valued
scenarios	1	3	1
data sample	2012 data partial	only 2011 data	2012 all data
mass point	6	5	10 per sign
results	no excess	no excess	no excess
interpretations	245 GeV	179 GeV	240 GeV

6.5 Summary of results about seesaw search

Seesaw search in all three types is ongoing. Theoreticians' picture as described in Table 6.5 shows that field is open. Many interesting final states are not yet investigated.

Table 6.5: Seesaw searches status. "ns" stays for not searched, "na" not applicable.

model	$l^{\pm}$	$l^{+}l^{-}$	$l^{\pm}l^{\pm}$	$l^{\pm}l^{+}l^{-}$	$l^{+}l^{+}l^{-}l^{-}$	$l^{\pm}l^{\pm}l^{+}l^{-}$
type I	ns	ns	ATLAS,CMS	ns	na	na
type I inverse	ns	ns	na	ns	na	na
type I LeftRight	ns	ATLAS	ATLAS,CMS	ns	na	na
type I LeftRight inverse	ns	ATLAS	na	ns	na	na
type I Z'	ns	ns	ns	ns	ns	na
type I Z' inverse	ns	ns	na	ns	ns	na
type II (large Y)	ns	ns	ATLAS	ATLAS, CMS	CMS	na
type II (small Y)	ns	ns	ns	ns	ns	na
type III	ns	ns	CMS	ATLAS	ATLAS	ns
type III inverse	ns	ns	ns	ns	ns	ns

Chapter 7

Interpretations of results

The analysis, which shows no evidence for seesaw type III model signal, sets limits on the production cross sections times the branching ratio of the considered process. Exclusion limits between combined channels are calculated at the 95% CL (Confidence Level) by employing the CL95 technique in the RooStats implementation [87], using Bayesian statistics and a flat prior for the signal production cross sections. The values of cross sections times branching ratio are translated in the corresponding lower limits on seesaw type III mediators mass.

7.1 Statistical approach

Seesaw type III search is a counting experiment, with one signal and three background contributions (SM processes, Dalitz and Fakes). CMS Higgs Combined Limit Analysis Toolkit [88] is used to set limits. Tool is stable for low background (order of 10-20 events) search. In the toolkit, the Bayesian method with MarkovChainMC algorithm [89], based on RootStats package [87], is chosen according with the CMS statistical committee guide. The MarkovChainMC algorithm computes the Bayesian observed limit using MC integration. For each channel, nuisance parameters are defined to describe the systematic signal uncertainty, the systematic background uncertainty as well as the statistical uncertainties in background and signal. The data cards are produced in a way such that the correlations are taken into account properly. Nuisance parameters are treated with the Log-normal parametrization. One channel of the statistical tool is a category at defined mass point and sign. Channels with no expected signal are not present. The Asymptotic likelihood method computes the expected limit and the uncertainty bands at 1 and 2 standard deviation(s) (σ).

7.2 NNLO corrections

The NNLO cross sections are obtained with the application of a common k factor. The ratio between NNLO and LO cross sections, estimated with MC signal samples, is about 1.35 at $\sim$ 400 GeV (see Table 1 in Reference [90]), the energy scale compatible with the seesaw type III search.

7.3 Exclusion limits

Limits are set on the supposed contributions from seesaw type III signal. Combination takes in accounts all categories and it is 1D limit calculated as a function of the seesaw mediators mass. All the information are included in the input cards used for the limit calculation. For each category the considered values are:

- the number of events for signal, SM backgrounds, Fake and Dalitz backgrounds;
- the six background uncertainties in Table 5.20;
- the total uncertainty due to trigger and object efficiency in Table 5.19.

The uncertainty values on signals are calculated for mass 180 GeV, sign $+$, and assumed to be constant (see Section 5.11). Combining the different categories with the same total charge, the systematic of the SM backgrounds are considered correlated, the systematic due to Fake and Dalitz events are considered uncorrelated.

Figures 7.1 and 7.2 depict the interpretation of the seesaw type III results. The solid blue line corresponds to the seesaw triplet production cross section at NNLO $\times$ BR (theoretic line). The light and dark shaded areas represent respectively the one and two standard deviation(s) (σ) limits on the expected results (dashed line) obtained from MC pseudo experiments. These uncertainties reflect the combined statistical and systematic SM contributions, assuming for the signal flavor democratic scenario with $V_\alpha = 10^{-6}$.

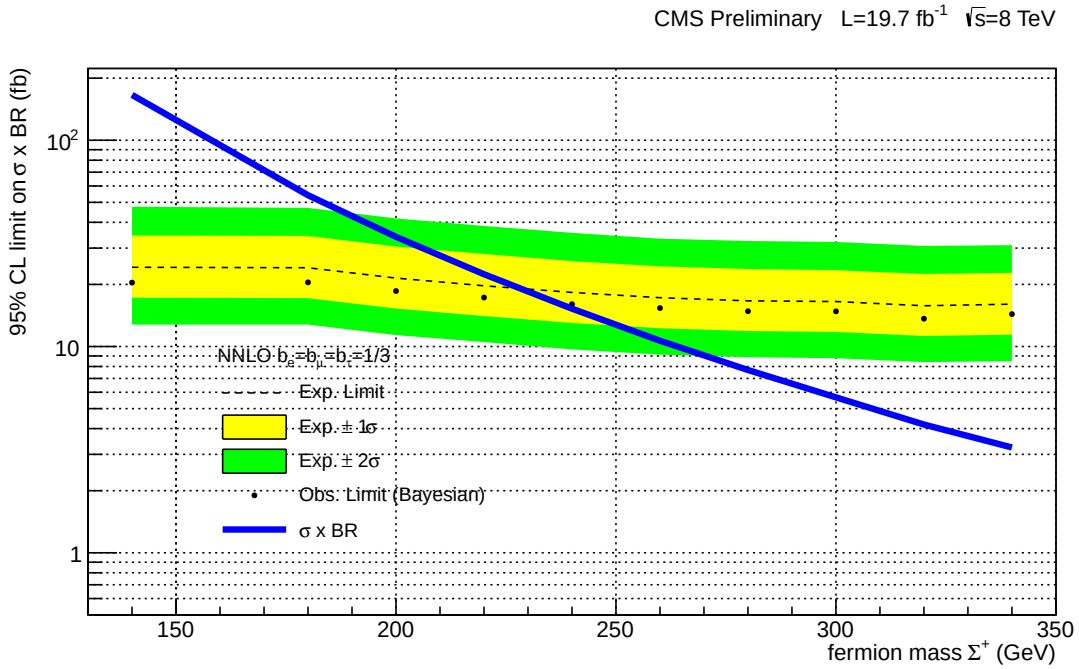

Figure 7.1: The expected and observed exclusion limits at 95% confidence on $\sigma \times$ BR as a function of the Σ mass. The light and dark shaded areas represent respectively the 1 standard deviation (σ) and 2 standard deviation (σ) limits on the expected results (dashed line) obtained from MC pseudo experiments. These uncertainties reflect the combined statistical and systematic SM contributions, assuming for the signal $b_e = b_\mu = b_\tau = 1/3$.

Tables 7.1 and 7.2 recap the information coming out the interpretations. The extracted upper limits at 95 % confidence level on cross sections $\times$BR of $\Sigma^{\pm}\Sigma^{0}$ to three charged lepton final

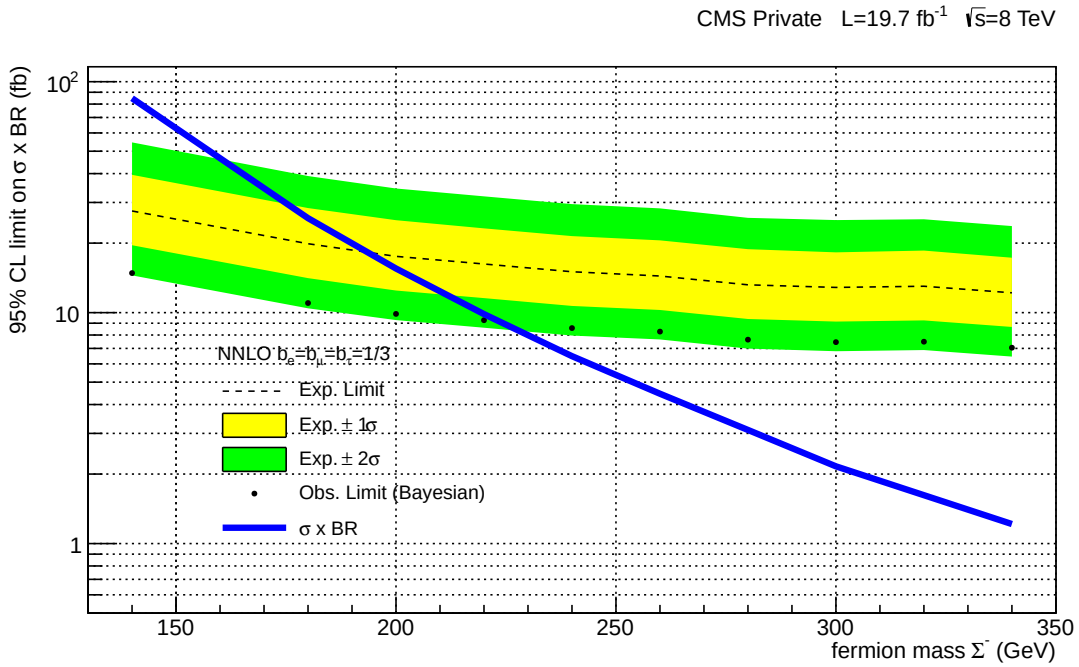

Figure 7.2: The expected and observed exclusion limits at 95% confidence on $\sigma \times$ BR as a function of the Σ mass. The light and dark shaded areas represent respectively the 1 standard deviation (σ) and 2 standard deviation (σ) limits on the expected results (dashed line) obtained from MC pseudo experiments. These uncertainties reflect the combined statistical and systematic SM contributions, assuming for the signal $b_e = b_\mu = b_\tau = 1/3$.

states in fb are set. Then, they are translated into lower limit on the corresponding seesaw mediator mass.

Table 7.1: Expected and observed upper limits at 95% CL on $\sigma \times$BR and their translation in lower limits at 95% CL for the mediator Σ^+ mass in flavor democratic scenario.

95% on $\sigma \times$ BR (fb)		95% on M_{Σ^+} GeV	
Exp.	Obs.	Exp.	Obs.
19	19	230	240

Table 7.2: Expected and observed upper limits at 95% CL on $\sigma \times$BR and their translation in lower limits at 95% CL for the mediator Σ^- mass in flavor democratic scenario.

95% on $\sigma \times$ BR (fb)		95% on M_{Σ^-} GeV	
Exp.	Obs.	Exp.	Obs.
16	8	200	240

The mass limit for the negative charge triplet is expected to be lower with respect to the positive charge because signal and SM background cross sections scale down of ~ 50 %, but Fake and Dalitz events should be independent to the charge.

7.4 Reinterpretation of results

Theorists propose a comparative review of seesaw signals at LHC experiments (see Reference [52]) with emphasis on multilepton final states and remark that some seesaw variant are not covered yet. They also give a critical summary of current experimental limits and suggest the reinterpretations of experimental searches. Seesaw type I and III have normal and inverse modes. All the three types follow a single or pair production, with or without extra particles. There are final states with one up to six charged leptons and different decay channels. In the seesaw signal zoo, the search described is for type III normal mode in pair production without extra particles and considering final states with exactly three charged leptons produced via W and Z bosons decays. Limits on seesaw type III are in the simplest flavor benchmarks, the flavor democratic scenario. A reinterpretation is proposed. It is possible to present general limits for seesaw type III normal mode, fixing flavor structure and let M_Σ arbitrary. A fully general limit is drawn in 2D plane [V_{eN}; $V_{\mu N}$], as exclusion regions in flavor mixing space for ten values of M_Σ. The coupling mixing parameters $V_{\alpha N}$ are the V_α defined in the Formula 2.9, N stands for the lightest of the three heavy neutrinos. Figure 7.3 is referred to results coming from 2011 CMS data analysis.

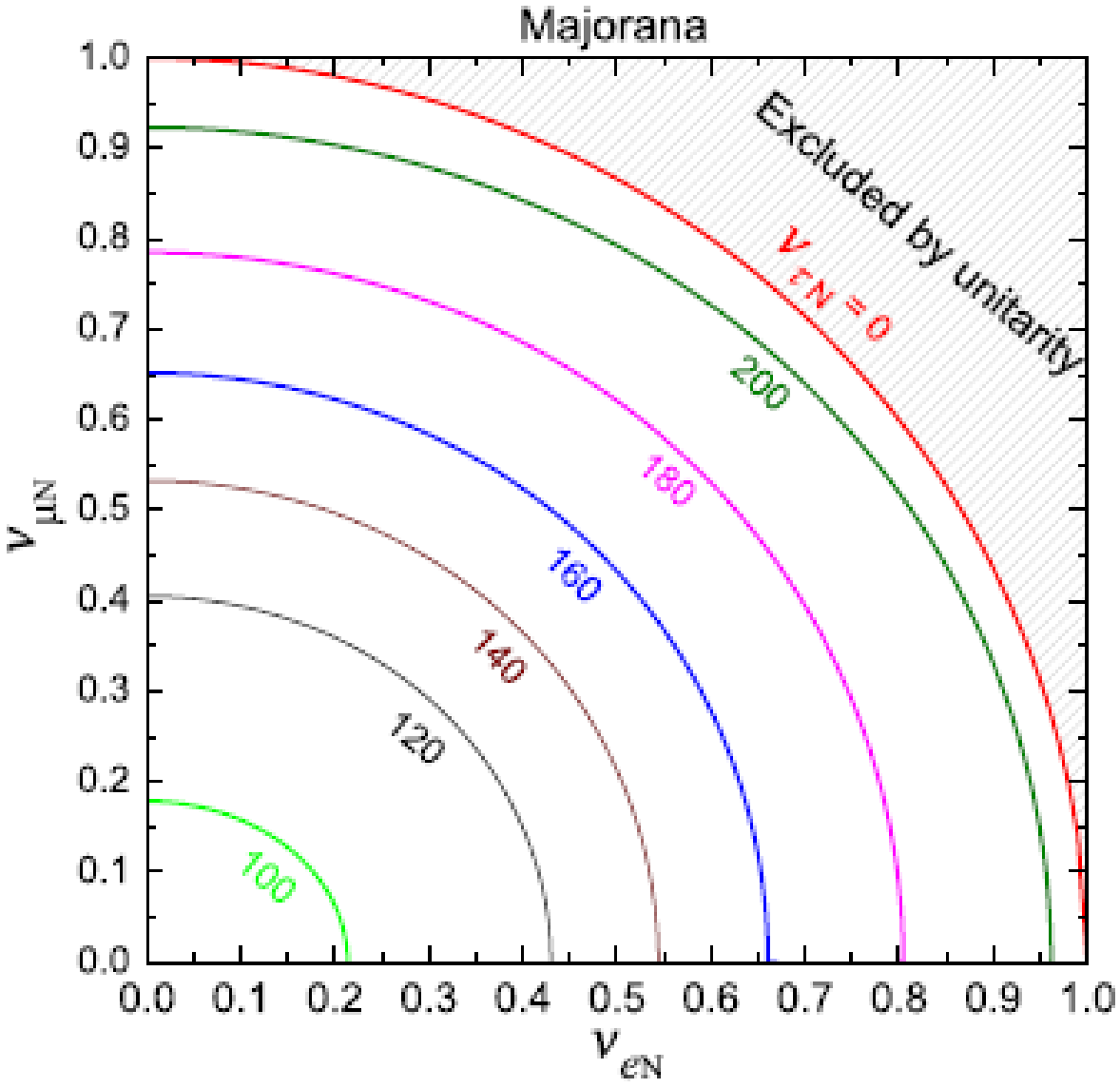

Figure 7.3: Reinterpretation of 2011 CMS results in 2D plane [V_{eN}; $V_{\mu N}$] [52].

Conclusion

The thesis has reported the analysis performed for the search of seesaw mechanism involving heavy fermion weak triplets mediators (type III). The signal is build in simplified model, for ten mediators mass values, from 140 GeV to 340 GeV, and with the mixing angles related to Yukawa couplings with all standard leptons at the "natural" value 10^{-6} . Signal production cross sections range from 122 fb for mediator positive charged at 140 GeV to 9 fb for mediator negative charged at 340 GeV. The data used for the analysis, corresponding to a total integrated luminosity of 19.7 fb^{-1}, were taken during the 2012 LHC operations with HLT dilepton triggers. The signal search has been performed looking for final states with three charged isolated leptons, jets and missing transverse energy. The major background contribution is given by SM processes, such as WZ and ZZ and WWW bosons production. Two background were obtained from data-driven methods to estimate photon asymmetric conversions (Dalitz) and non prompt leptons (Fake). The number of data events observed in all the categories is consistent with the number of predicted background events. No signal is found in the data within the sensitivity of the analysis. The results are interpreted giving the upper limits, at 95% confidence level, to the heavy fermion weak triplet mediators in the seesaw mechanism (type III model) cross sections times the branching ratio of the Σ mediators. Limits are set in flavor democratic scenario with natural mixing value of the Yukawa couplings $V_e = V_\tau = V_\mu = 10^{-6} = V_\alpha$: observed values are 19 fb for positive charged mediator, and 8 fb for negative charged mediator. The lower limit on mediators mass, at 95% confidence level, is observed at value $M_\Sigma = 240$ GeV.

The results with 8 TeV improve the limit on the positive charged mediator mass reported by CMS analysis at 7 TeV and, for the first time, explore the negative charged mediator.

Next LHC step, center of mass energy increased from 8 to 13 TeV in 2015, open new interesting possibilities to discover the seesaw type III mechanism or to increase the exclusion limit value of mediators mass.

Acknowledgements

I thank the technical and administrative staffs at Padua University, at National Institute of Nuclear Physics (INFN) National Laboratory of Legnaro and at CERN. Educational periods such specific schools, meetings, seminars were important and helpful in developing my PhD path: staffs gave me possibilities to participate and to present results at national and international conferences. I acknowledge support from all CMS Padova and LNL teams. Paolo Checchia, the CMS Padova team leader, and Ezio Torassa, the CMS Padova deputy team leader and my supervisor, helped me directly during three year as PhD student. Ugo Gasparini, my co spervisor from Padova group, and Gaetano Maron, my co supervisor from LNL team, designed my studies path regarding graduate courses and support teaching activities. Ezio, Paolo, Ugo and Gaetano proposed me for key role in CMS collaboration such as cDAQ shifter, DT detector on call expert shifter, DT trigger emulator responsible: these tasks are crucial in my future activities, so I hope to take advantages from those experiences. I thank Stefano Lacaprara for discussions about data analysis steps without any problems of time and for help during difficult periods. I acknowledge support from Massimo Biasotto and Michele Gulmini about specific sections in my thesis. I also thank Carla Biggio, theoretician colleague at INFN Genova, and Andrea Wulzer, theoretician colleague at INFN Padua, for the model discussions moments. I give a very special thank to CMS Padova previous PhD students: Mia Tosi, Paolo Bellan, Antonio Branca, Kostya Kanishev and Sara Vanini. Sara during 2013 spent a lot of time in my office to modify, refine, re tune, review, rebuild the analysis: she is a special extra tutor. Finally, a thought for future CMS Padova PhD students. I thank Alberto Zucchetta, Jacopo Pazzini and Martino Dall'Osso for common experiences in daily working and studying activities.
I wish a great future for all CMS Padova and LNL groups.

References

[1] S.L.Glashow, "Partial-Symmetries of Weak Interactions", *Nucl. Phys.* **22** (1961) 579, doi:doi:10.1016/0029-5582(61)90469-2.

[2] S.Weinberg, "A Model of Leptons", *Phys. Rev. Lett* **19** (1967) 1264, doi:doi:10.1103/PhysRevLett.19.1264.

[3] D.J.Gross and F.Wilczek, "Ultraviolet Behavior of Non-Abelian Gauge Theories", *Phys. Rev. Lett* **30** (1973) 1343, doi:doi:10.1103/PhysRevLett.30.1343.

[4] H.D.Politzer, "Reliable Perturbative Results for Strong Interactions?", *Phys. Rev. Lett* **30** (1973) 1346, doi:doi:10.1103/PhysRevLett.30.1346.

[5] CMS Collaboration, "Observation of a new boson at a mass of 125 GeV with the CMS experiment at the LHC", *Phys. Lett.* **B 716** (Jul, 2012) 30–61, doi:doi:10.1007/JHEP06(2013)081.

[6] ATLAS Collaboration, "Observation of a New Particle in the Search for the Standard Model Higgs Boson with the ATLAS Detector at the LHC", *Phys. Lett.* **B 716** (Jul, 2012) 1–29.

[7] ATLAS Collaboration, "Combined measurements of the mass and signal strength of the Higgs-like boson with the ATLAS detector using up to 25 /fb of proton-proton collision data", *ATLAS-CONF-2013-014* (March, 2013) doi:http://cds.cern.ch/record/1523727.

[8] CMS Collaboration, "Measurement of the properties of a Higgs boson in the four-lepton final state", *Phys. Rev.* **D** (2014).

[9] CMS Collaboration, "Measurement of Higgs boson production and properties in the WW decay channel with leptonic final states", *Journal of High Energy Physics* (2014).

[10] CMS Collaboration, "Search for new physics in events with same-sign dileptons and jets", *JHEP* (2013).

[11] CMS Collaboration, "Search for anomalous production of events with three or more leptons", *CMS Physics Analysis Summary* **SUS-13-002** (2013).

[12] K. Hirata, T. Kajita, M. Koshiba et al., "Observation of a neutrino burst from the supernova SN1987A", *Phys. Rev. Lett.* **58** (Apr, 1987) 1490–1493, doi:10.1103/PhysRevLett.58.1490.

[13] C. L. Cowan, F. Reines, F. B. Harrison et al., "Detection of the Free Neutrino: A Confirmation", *Science* **124** (1956) 103.

[14] C. L. Cowan and F. Reines, "The Neutrino", *Nature* **178** (1956) 446.

[15] WMAP Collaboration, "First Year Wilkinson Microwave Anisotropy Probe (WMAP) Observations: Determination of Cosmological Parameters", *Astrophys. J. Suppl.* **148** (2003) 175, doi:arXiv:astro-ph/0302209.

[16] SDSS Collaboration, "Cosmological parameters from SDSS and WMAP", *Phys. Rev.* **D69** (2004) 103501, doi:10.1103/PhysRevD.69.103501.

[17] K. Ichikawa, M. Fukugita, and M. Kawasaki, "Constraining neutrino masses by CMB experiments alone", *Phys. Rev.* **D71** (2005) 043001, doi:10.1103/PhysRevD.71.043001.

[18] F. Capozzi, G. Fogli, E. Lisi et al., "Status of three-neutrino oscillation parameters, circa 2013", *JHEP* (2013).

[19] DAYA BAY Collaboration, "Spectral measurement of electron antineutrino oscillation amplitude and frequency at Daya Bay", *Phys. Rev. Lett.* (2014).

[20] RENO Collaboration, "Recent Results from RENO", *talk at WIN 2013, XXIV International Workshops on Weak Interactions and Neutrinos* (2013) arXiv:hep.if.usp.br/WIN13.

[21] T2K Collaboration, "Evidence of electron neutrino appearance in a muon neutrino beam", *Phys. Rev.* **D88** (2013) 032002, doi:10.1103/PhysRevD.88.032002.

[22] T2K Collaboration, "Measurement of Neutrino Oscillation Parameters from Muon Neutrino Disappearance with an Off-axis Beam", *Phys. Rev. Lett.* **111** (2013) 211803.

[23] MINOS Collaboration, "Electron neutrino and antineutrino appearance in the full MINOS data sample", *Phys. Rev. Lett.* **110** (2013) 171801.

[24] MINOS Collaboration, "Measurement of Neutrino and Antineutrino Oscillations Using Beam and Atmospheric Data in MINOS", *Phys. Rev. Lett.* **110** (2013) 251801.

[25] T. Han and B. Zhang, "Signatures for Majorana neutrinos at hadron colliders", *Phys. Rev. Lett.* **97** (2006) doi:10.1103/PhysRevLett.97.171804.

[26] J. A.-S. F. del Aguila and R. Pittau, "Heavy neutrino signals at large hadron colliders", *JHEP* **0710** (2007) doi:10.1088/1126-6708/2007/10/047.

[27] J. Kersten and A. Y. Smirnov, "Right-Handed Neutrinos at LHC and the Mechanism of Neutrino Mass Generation", *Phys.Rev.* **D76** (2007) doi:10.1103/PhysRevD.76.073005.

[28] M. Muhlleitner and M. Spira, "A Note on Doubly-Charged Higgs Pair Production at Hadron Colliders", *Phys.Rev.* **D68** (2003) doi:10.1103/PhysRevD.68.117701.

[29] A. Akeroyd and M. Aoki, "Single and Pair Production of Doubly Charged Higgs Bosons at Hadron Colliders", *Phys.Rev.* **D72** (2005) doi:10.1103/PhysRevD.72.035011.

[30] Z.-z. X. W. Chao, Z.-G. Si and S. Zhou, "Correlative signatures of heavy Majorana neutrinos and doubly-charged Higgs bosons at the Large Hadron Collider", *Phys.Lett.* **B666** (2008) doi:10.1016/j.physletb.2008.08.003.

[31] H. L. R. Foot, X.-G. He, and G. Joshi, "See-saw neutrino masses induced by a triplet of leptons", *Z. Phys.* **C44** (1989) doi:10.1007/BF01415558.

[32] T. H. R. Franceschini and A. Strumia, "Type-III see-saw at LHC", *Phys.Rev.* **D78** (2008) doi:10.1103/PhysRevD.78.033002.

[33] F. del Aguila and J. Aguilar-Saavedra, "Distinguishing seesaw models at LHC with multi-lepton signals", *Nucl. Phys.* **B813** (2009) doi:10.1016/j.nuclphysb.2008.12.029.

[34] C. Biggio and F. Bonnet, "A Simple Realization of the Inverse Seesaw Mechanism", *Phys. Rev.* **D86** (2012) 035007, doi:10.1103/PhysRevD.86.035007.

[35] L3 Collaboration, "Search for isosinglet neutral heavy leptons in Z decays", *Phys. Lett.* **B295** (1992) 371, doi:10.1016/0370-2693(92)91579-X.

[36] DELPHI Collaboration, "Search for neutral heavy leptons produced in Z decays", *Z. Phys.* **C74** (1997) 57, doi:doi:10.1007/s002880050370.

[37] ATLAS Collaboration, "Inclusive search for same-sign dilepton signatures in pp collisions at 7 TeV with the ATLAS detector", *JHEP* **10** (2011) 107, doi:doi:10.1007/JHEP10(2011)107, arXiv:arXiv:1108.0366.

[38] ATLAS Collaboration, "Search for heavy neutrinos and right-handed W bosons in events with two leptons and jets in pp collisions at s = 7 TeV with the ATLAS detector", *Eur. Phys. J.* **C72** (2012) 2056, doi:doi:10.1140/epjc/s10052-012-2056-4, arXiv:arXiv:1203.5420.

[39] CMS Collaboration, "Search for heavy Majorana neutrinos in dimuon and dielectron events in pp collisions at 7 TeV", *Phys. Lett.* **B717** (2012) 109, doi:10.1016/j.physletb.2012.09.012, arXiv:arXiv:1207.6079.

[40] CMS Collaboration, "A search for a doubly-charged Higgs boson in pp collisions at 7 TeV", *Eur. Phys. J.* **C72** (2012) 2189, doi:10.1140/epjc/s10052-012-2189-5, arXiv:arXiv:1207.2666.

[41] M. Swartz, "Limits on doubly charged Higgs boson and lepton flavor violation", *Phys. Rev.* **D40** (1989) 1521, doi:10.1103/PhysRevD.40.1521.

[42] M. Swartz, "A search for doubly charged Higgs scalars in Z decay", *Phys. Rev. Lett.* **64** (1990) 2877, doi:10.1103/PhysRevLett.64.2877.

[43] H1 Collaboration, "Search for doubly-charged Higgs boson production at HERA", *Phys. Lett.* **B638** (2006) 432, doi:10.1016/j.physletb.2006.05.061, arXiv:arXiv:hep-ex/0604027.

[44] L3 Collaboration, "Search for doubly charged Higgs bosons at LEP", *Phys. Lett.* **B576** (2003) 18, doi:10.1016/j.physletb.2003.09.082, arXiv:arXiv:hep-ex/0309076.

[45] DELPHI Collaboration, "Search for doubly charged Higgs bosons at LEP-2", *Phys. Lett.* **B552** (2003) 127, doi:10.1016/S0370-2693(02)03125-8, arXiv:arXiv:hep-ex/0303026.

[46] OPAL Collaboration, "Search for the single production of doubly charged Higgs bosons and constraints on their couplings from Bhabha scattering", *Phys. Lett.* **B577** (2003) 93, doi:10.1016/j.physletb.2003.10.034, arXiv:arXiv:hep-ex/0308052.

[47] CDF Collaboration, "Search for new physics in high p T like-sign dilepton events at CDF II", *Phys. Rev. Lett.* **107** (2011) 181801, doi:10.1103/PhysRevLett.107.181801, arXiv:arXiv:1108.0101.

[48] ATLAS Collaboration, "Search for anomalous production of prompt like-sign muon pairs and constraints on physics beyond the Standard Model with the ATLAS detector", *Phys. Rev.* **D88** (2012) 032004, doi:10.1103/PhysRevD.85.032004, arXiv:arXiv:1201.1091.

[49] F. Del Aguila et al., "Effects of new leptons in electroweak precision data", *Phys. Rev.* **D78** (2008) 13, arXiv:arXiv:0803.4008.

[50] C. Biggio and F. Bonnet, "Implementation of the type III seesaw model in FeynRules/MadGraph and prospects for discovery with early LHC data", *Eur. Phys.J.* **C** (2012) 72:1899, doi:10.1140/epjc/s10052-012-1899-z.

[51] CMS Collaboration, "Search for heavy lepton partners of neutrinos in proton-proton collisions in the context of the type III seesaw mechanism", *Phys. Lett.* **B718** (2012) 348, arXiv:arXiv:1210.1797.

[52] J. Aguilar Saavedra, P. Boavida, and F. Joaquim, "Flavoured searches for type-III seesaw at the LHC", *Phys. Lett.* **D88** (2013) 113008, doi:10.1103/PhysRevD.88.113008, arXiv:arXiv:1308.3226.

[53] T. Sjostrand, "A model for initial state parton showers", *Phys. Lett.* **B157** (1985) 67.

[54] A. Alloul, N. Christensen, C. Degrande et al., "FeynRules 2.0 - A complete toolbox for tree-level phenomenology", *CERN-PH-TH/2013-239* (2013) arXiv:arXiv:1310.1921.

[55] J. Alwall, M. Herquet, et al., "MadGraph 5 : Going Beyond", *JHEP* **1106 128B517** (2011) 128, doi:10.1007/JHEP06(2011)128.

[56] T. Sjöstrand, S. Mrenna, and P. Skands, "PYTHIA 6.4 physics and manual", *JHEP* **05** (2006) 026, doi:10.1088/1126-6708/2006/05/026, arXiv:hep-ph/0603175.

[57] CMS Collaboration, "Detector and Software Technical Design Report", *CERN-LHCC-2006-001* **1** (2006) doi:http://cds.cern.ch/record/922757.

[58] C. Degrande et al., "UFO - The Universal FeynRules Output", *Comput. Phys. Commun.* **183** (2012) doi:10.1016/j.cpc.2012.01.022.

[59] S. Agostinelli et al., "GEANT4: A Simulation toolkit", *Nucl.Instrum.Meth.* **A506** (2003) 250, doi:10.1016/S0168-9002(03)01368-8.

[60] I. Wolfram Research, "Mathematica", *Version 9.0* (2012).

[61] CMS Collaboration, "The CMS experiment at the CERN LHC", *JINST* **03** (2008) S08004, doi:10.1088/1748-0221/3/08/S08004.

[62] CMS Collaboration, "Tracker Technical Design Report", *CERN/LHCC 98-6* (1998).

[63] CMS Collaboration, "CMS ECAL Technical Design Report", *CERN/LHCC 97-33* (1997).

[64] CMS Collaboration, "CMS HCAL Technical Design Report", *CERN/LHCC 97-31* (1997).

[65] CMS Collaboration, "CMS MUON Technical Design Report", *CERN/LHCC 97-32* (1997).

[66] M. Gulmini et al., "Run Control and Monitor System for the CMS experiment", in *Computing in high energy and nuclear physics*. 2003. La Jolla (California).

[67] M. Biasotto et al., "The Legnaro-Padova distributed Tier-2:challenges and results", in *Computing in high energy and nuclear physics*. 2013.

[68] CMS Collaboration, "Particle flow event reconstruction in CMS and performance for jets, taus, and missing transverse energy", *CMS Physics Analysis Summary* **CMS-PAS-PFT-09-001** (2009).

[69] CMS Collaboration, "Commissioning of the particle-flow event reconstruction with the first LHC collisions recorded in the CMS detector", *CMS Physics Analysis Summary* **CMS-PAS-PFT-10-001** (2010).

[70] CMS Collaboration, "Commissioning of the particle-flow reconstruction in minimum-bias and jet events from pp collisions at 7 TeV", *CMS Physics Analysis Summary* **CMS-PAS-PFT-10-002** (2010).

[71] CMS Collaboration, "Particle-flow commissioning with muons and electrons from J/Psi, and W events at 7 TeV", *CMS Physics Analysis Summary* **CMS-PAS-PFT-10-003** (2010).

[72] M. Cacciari, G. P. Salam, and G. Soyez, "The anti-k_t jet clustering algorithm", *JHEP* **04** (2008) 063, doi:10.1088/1126-6708/2008/04/063, arXiv:0802.1189.

[73] CMS Collaboration Collaboration, "Determination of Jet Energy Calibration and Transverse Momentum Resolution in CMS", *JINST* **6** (2011) 11002, doi:10.1088/1126-6708/2008/04/063, arXiv:1107.4277.

[74] Z. Was, "TAUOLA the library for tau lepton decay, and KKMC-KORALB-KORALZ status report", *Nucl.Phys.Proc.Suppl.* **98** (2001) 96, doi:10.1016/S0920-5632(01)01200-2, arXiv:hep-ph/0011305.

[75] CMS Collaboration, "Measurement of WZ production rate", *CMS Physics Analysis Summary* **CMS-PAS-SMP-12-006** (2013).

[76] CMS Collaboration, "Measurement of W+W- and ZZ production cross sections in pp collisions at sqrt(s) = 8 TeV", *Phys. Lett.* **B721** (2013) 190, doi:10.1016/j.physletb.2013.03.027, arXiv:arXiv:1301.4698.

[77] CMS Collaboration, "Measurement of the t t-bar production cross section in the dilepton channel in pp collisions at 8 TeV", *JHEP* (2014) arXiv:arXiv:1312.7582.

[78] CMS Collaboration, "Measurement of inclusive W and Z boson cross sections in pp collisions at 8 TeV", *CMS-PAS-SMP-12-011* (2014) arXiv:http://cds.cern.ch/record/1460098.

[79] CMS Collaboration, "Search for new physics in events with same-sign dileptons and b jets in pp collisions at 8TeV", *JHEP* **03** (2013) 037, doi:10.1007/JHEP03(2013)037.

[80] CMS Collaboration, "Background and Efficiency Determination Methods for Multilepton Analyses", *AN Analysis Note* **AN-2012-257** (2012).

[81] CMS Collaboration, "A search for anomalous production of events with three or more leptons using 19.5 /fb of 8 TeV LHC data", *AN Analysis Note* **AN-2012-343** (2012).

[82] CMS Collaboration, "Search for new physics in a final state with same-sign lepton pair, jets, and missinge transverse energy using the full 2012 CMS dataset", *AN Analysis Note* **AN-2013-120** (2013).

[83] CMS Collaboration, "Inclusive W/Z cross section at 8 TeV", *CMS Physics Analysis Summary* **CMS-PAS-SMP-12-011** (2013).

[84] ATLAS Collaboration, "ATLAS detector and physics performance : Technical Design Report, 2", *CERN-LHCC-99-015* (1999) arXiv:http://cds.cern.ch/record/391177.

[85] ATLAS Collaboration, "Search for Type III Seesaw Model Heavy Fermions in Events with Four Charged Leptons using 5.8 /fb of 8 TeV data with the ATLAS Detector", *ATLAS-CONF-2013-019* (2013) doi:http://cds.cern.ch/record/1525526.

[86] CMS Collaboration, "Search for heavy lepton partners of neutrinos in pp collisions at 8 TeV, in the context of type III seesaw mechanism", *CMS Physics Analysis Summary* **CMS-PAS-EXO-14-001** (2014).

[87] L. Moneta et al., "The RooStats Project", in *13th International Workshop on Advanced Computing and Analysis Techniques in Physics Research (ACAT2010)*. SISSA, 2010. arXiv:1009.1003. PoS(ACAT2010)057.

[88] ATLAS, CMS Collaboration, "Procedure for the LHC higgs boson search combination in Summer2011", atl-phys-pub 2011-11/cms note, 2011/005 (2011), LHCforse, (2011).

[89] C. Robert and G. Casella, "Monte Carlo statistical methods", *book* (2004) doi:ISBN0-387-21239-6.

[90] CMS Collaboration, "Search for W'/technirho in WZ using leptonic final states", *CMS Physics Analysis Summary* **CMS-PAS-EXO-12-025** (2013).

Appendix A

Definitions

Natural units are used (h=c=1). Energy is expressed in eV.

Discussing the physical dimensions of the detector, Cartesian coordinates are used, where x points inwards to the center of the accelerator, y is positive in the upwards vertical direction and z is aligned along the beam pipe (pointing towards the Jura mountains). The kinematics of physical events and certain aspects of the detector are discussed in terms of the coordinate system (η; ϕ; z). In the previous system, z is defined as in the Cartesian system and the azimuthal angle, ϕ, is given by: $\phi = arctan[\frac{y}{x}]$. The pseudo rapidity, η, is defined as $\eta = ln[tan(\frac{\theta}{2})]$, where θ is the polar angle $\theta = arctan[\frac{\sqrt{(x^2+y^2)}}{z}]$.

Appendix B

MADGRAPH cards

Parameter card for mass 180 GeV is reported. The other nine are similar. Process card for sign + is reported. Charge conjugation operator gives the card for sign -. Process card has 6 processes because processes with H boson are excluded. Run card is unique for all the production sample.

```
***********************************************************************
** PARAM CARD AUTOMATICALY GENERATED BY MG5 FOLLOWING UFO MODEL ****
***********************************************************************
** **
** Width set on Auto will be computed following the information **
** present in the decay.py files of the model. By default, **
** this is only 1to2 decay modes. **
** **
***********************************************************************


***********************************
** INFORMATION FOR CKMBLOCK
***********************************
Block ckmblock
1 0.000000e+00 * cabi
2 0.000000e+00 * theta13
3 0.000000e+00 * theta12
4 0.000000e+00 * theta23


***********************************
** INFORMATION FOR MASS
***********************************
Block mass
1 5.040000e-03 * MD
2 2.550000e-03 * MU
3 1.040000e-01 * MS
4 1.420000e+00 * MC
5 4.700000e+00 * MB
6 1.743000e+02 * MT
11 5.110000e-04 * Me
13 1.056600e-01 * MM
15 1.777000e+00 * MTA
23 9.118800e+01 * MZ
```

```
25 1.253000e+02 * MH
8000018 1.800000e+02 * Mtr0
8000020 1.800000e+02 * Mtrch
** Dependent parameters, given by model restrictions.
** Those values should be edited following the
** analytical expression. MG5 ignores those values
** but they are important for interfacing the output of MG5
** to external program such as Pythia.
21 0.000000 * g : 0.0
22 0.000000 * a : 0.0
24 79.825164 * w+
8000012 0.000000 * v1 : 0.0
8000014 0.000000 * v2 : 0.0
8000016 0.000000 * v3 : 0.0
***********************************
** INFORMATION FOR MIXING
***********************************
Block mixing
1 1.000000e-06 * Ve
2 1.000000e-06 * Vm
3 1.000000e-06 * Vtt


***********************************
** INFORMATION FOR NEWMASSES
***********************************
Block newmasses
1 0.000000e+00 * mv1
2 0.000000e+00 * mv2
3 0.000000e+00 * mv3
4 1.800000e+02 * mtr
5 1.800000e+02 * mtrm


***********************************
** INFORMATION FOR SMINPUTS
***********************************
Block sminputs
1 1.279000e+02 * aEWM1
2 1.166390e-05 * Gf
3 1.180000e-01 * aS


***********************************
** INFORMATION FOR YUKAWA
***********************************
Block yukawa
4 0.000000e+00 * ymc
5 4.700000e+00 * ymb
6 1.743000e+02 * ymt
13 0.000000e+00 * yme
```

14 0.000000e+00 * ymm
15 0.000000e+00 * ymtau

****
** INFORMATION FOR DECAY
****
*DECAY 4 1.000000e-01 * WC
*DECAY 5 1.000000e-01 * WB
*DECAY 6 1.508336e+00 * WT
*DECAY 15 1.000000e-01 * Wtau
*DECAY 23 2.441404e+00 * WZ
*DECAY 24 2.047600e+00 * WW
*DECAY 25 5.753088e-03 * WH
*DECAY 8000018 3.600000e-12 * Wtr0
*DECAY 8000020 3.600000e-12 * Wtrch
** Dependent parameters, given by model restrictions.
** Those values should be edited following the
** analytical expression. MG5 ignores those values
** but they are important for interfacing the output of MG5
** to external program such as Pythia.
*DECAY 1 0.000000 * d : 0.0
*DECAY 2 0.000000 * u : 0.0
*DECAY 3 0.000000 * s : 0.0
*DECAY 11 0.000000 * e- : 0.0
*DECAY 13 0.000000 * mu- : 0.0
*DECAY 21 0.000000 * g : 0.0
*DECAY 22 0.000000 * a : 0.0
*DECAY 8000012 0.000000 * v1 : 0.0
*DECAY 8000014 0.000000 * v2 : 0.0
*DECAY 8000016 0.000000 * v3 : 0.0

****
** INFORMATION FOR DECAY
****
DECAY 8000002 0.00000000e+00 * T1 decays
* BR NDA ID1 ID2
*
DECAY 25 5.4039e-03 * h decays
* BR NDA ID1 ID2
0.00000000e+00 2 -11 11 * BR(h to e+ e-)
0.00000000e+00 2 -11 13 * BR(h to e+ m-)
0.00000000e+00 2 -11 15 * BR(h to e+ tt-)
0.00000000e+00 2 -13 11 * BR(h to m+ e-)
0.00000000e+00 2 -13 13 * BR(h to m+ m-)
0.00000000e+00 2 -13 15 * BR(h to m+ tt-)
0.00000000e+00 2 -15 11 * BR(h to tt+ e-)
0.00000000e+00 2 -15 13 * BR(h to tt+ m-)
0.00000000e+00 2 -15 15 * BR(h to tt+ tt-)

0.00000000e+00 2 8000012 8000012 * BR(h to v1 v1)
0.00000000e+00 2 8000014 8000012 * BR(h to v2 v1)
0.00000000e+00 2 8000014 8000014 * BR(h to v2 v2)
0.00000000e+00 2 8000016 8000012 * BR(h to v3 v1)
0.00000000e+00 2 8000016 8000014 * BR(h to v3 v2)
0.00000000e+00 2 8000016 8000016 * BR(h to v3 v3)
1.00000000e+00 2 -5 5 * BR(h to b b)
0.00000000e+00 2 -4 4 * BR(h to c c)
0.00000000e+00 2 -1 1 * BR(h to d d)
0.00000000e+00 2 -3 3 * BR(h to s s)
0.00000000e+00 2 -2 2 * BR(h to u u)
*
DECAY 6 1.54424720e+00 * t decays
* BR NDA ID1 ID2
1.00000000e+00 2 5 24 * BR(t to b w+)
0.00000000e+00 2 1 24 * BR(t to d w+)
0.00000000e+00 2 3 24 * BR(t to s w+)
*
DECAY 8000020 1.6651e-11 * tr- decays
* BR NDA ID1 ID2
9.61000000e-02 2 11 23 * BR(tr- to e- z)
9.61000000e-02 2 13 23 * BR(tr- to m- z)
9.61000000e-02 2 15 23 * BR(tr- to tt- z)
2.01000000e-01 2 8000012 -24 * BR(tr- to v1 w-)
2.01000000e-01 2 8000014 -24 * BR(tr- to v2 w-)
2.01000000e-01 2 8000016 -24 * BR(tr- to v3 w-)
3.05300000e-02 2 11 25 * BR(tr- to e- h)
3.05300000e-02 2 13 25 * BR(tr- to m- h)
3.05300000e-02 2 15 25 * BR(tr- to tt- h)
*
DECAY -8000020 1.6651e-11 * tr+ decays
* BR NDA ID1 ID2
9.61000000e-02 2 -11 23 * BR(tr+ to e+ z)
9.61000000e-02 2 -13 23 * BR(tr+ to m+ z)
9.61000000e-02 2 -15 23 * BR(tr+ to tt+ z)
2.01000000e-01 2 8000012 24 * BR(tr+ to v1 w+)
2.01000000e-01 2 8000014 24 * BR(tr+ to v2 w+)
2.01000000e-01 2 8000016 24 * BR(tr+ to v3 w+)
3.05300000e-02 2 -11 25 * BR(tr+ to e+ h)
3.05300000e-02 2 -13 25 * BR(tr+ to m+ h)
3.05300000e-02 2 -15 25 * BR(tr+ to tt+ h)
*
DECAY 8000018 1.6651e-11 * tr0 decays
* BR NDA ID1 ID2
9.61000000e-02 2 8000012 23 * BR(tr0 to v1 z)
9.61000000e-02 2 8000014 23 * BR(tr0 to v2 z)
9.61000000e-02 2 8000016 23 * BR(tr0 to v3 z)
1.03360000e-01 2 -11 -24 * BR(tr0 to e+ w-)
1.03360000e-01 2 -13 -24 * BR(tr0 to m+ w-)

1.03360000e-01 2 -15 -24 * BR(tr0 to tt+ w-)
1.03360000e-01 2 11 24 * BR(tr0 to e- w+)
1.03360000e-01 2 13 24 * BR(tr0 to m- w+)
1.03360000e-01 2 15 24 * BR(tr0 to tt- w+)
3.05300000e-02 2 8000012 25 * BR(tr0 to v1 h)
3.05300000e-02 2 8000014 25 * BR(tr0 to v2 h)
3.05300000e-02 2 8000016 25 * BR(tr0 to v3 h)
*
DECAY 8000012 0.00000000e+00 * v1 decays
* BR NDA ID1 ID2
*
DECAY 8000014 0.00000000e+00 * v2 decays
* BR NDA ID1 ID2
*
DECAY 8000016 0.00000000e+00 * v3 decays
* BR NDA ID1 ID2
*
DECAY 24 2.0026e+00 * w+ decays
* BR NDA ID1 ID2
1.11158273e-01 2 8000012 -11 * BR(w+ to v1 e+)
0.00000000e+00 2 8000014 -11 * BR(w+ to v2 e+)
0.00000000e+00 2 8000016 -11 * BR(w+ to v3 e+)
0.00000000e+00 2 8000012 -13 * BR(w+ to v1 m+)
1.11158273e-01 2 8000014 -13 * BR(w+ to v2 m+)
0.00000000e+00 2 8000016 -13 * BR(w+ to v3 m+)
0.00000000e+00 2 8000012 -15 * BR(w+ to v1 tt+)
0.00000000e+00 2 8000014 -15 * BR(w+ to v2 tt+)
1.11158273e-01 2 8000016 -15 * BR(w+ to v3 tt+)
0.00000000e+00 2 4 -5 * BR(w+ to c b)
0.00000000e+00 2 2 -5 * BR(w+ to u b)
0.00000000e+00 2 4 -1 * BR(w+ to c d)
3.33275074e-01 2 2 -1 * BR(w+ to u d)
3.33275074e-01 2 4 -3 * BR(w+ to c s)
0.00000000e+00 2 2 -3 * BR(w+ to u s)
*
DECAY -24 2.0026e+00 * w- decays
* BR NDA ID1 ID2
1.11158273e-01 2 11 8000012 * BR(w- to e- v1)
0.00000000e+00 2 11 8000014 * BR(w- to e- v2)
0.00000000e+00 2 11 8000016 * BR(w- to e- v3)
0.00000000e+00 2 13 8000012 * BR(w- to m- v1)
1.11158273e-01 2 13 8000014 * BR(w- to m- v2)
0.00000000e+00 2 13 8000016 * BR(w- to m- v3)
0.00000000e+00 2 15 8000012 * BR(w- to tt- v1)
0.00000000e+00 2 15 8000014 * BR(w- to tt- v2)
1.11158273e-01 2 15 8000016 * BR(w- to tt- v3)
0.00000000e+00 2 5 -4 * BR(w- to b c)
0.00000000e+00 2 1 -4 * BR(w- to d c)
3.33275074e-01 2 3 -4 * BR(w- to s c)

```
0.00000000e+00 2 5 -2 * BR(w- to b u  )
3.33275074e-01 2 1 -2 * BR(w- to d u  )
0.00000000e+00 2 3 -2 * BR(w- to s u  )
*
DECAY 23 2.411e+00 * z decays
* BR NDA ID1 ID2
3.45411110e-02 2 11 -11 * BR(z to e- e+ )
3.45411110e-02 2 13 -13 * BR(z to m- m+ )
3.45411110e-02 2 15 -15 * BR(z to tt- tt+ )
0.00000000e+00 2 13 -11 * BR(z to m- e+ )
0.00000000e+00 2 15 -11 * BR(z to tt- e+ )
0.00000000e+00 2 11 -13 * BR(z to e- m+ )
0.00000000e+00 2 15 -13 * BR(z to tt- m+ )
0.00000000e+00 2 11 -15 * BR(z to e- tt+ )
0.00000000e+00 2 13 -15 * BR(z to m- tt+ )
6.87919610e-02 2 8000012 8000012 * BR(z to v1 v1 )
0.00000000e+00 2 8000014 8000012 * BR(z to v2 v1 )
0.00000000e+00 2 8000016 8000012 * BR(z to v3 v1 )
6.87919610e-02 2 8000014 8000014 * BR(z to v2 v2 )
0.00000000e+00 2 8000016 8000014 * BR(z to v3 v2 )
6.87919610e-02 2 8000016 8000016 * BR(z to v3 v3 )
1.50438357e-01 2 5 -5 * BR(z to b b  )
1.17680280e-01 2 4 -4 * BR(z to c c  )
1.52096994e-01 2 1 -1 * BR(z to d d  )
1.52096994e-01 2 3 -3 * BR(z to s s  )
1.17846144e-01 2 2 -2 * BR(z to u u  )
*


*============================================================
* QUANTUM NUMBERS OF NEW STATE(S) (NON SM PDG CODE)
*============================================================


Block QNUMBERS 8000012 * v1
1 0 * 3 times electric charge
2 2 * number of spin states (2S+1)
3 1 * colour rep (1: singlet, 3: triplet, 8: octet)
4 0 * Particle/Antiparticle distinction (0=own anti)
Block QNUMBERS 8000014 * v2
1 0 * 3 times electric charge
2 2 * number of spin states (2S+1)
3 1 * colour rep (1: singlet, 3: triplet, 8: octet)
4 0 * Particle/Antiparticle distinction (0=own anti)
Block QNUMBERS 8000016 * v3
1 0 * 3 times electric charge
2 2 * number of spin states (2S+1)
3 1 * colour rep (1: singlet, 3: triplet, 8: octet)
4 0 * Particle/Antiparticle distinction (0=own anti)
Block QNUMBERS 8000018 * tr0
```

```
1 0 * 3 times electric charge
2 2 * number of spin states (2S+1)
3 1 * colour rep (1: singlet, 3: triplet, 8: octet)
4 0 * Particle/Antiparticle distinction (0=own anti)
Block QNUMBERS 8000020 * tr-
1 -3 * 3 times electric charge
2 2 * number of spin states (2S+1)
3 1 * colour rep (1: singlet, 3: triplet, 8: octet)
4 1 * Particle/Antiparticle distinction (0=own anti)


*********************************************************************
* MadGraph/MadEvent *
* http://madgraph.hep.uiuc.edu *
* *
* run_card.dat *
* *
* This file is used to set the parameters of the run. *
* *
* Some notation/conventions: *
* *
* Lines starting with a '* ' are info or comments *
* *
* mind the format: value = variable ! comment *
*********************************************************************
*
*******************
* Running parameters
*******************
* *********************************************************************
* Tag name for the run (one word) *
*********************************************************************
seesaw = run_tag ! name of the run
*********************************************************************
* Run to generate the grid pack *
*********************************************************************
.false. = gridpack !True = setting up the grid pack
*********************************************************************
* Number of events and rnd seed *
* Warning: Do not generate more than 1M events in a single run *
* If you want to run Pythia, avoid more than 50k events in a run. *
*********************************************************************
1000000 = nevents ! Number of unweighted events requested
0 = iseed ! rnd seed (0=assigned automatically=default))
*********************************************************************
* Collider type and energy *
* lpp: 0=No PDF, 1=proton, -1=antiproton, 2=photon from proton, *
* 3=photon from electron *
*********************************************************************
1 = lpp1 ! beam 1 type
```

```
1 = lpp2 ! beam 2 type
4000 = ebeam1 ! beam 1 total energy in GeV
4000 = ebeam2 ! beam 2 total energy in GeV
*********************************************************************
* Beam polarization from -100 (left-handed) to 100 (right-handed) *
*********************************************************************
0 = polbeam1 ! beam polarization for beam 1
0 = polbeam2 ! beam polarization for beam 2
*********************************************************************
* PDF CHOICE: this automatically fixes also alpha_s and its evol. *
*********************************************************************
'cteq6l1' = pdlabel ! PDF set
*********************************************************************
* Renormalization and factorization scales *
*********************************************************************
F = fixed_ren_scale ! if .true. use fixed ren scale
F = fixed_fac_scale ! if .true. use fixed fac scale
91.1880 = scale ! fixed ren scale
91.1880 = dsqrt_q2fact1 ! fixed fact scale for pdf1
91.1880 = dsqrt_q2fact2 ! fixed fact scale for pdf2
1 = scalefact ! scale factor for event-by-event scales
*********************************************************************
* Matching - Warning! ickkw > 1 is still beta
*********************************************************************
1 = ickkw ! 0 no matching, 1 MLM, 2 CKKW matching
1 = highestmult ! for ickkw=2, highest mult group
1 = ktscheme ! for ickkw=1, 1 Durham kT, 2 Pythia pTE
1 = alpsfact ! scale factor for QCD emission vx
F = chcluster ! cluster only according to channel diag
T = pdfwgt ! for ickkw=1, perform pdf reweighting
5 = asrwgtflavor ! highest quark flavor for a_s reweight
*********************************************************************
* Automatic ptj and mjj cuts if xqcut ¿ 0
* (turn off for VBF and single top processes)
*********************************************************
T = auto_ptj_mjj ! Automatic setting of ptj and mjj
*********************************************************
* *********************************
* BW cutoff (M+/-bwcutoff*Gamma)
***********************************
15 = bwcutoff ! (M+/-bwcutoff*Gamma)
*********************************************************
* Apply pt/E/eta/dr/mij cuts on decay products or not
* (note that etmiss/ptll/ptheavy/ht/sorted cuts always apply)
*********************************************************
T = cut_decays ! Cut decay products
*********************************************************
* Number of helicities to sum per event (0 = all helicities)
* 0 gives more stable result, but longer run time (needed for
```

```
* long decay chains e.g.).
* Use ¿=2 if most helicities contribute, e.g. pure QCD.
*************************************************************
0 = nhel ! Number of helicities used per event
*******************
* Standard Cuts
*******************
* ****************************************************************
* Minimum and maximum pt's (for max, -1 means no cut) *
*******************************************************************
20 = ptj ! minimum pt for the jets
20 = ptb ! minimum pt for the b
0 = pta ! minimum pt for the photons
0 = ptl ! minimum pt for the charged leptons
0 = misset ! minimum missing Et (sum of neutrino's momenta)
0 = ptheavy ! minimum pt for one heavy final state
1.0 = ptonium ! minimum pt for the quarkonium states
-1 = ptjmax ! maximum pt for the jets
-1 = ptbmax ! maximum pt for the b
-1 = ptamax ! maximum pt for the photons
-1 = ptlmax ! maximum pt for the charged leptons
-1 = missetmax ! maximum missing Et (sum of neutrino's momenta)
*******************************************************************
* Minimum and maximum E's (in the lab frame) *
*******************************************************************
0 = ej ! minimum E for the jets
0 = eb ! minimum E for the b
0 = ea ! minimum E for the photons
0 = el ! minimum E for the charged leptons
-1 = ejmax ! maximum E for the jets
-1 = ebmax ! maximum E for the b
-1 = eamax ! maximum E for the photons
-1 = elmax ! maximum E for the charged leptons
*******************************************************************
* Maximum and minimum absolute rapidity (for max, -1 means no cut) *
*******************************************************************
5 = etaj ! max rap for the jets
5 = etab ! max rap for the b
5 = etaa ! max rap for the photons
5 = etal ! max rap for the charged leptons
0.6 = etaonium ! max rap for the quarkonium states
0 = etajmin ! min rap for the jets
0 = etabmin ! min rap for the b
0 = etaamin ! min rap for the photons
0 = etalmin ! main rap for the charged leptons
*******************************************************************
* Minimum and maximum DeltaR distance *
*******************************************************************
0.001 = drjj ! min distance between jets
```

0.001 = drbb ! min distance between b's
0 = drll ! min distance between leptons
0 = draa ! min distance between gammas
0.001 = drbj ! min distance between b and jet
0 = draj ! min distance between gamma and jet
0 = drjl ! min distance between jet and lepton
0 = drab ! min distance between gamma and b
0 = drbl ! min distance between b and lepton
0 = dral ! min distance between gamma and lepton
-1 = drjjmax ! max distance between jets
-1 = drbbmax ! max distance between b's
-1 = drllmax ! max distance between leptons
-1 = draamax ! max distance between gammas
-1 = drbjmax ! max distance between b and jet
-1 = drajmax ! max distance between gamma and jet
-1 = drjlmax ! max distance between jet and lepton
-1 = drabmax ! max distance between gamma and b
-1 = drblmax ! max distance between b and lepton
-1 = dralmax ! maxdistance between gamma and lepton
****
* Minimum and maximum invariant mass for pairs *
****
0 = mmjj ! min invariant mass of a jet pair
0 = mmbb ! min invariant mass of a b pair
0 = mmaa ! min invariant mass of gamma gamma pair
0 = mmll ! min invariant mass of l+l- (same flavour) lepton pair
-1 = mmjjmax ! max invariant mass of a jet pair
-1 = mmbbmax ! max invariant mass of a b pair
-1 = mmaamax ! max invariant mass of gamma gamma pair
-1 = mmllmax ! max invariant mass of l+l- (same flavour) lepton pair
****
* Minimum and maximum invariant mass for all letpons *
****
0 = mmnl ! min invariant mass for all letpons (l+- and vl)
-1 = mmnlmax ! max invariant mass for all letpons (l+- and vl)
****
* Minimum and maximum pt for 4-momenta sum of leptons *
****
0 = ptllmin ! Minimum pt for 4-momenta sum of leptons(l and vl)
-1 = ptllmax ! Maximum pt for 4-momenta sum of leptons(l and vl)
****
* Inclusive cuts *
****
0 = xptj ! minimum pt for at least one jet
0 = xptb ! minimum pt for at least one b
0 = xpta ! minimum pt for at least one photon
0 = xptl ! minimum pt for at least one charged lepton
****
* Control the pt's of the jets sorted by pt *

```
*********************************************************************
0 = ptj1min ! minimum pt for the leading jet in pt
0 = ptj2min ! minimum pt for the second jet in pt
0 = ptj3min ! minimum pt for the third jet in pt
0 = ptj4min ! minimum pt for the fourth jet in pt
-1 = ptj1max ! maximum pt for the leading jet in pt
-1 = ptj2max ! maximum pt for the second jet in pt
-1 = ptj3max ! maximum pt for the third jet in pt
-1 = ptj4max ! maximum pt for the fourth jet in pt
0 = cutuse ! reject event if fails any (0) / all (1) jet pt cuts
*********************************************************************
* Control the pt's of leptons sorted by pt *
*********************************************************************
0 = ptl1min ! minimum pt for the leading lepton in pt
0 = ptl2min ! minimum pt for the second lepton in pt
0 = ptl3min ! minimum pt for the third lepton in pt
0 = ptl4min ! minimum pt for the fourth lepton in pt
-1 = ptl1max ! maximum pt for the leading lepton in pt
-1 = ptl2max ! maximum pt for the second lepton in pt
-1 = ptl3max ! maximum pt for the third lepton in pt
-1 = ptl4max ! maximum pt for the fourth lepton in pt
*********************************************************************
* Control the Ht(k)=Sum of k leading jets *
*********************************************************************
0 = htjmin ! minimum jet HT=Sum(jet pt)
-1 = htjmax ! maximum jet HT=Sum(jet pt)
0 = ihtmin !inclusive Ht for all partons (including b)
-1 = ihtmax !inclusive Ht for all partons (including b)
0 = ht2min ! minimum Ht for the two leading jets
0 = ht3min ! minimum Ht for the three leading jets
0 = ht4min ! minimum Ht for the four leading jets
-1 = ht2max ! maximum Ht for the two leading jets
-1 = ht3max ! maximum Ht for the three leading jets
-1 = ht4max ! maximum Ht for the four leading jets
*********************************************************************
* WBF cuts *
*********************************************************************
0 = xetamin ! minimum rapidity for two jets in the WBF case
0 = deltaeta ! minimum rapidity for two jets in the WBF case
*********************************************************************
* maximal pdg code for quark to be considered as a light jet *
* (otherwise b cuts are applied) *
*********************************************************************
5 = maxjetflavor ! Maximum jet pdg code
*********************************************************************
* Jet measure cuts *
*********************************************************************
20 = xqcut ! minimum kt jet measure between partons
*********************************************************************
```

```
************************************************************
** MadGraph 5 *
** *
** * * *
** * * * * *
** * * * * 5 * * * * *
** * * * * *
** * * *
** *
** *
** VERSION 1.5.7 2013-01-15 *
** *
** The MadGraph Development Team - Please visit us at *
** https://server06.fynu.ucl.ac.be/projects/madgraph *
** *
************************************************************
** *
** Command File for MadGraph 5 *
** *
** run as ./bin/mg5 filename *
** *
************************************************************


set group_subprocesses Auto
set ignore_six_quark_processes False
set gauge unitary
set complex_mass_scheme False
import model sm
define p = g u c d s u~ c~ d~ s~
define j = g u c d s u~ c~ d~ s~
define l+ = e+ mu+
define l- = e- mu-
define vl = ve vm vt
define vl~ = ve~ vm~ vt~
import model typeIIIAG180_UFO
define vl = ve vm vt
define vl~ = ve~ vm~ vt~
define vl = v1 v2 v3
define l+ = e+ mu+ ta+
define l- = e- mu- ta-
generate p p > tr- tr0, (tr- > w- vl, w- > l- vl), (tr0 > w+ l-, w+ > l+ vl)
add process p p > tr- tr0, (tr- > w- vl, w- > l- vl), (tr0 > w- l+, w- > l- vl)
add process p p > tr- tr0, (tr- > z l-, z > vl vl), (tr0 > w+ l-, w+ > l+ vl)
add process p p > tr- tr0, (tr- > z l-, z > vl vl), (tr0 > w- l+, w- > l- vl)
add process p p > tr- tr0, (tr- > z l-, z > j j), (tr0 > w- l+, w- > l- vl)
add process p p > tr- tr0, (tr- > z l-, z > j j), (tr0 > w+ l-, w+ > l+ vl)
output PROC_typeIIIAG180_UFO_minus
```

```
************************************************************
** MadGraph 5 *
** *
** * * *
** * * * * *
** * * * * 5 * * * * *
** * * * * *
** * * *
** *
** *
** VERSION 1.5.7 2013-01-15 *
** *
** The MadGraph Development Team - Please visit us at *
** https://server06.fynu.ucl.ac.be/projects/madgraph *
** *
************************************************************
** *
** Command File for MadGraph 5 *
** *
** run as ./bin/mg5 filename *
** *
************************************************************


set group_subprocesses Auto
set ignore_six_quark_processes False
set gauge unitary
set complex_mass_scheme False
import model sm
define p = g u c d s u  c  d  s
define j = g u c d s u  c  d  s
define l+ = e+ mu+
define l- = e- mu-
define vl = ve vm vt
define vl  = ve  vm  vt
import model typeIIIAG180_UFO
define vl = ve vm vt
define vl  = ve  vm  vt
define vl = v1 v2 v3
define l- = e- mu- ta-
define l+ = e+ mu+ ta+
generate p p > tr+ tr0, (tr+ > w+ vl, w+ > l+ vl), (tr0 > w+ l-, w+ > l+ vl)
add process p p > tr+ tr0, (tr+ > w+ vl, w+ > l+ vl), (tr0 > w- l+, w- > l- vl)
add process p p > tr+ tr0, (tr+ > z l+, z > vl vl), (tr0 > w+ l-, w+ > l+ vl)
add process p p > tr+ tr0, (tr+ > z l+, z > vl vl), (tr0 > w- l+, w- > l- vl)
add process p p > tr+ tr0, (tr+ > z l+, z > j j), (tr0 > w- l+, w- > l- vl)
add process p p > tr+ tr0, (tr+ > z l+, z > j j), (tr0 > w+ l-, w+ ¿ l+ vl)
output PROC_typeIIIAG180_UFO_plus
```

Appendix C

Hadronization fragment

Hadronization fragment code is:

```
import FWCore.ParameterSet.Config as cms

from Configuration.Generator.PythiaUEZ2starSettings4_cfi import *
from GeneratorInterface.ExternalDecays.TauolaSettings_cff import *

generator = cms.EDFilter("Pythia6HadronizerFilter",
pythiaHepMCVerbosity = cms.untracked.bool(True),
maxEventsToPrint = cms.untracked.int32(0),
pythiaPylistVerbosity = cms.untracked.int32(1),
comEnergy = cms.double(8000.0),
ExternalDecays = cms.PSet(
Tauola = cms.untracked.PSet(
TauolaPolar,
TauolaDefaultInputCards
),
parameterSets = cms.vstring('Tauola')
), UseExternalGenerators = cms.untracked.bool(True),
PythiaParameters = cms.PSet(
pythiaUESettingsBlock,
processParameters = cms.vstring('MSEL=0 ! User defined processes',
'PMAS(5,1)=4.8 ! b quark mass',
'PMAS(6,1)=172.5 ! t quark mass'),
# This is a vector of ParameterSet names to be read, in this order
parameterSets = cms.vstring('pythiaUESettings',
'processParameters'
)
)
)

configurationMetadata = cms.untracked.PSet(
version = cms.untracked.string('$Revision : 1.2$'),
name = cms.untracked.string ('$Source : /afs/cern.ch/project/cvs/reps/CMSSW/CMSSW/
Configuration/GenProduction/python/EightTeV
/Hadronizer_TuneZ2star_8TeV_generic_LHE_pythia_tauola_cff.py,v$'),
```

annotation = cms.untracked.string('runs Z2* Pythia6')
)

The program takes as input the hadronization fragment, the simulation steps to be produced (GEN stays for generation, SIM for simulation), the beam spot to use depending on scenario, the conditions about detectors calibration and alignement (i.e. the Global Tag), the pileup situation, the datamix config to use, the event content to write in the output root file, the datatier to use, the input file with path, the output file name with path, the input file type (LHE), the number of events to produce. The LHE file generation command line is:
cmsDriver.py
Configuration/GenProduction/python/EightTeV/
Hadronizer_TuneZ2star_8TeV_generic_LHE_pythia_tauola_cff.py
–step GEN,SIM
–beamspot Realistic8TeVCollision
–conditions START53_V7C::All
–pileup NoPileUp
–datamix NODATAMIXER
–eventcontent RAWSIM
–datatier GEN-SIM
–filein=file:/tmp/gozzelin/unweighted_events_180plus.lhe
–fileout file:180plus.root
–filetype LHE -n 10

Appendix D

Samples details

Sample are treated in software version CMSSW_5_3_X with Physics Analysis Toolkit version 19, called Padua Prod6.

Table D.1 describes MC background samples considered. Table D.2 shows 2012 data samples at 8 TeV, with corresponding intregrated luminosity. Table D.3 recaps MC signal samples, with cross sections at LO.

Table D.1: Monte Carlo backgrounds samples in Summer12_DR53X-PU_S10_START53_V7A-vX/AODSIM.

Name	Sample
WW	/WW_TuneZ2star_8TeV_pythia6_tauola/
WZ	/WZ_TuneZ2star_8TeV_pythia6_tauola/
ZZ	/ZZ_TuneZ2star_8TeV_pythia6_tauola/
WWW	/WWWJets_8TeV-madgraph/
$t\bar{t}$	/TTJets_FullLeptMGDecays_8TeV-madgraph-tauola/
W+jet	/WJetsToLNu_TuneZ2Star_8TeV-madgraph-tarball/
Z+jet	/DYJetsToLL_M-50_TuneZ2Star_8TeV-madgraph-tarball/
DY	/DYJetsToLL_M-10To50_TuneZ2Star_8TeV-madgraph/

Table D.2: 2012 proton proton collisions data samples.

Data set	Integrated lumi (fb^{-1})
/DoubleElectron/Run2012A-22Jan2013-v1/AOD	0.876
/DoubleElectron/Run2012B-22Jan2013-v1/AOD	4.412
/DoubleElectron/Run2012C-22Jan2013-v1/AOD	7.055
/DoubleElectron/Run2012D-22Jan2013-v1/AOD	7.369
DoubleEle total	19.710
/DoubleMu/Run2012A-22Jan2013-v1/AOD	0.876
/DoubleMuParked/Run2012B-22Jan2013-v1/AOD	4.412
/DoubleMuParked/Run2012C-22Jan2013-v1/AOD	7.017
/DoubleMuParked/Run2012D-22Jan2013-v1/AOD	7.369
DoubleMuParked total	19.674
/MuEG/Run2012A-22Jan2013-v1/AOD	0.876
/MuEG/Run2012B-22Jan2013-v1/AOD	4.412
/MuEG/Run2012C-22Jan2013-v1/AOD	7.055
/MuEG/Run2012D-22Jan2013-v1/AOD	7.360
MuEG total	19.703

In data DoubleMuParked Run A events triggered by Mu17Mu8 are only partially present.

Table D.3: Monte Carlo signal samples.

Signal Sample	σ (pb)
/SeesawTo3Lminus_M-140_FDS_TuneZ2_8TeV-madgraph/Summer12_DR53X-PU_S10_START53_V19-v1/AODSIM	0.0628
/SeesawTo3Lminus_M-180_FDS_TuneZ2_8TeV-madgraph/Summer12_DR53X-PU_S10_START53_V19-v1/AODSIM	0.0190
/SeesawTo3Lminus_M-200_FDS_TuneZ2_8TeV-madgraph/Summer12_DR53X-PU_S10_START53_V19-v1/AODSIM	0.0115
/SeesawTo3Lminus_M-220_FDS_TuneZ2_8TeV-madgraph/Summer12_DR53X-PU_S10_START53_V19-v1/AODSIM	0.0073
/SeesawTo3Lminus_M-240_FDS_TuneZ2_8TeV-madgraph/Summer12_DR53X-PU_S10_START53_V19-v1/AODSIM	0.0048
/SeesawTo3Lminus_M-260_FDS_TuneZ2_8TeV-madgraph/Summer12_DR53X-PU_S10_START53_V19-v1/AODSIM	0.0033
/SeesawTo3Lminus_M-280_FDS_TuneZ2_8TeV-madgraph/Summer12_DR53X-PU_S10_START53_V19-v1/AODSIM	0.0023
/SeesawTo3Lminus_M-300_FDS_TuneZ2_8TeV-madgraph/Summer12_DR53X-PU_S10_START53_V19-v1/AODSIM	0.0016
/SeesawTo3Lminus_M-320_FDS_TuneZ2_8TeV-madgraph/Summer12_DR53X-PU_S10_START53_V19-v1/AODSIM	0.0012
/SeesawTo3Lminus_M-340_FDS_TuneZ2_8TeV-madgraph/Summer12_DR53X-PU_S10_START53_V19-v1/AODSIM	0.0009
/SeesawTo3Lplus_M-140_FDS_TuneZ2_8TeV-madgraph/Summer12_DR53X-PU_S10_START53_V19-v1/AODSIM	0.1229
/SeesawTo3Lplus_M-180_FDS_TuneZ2_8TeV-madgraph/Summer12_DR53X-PU_S10_START53_V19-v1/AODSIM	0.0401
/SeesawTo3Lplus_M-200_FDS_TuneZ2_8TeV-madgraph/Summer12_DR53X-PU_S10_START53_V19-v1/AODSIM	0.0252
/SeesawTo3Lplus_M-220_FDS_TuneZ2_8TeV-madgraph/Summer12_DR53X-PU_S10_START53_V19-v1/AODSIM	0.0166
/SeesawTo3Lplus_M-240_FDS_TuneZ2_8TeV-madgraph/Summer12_DR53X-PU_S10_START53_V19-v1/AODSIM	0.0113
/SeesawTo3Lplus_M-260_FDS_TuneZ2_8TeV-madgraph/Summer12_DR53X-PU_S10_START53_V19-v1/AODSIM	0.0079
/SeesawTo3Lplus_M-280_FDS_TuneZ2_8TeV-madgraph/Summer12_DR53X-PU_S10_START53_V19-v1/AODSIM	0.0057
/SeesawTo3Lplus_M-300_FDS_TuneZ2_8TeV-madgraph/Summer12_DR53X-PU_S10_START53_V19-v1/AODSIM	0.0042
/SeesawTo3Lplus_M-320_FDS_TuneZ2_8TeV-madgraph/Summer12_DR53X-PU_S10_START53_V19-v1/AODSIM	0.0031
/SeesawTo3Lplus_M-340_FDS_TuneZ2_8TeV-madgraph/Summer12_DR53X-PU_S10_START53_V19-v1/AODSIM	0.0024

Table D.4 recaps information to ask the signal production with the CMS official Full Sim chain. The main points deal the sample name containing reference to the model, the final state, the charge, the mass, the scenario, the hadronization features, the event generation program name, the number of events to be generated, the signal cross section coming from Madgraph at LO, the number of event generated in local test, the Central Processing Unit (CPU) time in second used to generate events during the test, the output test file size in Byte.

Sample info,Sample name	Events	σ (pb)	Test events	Time	Size(B)	Time/ev (s)	Size/ev (kB)
M=140,sign -,SeesawTo3Lminus_M-140_FDS_TuneZ2_8TeV-madgraph	450000	0.0628	50	3105	$3.30*10^7$	62	660
M=180,sign -,SeesawTo3Lminus_M-180_FDS_TuneZ2_8TeV-madgraph	450000	0.0190	10	985	$6.00*10^6$	99	600
M=200,sign -,SeesawTo3Lminus_M-200_FDS_TuneZ2_8TeV-madgraph	450000	0.0115	10	705	$6.50*10^6$	71	650
M=220,sign -,SeesawTo3Lminus_M-220_FDS_TuneZ2_8TeV-madgraph	450000	0.0073	10	716	$6.10*10^6$	72	610
M=240,sign -,SeesawTo3Lminus_M-240_FDS_TuneZ2_8TeV-madgraph	450000	0.0048	10	630	$5.60*10^6$	63	560
M=260,sign -,SeesawTo3Lminus_M-260_FDS_TuneZ2_8TeV-madgraph	450000	0.0033	10	815	$6.40*10^6$	82	640
M=280,sign -,SeesawTo3Lminus_M-280_FDS_TuneZ2_8TeV-madgraph	450000	0.0023	10	751	$6.70*10^6$	75	670
M=300,sign -,SeesawTo3Lminus_M-300_FDS_TuneZ2_8TeV-madgraph	450000	0.0016	10	705	$6.10*10^6$	71	610
M=320,sign -,SeesawTo3Lminus_M-320_FDS_TuneZ2_8TeV-madgraph	450000	0.0012	10	665	$6.20*10^6$	67	620
M=340,sign -,SeesawTo3Lminus_M-340_FDS_TuneZ2_8TeV-madgraph	450000	0.0009	10	711	$5.80*10^6$	71	580
M=140,sign +,SeesawTo3Lplus_M-140_FDS_TuneZ2_8TeV-madgraph	450000	0.1229	10	720	$7.10*10^6$	72	710
M=180,sign +,SeesawTo3Lplus_M-180_FDS_TuneZ2_8TeV-madgraph	450000	0.0401	10	650	$6.00*10^6$	65	600
M=200,sign +,SeesawTo3Lplus_M-200_FDS_TuneZ2_8TeV-madgraph	450000	0.0252	10	607	$5.80*10^6$	61	580
M=220,sign +,SeesawTo3Lplus_M-220_FDS_TuneZ2_8TeV-madgraph	450000	0.0166	10	660	$6.60*10^6$	66	660
M=240,sign +,SeesawTo3Lplus_M-240_FDS_TuneZ2_8TeV-madgraph	450000	0.0113	10	694	$7.50*10^6$	69	750
M=260,sign +,SeesawTo3Lplus_M-260_FDS_TuneZ2_8TeV-madgraph	450000	0.0079	10	695	$6.10*10^6$	70	610
M=280,sign +,SeesawTo3Lplus_M-280_FDS_TuneZ2_8TeV-madgraph	450000	0.0057	10	741	$7.10*10^6$	74	710
M=300,sign +,SeesawTo3Lplus_M-300_FDS_TuneZ2_8TeV-madgraph	450000	0.0042	10	788	$8.30*10^6$	79	830
M=320,sign +,SeesawTo3Lplus_M-320_FDS_TuneZ2_8TeV-madgraph	450000	0.0031	10	695	$6.20*10^6$	70	620
M=340,sign +,SeesawTo3Lplus_M-340_FDS_TuneZ2_8TeV-madgraph	450000	0.0024	10	855	$7.10*10^6$	86	710

Table D.4: Monte Carlo signal samples request for official Full Sim production.